Microscopic Theory of the Relaxation Dynamics of Magnetic Impurities

Dissertation

zur Erlangung des Doktorgrades

an der Fakultät für Mathematik, Informatik und Naturwissenschaften

Fachbereich Physik

der Universität Hamburg

vorgelegt von

Michael Lukas Sebastian Elbracht

Hamburg, Oktober 2024

Abstract

In this thesis, the real-time relaxation dynamics of different kinds of impurity models was investigated. The main focus was on quantum-classical hybrid models where one to two classical spins were coupled to a quantum host system of non-interacting itinerant electrons. These systems can only be propagated for a limited time before finite-size effects due to reflections at the system's boundaries set in and disturb the dynamics of the system at the impurities. Since the necessary system sizes would result in too long computation times, it is not feasible to simply increase the system size to raise the propagation time limit. To circumvent this problem, the Lindblad master equation was used to create so-called absorbing boundary conditions. There, the outermost electron sites of the system are coupled to an absorbing bath, which prevents reflections at the system's boundaries by absorbing the outgoing excitations. The construction of these absorbing boundary conditions requires some caution, as these absorbing boundaries should not initiate a dynamics on their own, which would disturb the dynamics of the system in its own way.

After applying these absorbing boundary conditions successfully to a simple toy-model to validate their effectiveness, they were used to investigate the relaxation behavior of a classical spin driven in a magnetic field and coupled to a topological insulator in the form of a Su-Schrieffer-Heeger (SSH) model. As this model features a band gap, it is clear that the system can only relax for sufficiently strong excitations. However, for the SSH model, there are edge states inside the band gap, which lead to a more intricate relaxation behavior of the classical spin. Consequently, the connection between the relaxation of the classical spin and the different parameters of the system was investigated. When explicitly considering retardation effects and dynamic spin-exchange processes, the relaxation behavior can be explained by means of a renormalized linear-response framework.

Going on, lastly, three different two-impurity models were investigated: one purely quantum mechanical (electron impurities coupled to an electron host system), one purely classical (classical spin impurities coupled to a host system of classical spins), and one quantum-classical model (classical spins coupled to an electron host system). While in all of these three models the system relaxed locally into its ground state for nearest-neighbor impurities, for next-nearest-neighbor impurities all these systems exhibited strongly delayed relaxation or even no relaxation at all. The underlying mechanisms behind these relaxation behaviors were investigated and found to involve impurity-induced bound states, emerging approximately conserved local observables, and cancellation of local and non-local damping effects.

Zusammenfassung

In dieser Arbeit wurde die Realzeit-Relaxationsdynamik von verschiedenen Störstellen-modellen untersucht. Das Hauptaugenmerk lag dabei auf einem quantenklassischen Hybridmodell. In diesem Modell werden ein bis zwei klassische Spins an ein quanten-mechanisches Substrat aus nicht wechselwirkenden Elektronen gekoppelt. Diese Systeme können nur für eine begrenzte Zeit propagiert werden, da nach einer gewissen Zeit die Dynamik des Systems an den Störstellen durch Finite-size-Effekte in Form von Reflexionen an den Systemrändern gestört wird. Es ist außerdem nicht möglich, die Systemgröße einfach zu erhöhen, um die Ausbreitungszeitgrenze anzuheben, weil die erforderlichen Systemgrößen zu lange Rechenzeiten zur Folge hätten. Um dieses Problem zu umgehen, wurde die Lindblad-Mastergleichung verwendet, um sogenannte absorbierende Randbedingungen zu kreieren. Dabei werden die äußersten Elektronen-plätze des Systems an ein absorbierendes Bad gekoppelt, das durch Absorption der herauslaufenden Anregungen Reflexionen an den Systemrändern verhindert. Die Kon-struktion dieser absorbierenden Randbedingungen erfordert aber eine gewisse Vorsicht, da diese absorbierenden Ränder von sich aus keine eigene Dynamik auslösen dürfen, welche sonst die Dynamik des Systems auf ihre eigene Art und Weise stören würde. Nachdem diese absorbierenden Randbedingungen erfolgreich an einem einfachen Test-modell getestet wurde, wurden sie verwendet, um das Relaxationsverhalten eines klassi-schen Spins in einem Magnetfeld zu untersuchen, welcher an einen topologischen Isola-tor in Form eines Su-Schrieffer-Heeger (SSH) Modells gekoppelt ist. Da das SSH Modell eine Bandlücke aufweist, ist es klar, dass der klassische Spin nur bei ausreichend starken Anregungen relaxieren kann. Beim SSH Modell gibt es jedoch Randzustände innerhalb der Bandlücke, die das Relaxationsverhalten des Spins komplizierter machen. Es wurde deshalb der Zusammenhang zwischen der Relaxation des Spins und den verschiedenen Parametern des Systems untersucht. Dies hat ergeben, dass, wenn Retardatierungsef-fekte und dynamische Spin-Austauschprozesse berücksichtigt werden, das Relaxations-verhalten mittels eines renormierten Linear-Response-Verfahrens erklärt werden kann. Zuletzt wurden drei verschiedene Zwei-Störstellenmodelle untersucht: ein rein quanten-mechanisches (Elektronen Störstellen auf einem Elektronen Substrat), ein rein klassi-sches (klassische Spins auf einem klassischen Spin Substrat) und ein quantenklassisches Modell (klassische Spins auf einem Elektronen Substrat). Während das System in allen drei Modellen bei benachbarten Störstellen lokal zu seinem Grundzustand relaxiert, zei-gen alle diese Systeme bei übernächsten benachbarten Störstellen eine stark verzögerte oder sogar gar keine Relaxation. Die Mechanismen hinter diesem Relaxationsverhalten wurden untersucht und es wurde herausgefunden, dass diese aufkommende annähernd erhaltene lokale Observablen, durch Störstellen induzierte gebundene Zustände und die gegenseitige Aufhebung lokaler und nichtlokaler Dämpfungseffekte beinhalten.

Contents

Formalities

Unless stated otherwise we use natural units ($\hbar = 1$) all throughout this thesis and corresponding papers.

We refer to the papers building up this cumulative thesis with roman numerals [I-IV]. Additionally, to reduce clutter whenever we reference a figure or something similar in one of the papers, we indicate this by a roman numeral in front of the figure number, e.g., Fig. I-6 references figure six in paper I. As all relevant papers are included in this thesis all respective figures and similar can still be found inside the thesis.

In chapters 4, 5, and 6 we discuss the papers. For a better understanding, it is helpful to read the papers first before looking at the rest of the respective chapter. However, for formatting reasons, the papers are always found at the end of each respective chapter. Also note that this PhD thesis is a continuation of my Master thesis: "Spin relaxation dynamics in the multi-impurity classical-spin Kondo model with dissipative boundaries" (2019). There are some similarities between the two theses regarding the content connected to the first publication [I]. However, the respective content (mainly the construction of the absorbing boundary conditions) was revised and done more rigorously in [I] and this thesis, so that it represents its own and new work.

1 – List of Publications

This cumulative thesis is based on the three publications [I], [II] and [III], which are listed in chronological order below and are also presented in this thesis in this order. There is also a further publication [IV]. However, with the exception of a very small remark in chapter 6, no reference is made to it in this thesis, as it is about work done prior to the PhD project.

The first paper [I] is presented in chapter 4, in which, we introduce the concept of "absorbing boundary conditions" (ABC). For the ABC, we couple the edges of a system to an absorbing bath and tune this bath absorption in such a way that it mimics an infinitely large system. This enables us to propagate the system on much longer timescales than without ABC, as the finite-size effects, which normally appear due to reflections at the system's boundaries, are suppressed by the ABC. We then apply the ABC to a toy-model of a classical spin in a magnetic field coupled to a host system of non-interacting itinerant electrons and compute the long-time relaxation dynamics of the classical spin.

In chapter 5 we present the second paper [II], where we apply the ABC to a quantum-classical system of a classical spin in a magnetic field coupled to a host system in form of an SSH model, which is an example for a topological insulator. The electronic structure features an easy to control band gap with potential edge states inside the band gap. We investigate the real-time relaxation dynamics of the classical spin and how it is influenced by the size of the band gap and the possible edge states.

Finally, the third paper [III] is discussed in chapter 6, where we investigate the real-time relaxation dynamics of different classical, quantum-classical and purely quantum mechanical two-impurity models. Despite their different natures, these models show a similar relaxation dynamics; however, we analyzed these models and found different explanations for each model, respectively.

Many thanks to the American Physical Society and their journals for the permission to include the papers in this thesis.

Publications:

[I] **M. Elbracht** and M. Potthoff, Accessing long timescales in the relaxation dynamics of spins coupled to a conduction-electron system using absorbing boundary conditions, Phys. Rev. B **102**, 115434 (2020).

[II] **M. Elbracht** and M. Potthoff, Long-time relaxation dynamics of a spin coupled to a chern insulator, Phys. Rev. B **103**, 024301 (2021).

[III] **M. Elbracht** and M. Potthoff, Prerelaxation in quantum, classical, and quantum-classical two-impurity models, Phys. Rev. Res. **6**, 033275 (2024).

[IV] **M. Elbracht**, S. Michel, and M. Potthoff, Topological spin torque emerging in classical spin systems with different timescales, Phys. Rev. Lett. **124**, 197202 (2020).

Declaration of Contribution

[I] M. Elbracht wrote the code for the numerical calculations using standard numerical solvers [1, 2], performed all numerical simulations and created all plots. Both authors participated in the planning of the project, the analysis of the numerical results and the writing of the paper.

[II] M. Elbracht wrote the code for the numerical calculations by modifying his code from [I], performed all numerical calculations and created all plots. Both authors participated in the planning of the project, the analysis of the numerical results and the writing of the paper.

[III] M. Elbracht wrote the code, performed all numerical calculations and created all plots. Both authors participated in the planning of the project, the analysis of the numerical results and the writing of the paper.

[IV] M. Elbracht performed initial calculations and analysis of the problem in his bachelor thesis. This mainly includes writing the code to perform the numerical calculations for Fig. 2 in the paper and performing initial analytical investigation. This was later continued by S. Michel, who refined the framework of adiabatic spin dynamics and expanded upon it. The paper was for the most part written by M. Potthoff.

2 – Introduction

Not even a hundred years ago electronic calculators did not exist. Nowadays, they can be found as a by-product on every commercially available smartphone. This is thanks to humanity's never-ending technological advancement, which, among other things, include the first bipolar transistor discovered by Bardeen, Shockley and Brattain in 1947, for which they later won the Nobel prize in physics in 1956. These transistors went on to revolutionize electronic technology and completely replaced the vacuum tube in the 1960s as the de facto control element in electronic circuits. Also at this time, in 1965, Moore's law was formulated, in which Gordon Moore, one of the later co-founders of the semiconductor chip manufacturer Intel, predicted that every one to two years the transistor density on computer chips doubles. This "law" might be in itself a self-fulfilling prophecy; nevertheless, that it more or less has held true until today is a quite remarkable achievement. Over the years, however, the boundaries of what is possible in semiconductor technology came closer and closer. Hence, to keep up with the pace of technological advancements new avenues have to be explored.

One possible option might be in the area of spintronics [3–5]. In spintronics, it is the idea to utilize the spin degrees of freedom of electrons to store and transport information in addition to the conventional use of electronic charge [3]. This idea originates from discoveries made in spin-dependent electron transport, e.g., the discovery of the Giant Magnetoresistance in 1988 [6–8]. The Giant Magnetoresistance enables us to control the electric resistance by changing the magnetization in ferromagnetic layers in heterostructures [3]. The development in spintronics has also already reached the point where first logical gates using only spin degrees of freedom were constructed [9,10]. For this, atomic spins of adatoms adsorbed on a non-magnetic metallic surface were utilized. With the help of a scanning tunnel microscope these adatoms can be placed in the, for the logical gate needed, specific geometries. Later, a spin-polarized scanning tunnel microscope can be used to read out the input and output adatoms of the logical gate. The functionality of these logical gates is based on the interaction between the local magnetic moments of the adatoms in the gate, which is described via an effective Rudermann-Kittel-Kasuya-Yosida (RKKY) coupling [11–13], that is mediated by the electrons in the non-magnetic metallic substrate surface. The transport of information via the magnetic degrees of freedom is advantageous compared to the conventional transport using electrical currents as it is much faster. The needed time to transport information in such a construction is solely limited by the typical dura-

tion for an adatom spin to flip and is approximately 200 fs (for Fe atoms on a Cu(111) surface) [10, 14], promising the possibility of high-speed operations.

These experimental results are very impressive and therefore we want to shed a light on these phenomena from a theoretical perspective. A standard way to treat spintronics theoretically is to use the phenomenological Landau-Lifshitz-Gilbert (LLG) equation [15, 16]

$$\frac{d}{dt}\boldsymbol{S}_m(t) = \boldsymbol{S}_m \times \boldsymbol{B} + \sum_n J_{mn}\boldsymbol{S}_m(t) \times \boldsymbol{S}_n(t) + \sum_n \alpha_{mn}\boldsymbol{S}_m(t) \times \left(\frac{d}{dt}\boldsymbol{S}_n(t)\right) \quad (2.1)$$

here in the form presented in [17]. The magnetic moments $\boldsymbol{S}_m$, representing for example the adatoms in a logical gate, interact via an effective RKKY interaction J_{mn} and can be driven in an (external) magnetic field $\boldsymbol{B}$. The last term of the LLG equation is dissipative and leads to a damping of the magnetic moments. The strength and form of this damping is described by the Gilbert dampings α_{mn} [16, 18]. The Gilbert damping describes dissipation effects induced, for example, by the (non-magnetic metallic) substrate. Compared to the problem of a condensed matter system with many interacting electrons the LLG equation is rather simple as it only contains classical degrees of freedom in form of magnetic moments. All the contributions of the system to the dynamics of the magnetic moments, for example by a substrate, are absorbed into the RKKY interaction and the Gilbert damping. Despite or perhaps because of the simplicity of the LLG equation it has become a fundamental dynamical system in applied magnetism [19–22].

However, sometimes the treatment of the problem via the LLG equation might be "too simplistic". There might be parameter regimes where it is not possible to capture the influence of the substrate solely by the RKKY interaction and the Gilbert damping. There, a more intricate treatment of the substrate is needed, where the substrate is treated explicitly and not only on an effective level. Indeed, in the past it was shown that there are cases where the LLG equation gives different results than an explicit treatment of the substrate [17, 23, 24].

A way to realize such a treatment is to consider impurity models. These models consist of two parts. Firstly, a large host system, which takes the same role as the metallic substrate in the experimental setup. Normally, we choose a tight-binding system of non-interacting itinerant electrons for the host system. This is a standard model for describing metallic materials and is relatively easy to use as the electrons are non-interacting, such that correlation effects can be neglected. Secondly, a very small amount of impurities attached to (typically somewhere in the bulk of) the host system. The impurities are used to describe the magnetic adatoms in the experimental setup and correspond to the local magnetic moments in the LLG equation, Eq. (2.1). For

that, most of the time, we choose the impurities to be classical spins, which represent the magnetic properties of the adatoms. Of course, one could also consider quantum mechanical spins for the impurities to also capture effects like the Kondo effect [17, 25, 26], but that would make all calculations much more difficult due to correlation effects between the quantum spin and the electrons in the host system. Hence, as a trade-off, we employ classical spin impurities so that we do not have to deal with these correlation effects and get a more easily accessible system.

We call the combination of a host system of non-interacting electrons and classical spin impurities "quantum-classical Kondo impurity model". However, even this most basic model with classical impurities struggles with a fundamental problem of impurity models: the occurrence of finite-size effects. In general we are interested in the real time dynamics of the considered systems. So how do specific observables, like local magnetic moments or energy density, evolve over time? Generally, these observables we are interested in are local and confined to an area in the vicinity of the impurities. Normally, we consider a system that is initially at rest and then is instantaneously and locally excited at the impurities. Mathematically, this is done by a parameter quench, e.g., switching on the host-impurity interaction or changing the local magnetic moments of the impurities. In the experiment on the other hand one could imagine something like suddenly changing the magnetization of the adatoms by using a spin-polarized scanning tunnel microscope.

As the system is no longer in an equilibrium anymore, dynamics set in, and the initial local excitations are then slowly dissipated from the impurities into the bulk of the host system. This then typically goes on and on until either the excitations are completely dissipated into the bulk or, in the more common case, the excitations, which traveled through the system, were reflected at the system's boundary and then traveled back, reach the impurities again and disturb the dynamics. In the experiment the substrate is macroscopically large and this does not happen, although there are of course different problems and difficulties like artifacts induced by local defects, too high temperatures, sensitivity to mechanical vibrations (of, e.g., vacuum pumps) or the desire for high magnetic fields [27, 28]. On the other hand, in the theoretical calculations, it is impossible to consider a macroscopically large host system since we are limited by what is feasible to calculate numerically. While the host system is typically much larger than the area around the impurities, it is in general not large enough to not have to worry about finite-size effects.

As a rule of thumb the numerical computation time scales approximately as $t \propto L^3$. In reality, this means that we are confined to system sizes of $L \approx 1000$ before calculations take too long. This is by no means macroscopically large and leads to the above mentioned problem of reflected excitations disturbing the dynamics at the impurities. There are some ways one could try to mitigate this. For example, one could use periodic

boundary conditions for the host system. We simply attach one boundary of the host system to the opposite boundary. So a one-dimensional chain becomes a ring, a two-dimensional lattice becomes a torus and so on. While this reduces the finite-size effects somewhat, it is by no means sufficient to fully suppress them.

We therefore elect to introduce a different kind of boundary conditions, which we call absorbing boundary conditions (ABC). The idea is to just consider a relatively small host system of about $L \approx 50$ sites and then attach an absorbing bath to its boundary. In the ideal case, the baths absorb the outgoing excitations without reflecting them back and thereby mimic the existence of a macroscopically large host system. Of course this is easier said than done and one would have to make sure that the absorbing bath does not influence the dynamics of the system in any other way. The construction of these ABC was one major part of this PhD project.

This thesis is built up as follows. At first, in chapter 3 we give a summary of the theoretical background and concepts used during this PhD project. In chapter 4 we present the first scientific paper [I] in which we constructed the ABC and link it to other scientific works. Following on, chapter 5 is about the second scientific paper [II], where we applied the ABC to investigate the relaxation dynamics of a classical spin coupled to a topological insulator and how the relaxation depends on the size of the band gap and on the topological trivial and non-trivial phase. At last, before we summarize the results and give a short outlook, we discuss the final scientific paper [III] where we found an odd relaxation behavior in models with two impurities. However, we found the same odd behavior for three different kind of models, a purely quantum mechanical, a purely classical and a quantum-classical model. We study each of these models and for each explain the reason behind the odd relaxation behavior.

3 – Models and Methods

During the work for this thesis, different kinds of models were considered, and various methods were used to investigate them. All of these models, however, have in common that they are some kind of impurity model. This means all models consist of two different parts. Firstly, a host system like a tight-binding system of non-interacting electrons or a classical Heisenberg system. This host system is typically large with over $L \gtrsim 10^3$ sites. Secondly, the impurities, for example classical spins, which are coupled to the host system. A schematic sketch of an impurity model is shown in Fig. 3.1, which together with its caption was taken from [III].

The number of impurities N is typically small compared to the number of sites in the host system: $N \approx 1, 2, ... < 10$. Each of the impurities $m \in \{1, ..., N\}$ is coupled to a site i_m of the host system. Usually these sites i_m are in the same vicinity and close to each other: $|i_{m_1} - i_{m_2}| < 10$. The consequence of this is that only a small part of the host system is directly influenced by the impurities, as the majority of the host system "does not see" the impurities and is only indirectly influenced by them via the inter-host system interactions.

All through out this thesis, the host system is initially in or close to its ground state, such that there is basically no excitation energy left in the host system. The system then is excited at the impurities, typically via some local parameter quench, which then initiates a dynamics. Over time this dynamics spreads out throughout the whole system as the initial excitation at the impurities is dissipated into the bulk system. Generally, we then are interested in the real-time dynamics of the degrees of freedom of the system in the vicinity of the impurities, so for example in the time evolution of local observables at the impurities. In general the observed dynamics is expected to show a relaxation of the system, as the initially local excitation wants to spread out throughout the whole system, lowering the local energy at the impurities. The system around the impurities, therefore, most often tends to some local ground state after some time. However, this does not always have to be the case as can be seen in the publications [I-III] on which this thesis is based, where the investigation of the relaxation dynamics for different kinds of impurity models was the main goal.

The relaxation behavior of non-equilibrium states in general is a major problem in theoretical solid state physics. There are many different theories, which try to predict whether a specific system relaxes, when the ergodicity of a system is violated or whether it thermalizes. In classical physics, for example, the ergodicity of a system
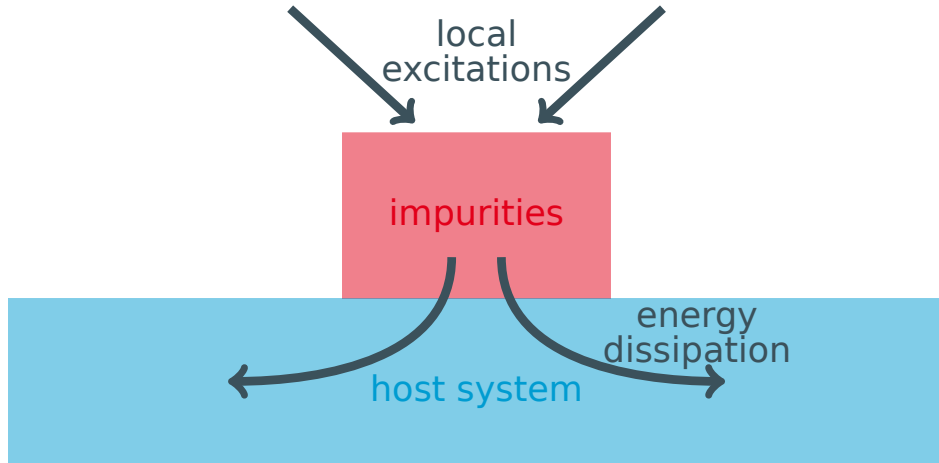
Figure 3.1: *Typical structure of an impurity model. The impurities are coupled to a much larger host system. After an initial local excitation, the full system, impurities plus host, is expected to relax locally in its ground state in the vicinity of the impurities after the excitation energy is dissipated into the bulk.*

is typically violated if there is a sufficient number of integrals of motion and in general this means that the system is integrable and can be solved analytically. In cases where the equations of motion cannot be solved analytically there are theories like the Kolmogorov-Arnold-Moser theorem (KAM theorem) [29–31], which makes a prediction about the ergodicity of a system close to an integrable one.

In quantum mechanics the "eigenstate thermalization hypothesis" (ETH) [32–35] predicts the relaxation behavior of isolated systems in a non-equilibrium state. Usually, such systems are ergodic and their dynamics show a relaxation to a thermal state. Like in the classical case, however, the existence of many integrals of motion can disturb the ergodicity of the system. The system then no longer relaxes to a thermal state and it instead relaxes to a non-thermal steady state, which is often predicted by the generalized Gibbs ensemble [36–39]. There, the non-thermal steady state is found by maximizing the entropy of the system under the restrictions to the dynamics given by the integrals of motion.

During this thesis, the relaxation dynamics of different kinds of impurity models was investigated. This includes fully classical [III], fully quantum mechanical [III] and quantum-classical hybrid systems [I-III]. These impurity models show all kinds of different relaxation behaviors from expected full relaxation to no relaxation at all. In a sense, the dynamics of these impurity models shows parallels to the prior mentioned KAM theorem and ETH theories, as these impurity models are often close to integrable models, namely their non-impurity counter parts. The main goal of this thesis was to investigate and explain the different relaxation behaviors of these models using various different techniques for analyzing the dynamics of the respective systems.

3.1 – Non-Interacting Electrons

For most of the impurity models considered in this thesis, the host system is a one-dimensional chain of itinerant non-interacting electrons. Mathematically, this can be described by the well-known (spinful) tight-binding Hamiltonian in second quantization

$$\hat{H}_{\text{host}} = -\sum_{ij\sigma\nu} T_{i\sigma j\nu}\hat{c}_{i\sigma}^{\dagger}\hat{c}_{j\nu} \ , \tag{3.1}$$

with a nearest-neighbor only and spin conserving hopping $T_{i\sigma j\nu} = T_{ij}\delta_{ij\pm1}\delta_{\sigma\nu}$. Spin conserving hopping means that we basically have two seperate spinless tight-binding models not interacting with each other. However, we still introduce the model with spin degrees of freedom, as it will be helpful later on. The operators $\hat{c}_{i\sigma}^{\dagger}$ and $\hat{c}_{i\sigma}$ create or annihilate respectively an electron at the lattice site i with a spin projection of $\sigma \in \{\uparrow,\downarrow\}$ and are adjoint to each other. Typically, the hopping is the same everywhere in the system, so $T_{ij} = T$ for $|i - j| = 1$ with the exception of section 3.2 where we consider alternating hopping amplitudes. Combining a lattice index and spin index to a multi index $\boldsymbol{\alpha} = (i, \sigma)$, the hopping can be expressed in matrix form as the hopping matrix

$$\boldsymbol{T} = (T_{\boldsymbol{\alpha}\boldsymbol{\alpha}'})_{\boldsymbol{\alpha}=1\uparrow,1\downarrow,\dots,L\uparrow,L\downarrow;\ \boldsymbol{\alpha}'=1\uparrow,1\downarrow,\dots,L\uparrow,L\downarrow}. \tag{3.2}$$

As there are only terms quadratic in the creation and annihilation operators in the Hamiltonian, Eq. (3.1), the system is not correlated. This makes it much easier to describe and calculate the dynamics of the system as one can reduce the dynamics to a one-particle picture. For that, we introduce the one-particle reduced density matrix $\boldsymbol{\rho}$, whose elements are:

$$\rho_{\boldsymbol{\alpha}\boldsymbol{\alpha}'}(t) = \rho_{i\sigma j\nu}(t) := \langle\hat{c}_{j\nu}^{\dagger}\hat{c}_{i\sigma}\rangle_t, \tag{3.3}$$

given by the expectation values of creation-annihilation operator tuples at time t. The one-particle reduced density matrix operates only on the one-particle part of the Hilbert space and, hence, has exponentially fewer elements ($2L \times 2L$) than the full density matrix ($\sim 4^L$). Consequently, it is possible to calculate the dynamics of the system for much larger system sizes and longer time scales than for a correlated system. The equation of motion in terms of the one-particle reduced density matrix is given by a von Neumann equation

$$i\frac{d}{dt}\boldsymbol{\rho}(t) = [\boldsymbol{T}, \boldsymbol{\rho}(t)] \ , \tag{3.4}$$

where the time derivative of the one-particle reduced density matrix is given by the commutator of itself and the hopping matrix.

This equation of motion can be easily solved analytically by

$$\boldsymbol{\rho}(t) = \boldsymbol{U}(t,0)\boldsymbol{\rho}_0\boldsymbol{U}(t,0)^{-1} \ , \tag{3.5}$$

where $\boldsymbol{\rho}_0 = \boldsymbol{\rho}(t=0)$ is the one-particle reduced density matrix at $t = 0$ and where $\boldsymbol{U}(t,t')$ is the unitary time-evolution matrix. Note, however, that to obtain the time-evolution matrix one still has to calculate the matrix exponentials

$$\boldsymbol{U}(t,t') = \exp\left(-i\boldsymbol{T}(t - t')\right) \ , \tag{3.6}$$

which for too large system sizes is in most cases not feasible analytically and might still be quite taxing numerically. If, for example, the system were invariant under translations, e.g., by considering periodic boundary conditions, one could Fourier transform the system to the momentum space and solve it there analytically. However, this is not of much use for us, as we always consider impurity models, whose impurities would break any existing translation symmetry of the system. Nevertheless, periodic boundary conditions make it easier to give analytic expressions for the one-particle eigenenergies and eigenstates. For a given $k_j = \frac{2(j-1)\pi}{L}$, $j \in \{1, 2, ..., L\}$ the one-particle eigenstates of a spinless tight-binding model are given by $\varphi_k(l) := e^{ik_j R_l}$, where R_l indicates the coordinate of the electron site l, typically we choose $R_l = l$. The eigenstates all extend over the whole system and have an increasing number of nodes. The one-particle eigenenergies ε_{k_j}, on the other hand, are given by the tight-binding dispersion

$$\varepsilon_{k_j} = -2T\cos(k_j) \ . \tag{3.7}$$

3.2 – SSH Model

Topological insulators [40,41] are states of quantum matter, which, while still featuring a bulk band gap like ordinary insulators, cannot be adiabatically connected to them. In other words, by adiabatically varying the parameters of the Hamiltonian, the spectrum

Figure 3.2: *Sketch of a one-dimensional SSH model. The different electron sites (blue dots) are connected via an alternating electron hopping T_1 (weaker) and T_2 (stronger).*

of a topological insulator cannot be deformed to that of an ordinary insulator without becoming a conduction state somewhere during the deformation. Often they are set apart by the existence of protected gapless conducting states at their edge or surface. The SSH model is one of the most basic examples for such a topological insulator. However, topological systems and their theory, like the tenfold classification of topological insulators and superconductors [42–45], are not the main focus of this thesis and we are much more interested in the properties of the SSH model, namely that it has a tuneable bulk band gap and that it may feature edge states inside the gap. We are not going to compute topological invariants like Chern numbers nor are we going to compute phase diagrams of the different topological phases or discuss the different symmetry classes characterizing topological insulators [46].

The SSH model is still a tight-binding model, so everything from the previous section still holds true for the SSH model. However, it features an alternating electron hopping between the sides, which leads to some interesting properties. We express the hopping in the following way:

$$T_{12} = T_{34} = T_{56} = ... =: T_1 \tag{3.8}$$

$$T_{23} = T_{45} = T_{67} = ... =: T_2 \ , \tag{3.9}$$

where

$$T_1 = T - \delta T \text{ and } T_2 = T + \delta T \ . \tag{3.10}$$

A sketch of the spinful SSH model is shown in Fig. 3.2 and its Hamiltonian for L electron sites, therefore, reads:

$$\hat{H} = -\sum_{i=1}^{L-1} \sum_{\sigma=\uparrow,\downarrow} \left[\left(T + (-1)^i \delta T\right) \hat{c}_{i\sigma}^\dagger \hat{c}_{i+1\sigma} + \text{H.c.} \right] \ . \tag{3.11}$$

For $\delta T = 0$ one would receive the same tight-binding model of a simple metal as in Eq. (3.1) while any non-zero δT leads to a finite bulk band gap of

$$\Delta = 4|\delta T| = 2|T_1 - T_2| \tag{3.12}$$

between the highest valence band state and the lowest conduction band state. The sign of δT is also important as for $\delta T < 0$ the system is in a topologically trivial insulator state. For $\delta T > 0$, on the other hand, the system is in a topologically non-trivial state and there are two spin-degenerate edge states inside the bulk band gap at zero energy. They are called edge states, because they are exponentially located at the edge of the system. In the limit $L \to \infty$ one can write down an analytical expression of the edge states. In this limit the edge state with spin projection σ is given by [47]:

$$|\text{edge}, \sigma\rangle = \sum_{i=1}^{\infty} c_i |i, \sigma\rangle \tag{3.13}$$

with coefficients $c_i = 0$ for even site indices i and

$$c_i = \left(-\frac{T_1}{T_2}\right)^{\frac{i-1}{2}} \sqrt{1 - \frac{T_1^2}{T_2^2}} \tag{3.14}$$

for odd i. As $T_1 < T_2$, these coefficients go to zero exponentially for increasing i, since $\lim_{i\to\infty} \left(-\frac{T_1}{T_2}\right)^{\frac{i-1}{2}} = 0$.

3.3 – Classical Spin Impurities

In most of our research we consider setups with a quantum mechanical host system of non-interacting electrons, to which we couple a small number of impurities in form of classical spins. We choose classical spins instead of quantum spins mainly because it makes the necessary calculations much easier, if not even possible in the first place. On the other hand for quantum spin impurities we would get the conventional Kondo model [25, 26], which features an anomalous behavior of the electric resistivity in presence of magnetic impurities, the so-called Kondo effect. This Kondo effect is not present for classical spin impurities. However, computing the real-time dynamics is much more difficult for quantum spin impurities as the system would be correlated at the sites the impurity spins are coupled to. It would require the use of much more intricate techniques like, for example, time-dependent density matrix renormalization group [48–54].

Estimating the quality of the classical spin approximation is difficult [55–57], however, for one-dimensional systems one can quantitatively compare the dynamics with full

quantum calculations [24]. There it was found that, especially for large spin-quantum numbers and for strong external magnetic fields, the classical-spin approximation is similar to its full-quantum counterpart.

The classical spin impurities lead to two additional terms in the Hamiltonian. To the original Hamiltonian of the host system Eq. (3.1), we add an exchange interaction term $\hat{H}_{\text{ex}}$ describing the interaction between the impurity spins and the host system and a magnetic field term H_B describing the interaction of the impurity spins with an (optional) magnetic field $\boldsymbol{B}_m$:

$$\hat{H} = \hat{H}_{\text{host}} + \hat{H}_{\text{ex}} + H_B \tag{3.15}$$

with

$$\hat{H}_{\text{ex}} = \sum_m K \boldsymbol{S}_m \hat{\boldsymbol{s}}_{i_m} \tag{3.16}$$

and

$$H_B = -\sum_m \boldsymbol{B}_m \boldsymbol{S}_m \ . \tag{3.17}$$

There, $\boldsymbol{S}_m$ are the classical impurity spins with a length of $S = |\boldsymbol{S}_m| = \frac{1}{2}$, when not mentioned otherwise, and

$$\hat{\boldsymbol{s}}_{i_m} = \frac{1}{2} \sum_{\sigma\nu} \hat{c}^\dagger_{i_m\sigma} \boldsymbol{\tau}_{\sigma\nu} \hat{c}_{i_m\nu} \tag{3.18}$$

are the local magnetic moments of the sites the impurities are coupled to, where $\boldsymbol{\tau}$ denotes the vector of Pauli matrices:

$$\boldsymbol{\tau} := \begin{pmatrix} \boldsymbol{\sigma}_x \\ \boldsymbol{\sigma}_y \\ \boldsymbol{\sigma}_z \end{pmatrix} \ . \tag{3.19}$$

Combining classical impurity spins with a quantum mechanical host system requires some thought about how to treat the quantum mechanical degrees of freedom when deriving the equations of motion for the classical degrees of freedom and vice versa. How to handle such a quantum-classical system is described in [58], and its application

to our systems is described in the following.

For the equations of motion for the quantum degrees of freedom we can treat the classical impurity spins as time-dependent external magnetic fields. We can absorb their effect on the electrons into the hopping matrix, resulting in the so-called effective hopping matrix $\boldsymbol{T}_{\mathrm{eff}}$:

$$T_{i\sigma j\nu}^{(\mathrm{eff})}(t) = T_{i\sigma j\nu} + \frac{K}{2}\sum_m \boldsymbol{S}_m(t)\boldsymbol{\tau}_{\sigma\nu}\delta_{ii_m}\delta_{ij} \ , \tag{3.20}$$

which then replaces the normal hopping matrix in Eq. (3.4) and leads to the new equation of motion:

$$i\frac{d}{dt}\boldsymbol{\rho}(t) = [\boldsymbol{T}_{\mathrm{eff}}\left(\boldsymbol{S}_1(t), \boldsymbol{S}_2(t), ...\right), \boldsymbol{\rho}(t)] \ . \tag{3.21}$$

For the equations of motion for the classical degrees of freedom, we have to think about how to treat the quantum part of the system as the equation of motions have to be classical. This is done by taking the expectation values of the quantum degrees of freedom. We then can derive the equations of motion easily by using the Spin-Poisson bracket [59, 60] to arrive at:

$$\frac{d}{dt}\boldsymbol{S}_m = \frac{\partial\langle\hat{H}\rangle_t}{\partial\boldsymbol{S}_m}\times\boldsymbol{S}_m = \frac{\partial\left(\langle\hat{H}_{\mathrm{ex}}\rangle_t + H_B\right)}{\partial\boldsymbol{S}_m}\times\boldsymbol{S}_m = (K\langle\hat{\boldsymbol{s}}_{i_m}\rangle_t - \boldsymbol{B}_m)\times\boldsymbol{S}_m \ . \tag{3.22}$$

Together Eq. (3.21) and Eq. (3.22) form a complete set of equations of motion for the quantum-classical hybrid model. Due to the addition of the classical spin(s), however, the equations of motion are not in general analytically solvable anymore in contrast to a pure tight-binding model. Therefore, the dynamics has to be calculated by using standard numerical techniques for solving ordinary differential equations like a Runge-Kutta method [1, 2].

3.4 – Linear-Response Theory

Linear-response theory enables us to predict the time-dependent response of a system to a (weak) time-dependent perturbation. This can be helpful for the analysis of our quantum-classical impurity models, as we can treat the coupling of the impurities to the host system as a perturbation, to which we can then compute the response of the host system. In the following, we will introduce the basics of linear-response theory. The derivation is based on and follows [61]. At the end of the derivation we then show

how to apply the linear-response theory to our systems.

Suppose we have some system with a time independent Hamiltonian $\hat{H}_0$. We add a time-dependent linear coupling $\lambda_B(t)\hat{B}$ to the system described by an observable $\hat{B}$ and a time-dependent coupling parameter $\lambda_B(t)$. The full Hamiltonian is therefore given by:

$$\hat{H} = \hat{H}_0 + \lambda_B(t)\hat{B} \; . \tag{3.23}$$

At time $t = -\infty$ the system shall be in an equilibrium, hence, $\lambda_B(t = -\infty) = 0$. Our goal is now to calculate the response of some non-explicitly time-dependent observable $\hat{A}$ to the perturbation, which is given by

$$\frac{\delta\langle\hat{A}\rangle_t}{\delta\lambda_B(\tau)}\big|_{\lambda_B(\tau)\equiv 0} \; . \tag{3.24}$$

The time expectation value of $\hat{A}$ is easily calculated by

$$\langle\hat{A}\rangle_t = \text{tr}\left(\hat{\rho}(t)\hat{A}\right) \; . \tag{3.25}$$

However, for that we need to know the density operator $\hat{\rho}(t)$. In the equilibrium at $t = -\infty$, so without the perturbation, the density operator is given by

$$\hat{\rho}_0 := \hat{\rho}(t = -\infty) = \frac{1}{Z_0}\exp\left(-\beta\hat{H}_0\right) \tag{3.26}$$

with the partition function $Z_0 = \text{tr}\left(\exp\left(-\beta\hat{H}_0\right)\right)$. We now know how the density operator looks like at $t = -\infty$, but we still need its time evolution to compute the expectation value in Eq. (3.25). The time evolution of the density operator is given by the von Neumann equation:

$$i\frac{d}{dt}\hat{\rho}(t) = \left[\hat{H}(t), \hat{\rho}(t)\right] \; . \tag{3.27}$$

In general for weak perturbations it is helpful to switch to the interaction picture, which is the same as the Heisenberg picture but with respect to the unperturbed Hamiltonian $\hat{H}_0$ only. In the interaction picture operators $\hat{O}_I(t)$ are defined by

$$\hat{O}_I(t) = \exp\left(i\hat{H}_0 t\right) \hat{O} \exp\left(-i\hat{H}_0 t\right) . \tag{3.28}$$

On the other hand, the statistical expectation values have the same form in the interaction picture

$$\langle \hat{A} \rangle_t = \text{tr}\left(\hat{\rho}_I(t)\hat{A}_I(t)\right) . \tag{3.29}$$

The time evolution of the density operator is again given by a von Neumann like equation:

$$\frac{d}{dt}\hat{\rho}_I(t) = i\left[\hat{B}_I(t), \hat{\rho}_I(t)\right]\lambda_B(t) , \tag{3.30}$$

where the Hamiltonian is replaced by the time-dependent perturbation: $\lambda_B(t)\hat{B}_I(t)$. We now need to solve this equation, but have to keep the restrictions given by Eq. (3.26) in mind. Doing that, one can receive the following integral equation by integrating Eq. (3.30):

$$\hat{\rho}_I(t) = \hat{\rho}_0 + i \int_{-\infty}^{t} d\tau \left[\hat{B}_I(\tau), \hat{\rho}_I(\tau)\right]\lambda_B(\tau) . \tag{3.31}$$

There is still a $\hat{\rho}_I(\tau)$ remaining under the integral in Eq. (3.31) and without solving the integral it is not possible to get rid of it. However we can generate an iterative solution by repeatingly inserting Eq. (3.31) into itself. As the perturbation $\lambda_B(\tau)\hat{B}_I(\tau)$ only appears in linear order under the integral, the iterative solution generates with each iteration additional terms with increasing order in the perturbation term. For example up to second order in the perturbation one would receive

$$\hat{\rho}_I(t) = \hat{\rho}_0 + i \int_{-\infty}^{t} d\tau \left[\hat{B}_I(\tau), \hat{\rho}_0\right]\lambda_B(\tau)$$
$$- \int_{-\infty}^{t} d\tau' \int_{-\infty}^{t} d\tau \left[\hat{B}_I(\tau), \left[\hat{B}(\tau'), \hat{\rho}_0\right]\right]\lambda_B(\tau)\lambda_B(\tau') . \tag{3.32}$$

Theoretically, we could perform this iteration forever. However, in linear-response theory we make an approximation and only consider terms of linear order in the perturbation and discard the rest. Hence, in linear-response theory the density operator is given by

$$\hat{\rho}_I(t) = \hat{\rho}_0 + i \int_{-\infty}^{t} d\tau \left[\hat{B}_I(\tau), \hat{\rho}_0 \right] \lambda_B(\tau) . \tag{3.33}$$

Finally, we can use Eq. (3.33) and insert it into Eq. (3.29) to receive the so-called Kubo formula

$$\delta \langle \hat{A} \rangle_t = \langle \hat{A} \rangle_t - \langle \hat{A} \rangle_{\rho_0} = \int_{-\infty}^{t} d\tau \lambda_B(\tau) \chi_{A,B}(t, \tau) . \tag{3.34}$$

There, $\chi_{A,B}(t, \tau)$ is the response function or so-called retarded susceptibility:

$$\chi_{A,B}(t, \tau) = \frac{\delta \langle \hat{A} \rangle_t}{\delta \lambda_B(\tau)} \Big|_{\lambda_B(\tau) \equiv 0} = i \left\langle \left[\hat{A}_I(t), \hat{B}_I(\tau) \right] \right\rangle_{\rho_0} \Theta(t - \tau) , \tag{3.35}$$

where $\Theta(t - \tau)$ is the Heaviside function. The Heaviside function ensures causality, such that the expectation value $\langle \hat{A} \rangle_t$ can only be influenced by perturbations $\hat{B}_I(\tau)$ at times $\tau < t$. Note that the susceptibility $\chi_{A,B}(t, \tau)$ depends only on the time difference $t - \tau$:

$$\chi_{A,B}(t, \tau) = \chi_{A,B}(t - \tau) . \tag{3.36}$$

In our work, we treat the spin impurities as perturbations in the sense of linear-response theory. The impurities are attached to the system at time $t = 0$. The classical spins are treated as the time-dependent coupling $\lambda_B(t)$, while the components of the local magnetic moments, which couple to the classical spins, function as observables $\hat{B}$. For example, for one impurity spin, we would have:

$$\lambda_B(t) = K S_1^\beta(t) \Theta(t) \tag{3.37}$$

$$\hat{B} = \hat{s}_{i_1}^\beta , \tag{3.38}$$

where $\beta = x, y, z$. We then are interested in the response of the component $\hat{A}(t) = \hat{s}_{i_1}^\alpha$ to the perturbation $\lambda_B(t)\hat{B} = K S_1^\beta(t) \hat{s}_{i_1}^\beta \Theta(t)$. The response is given by the retarded spin susceptibility

$$\chi_{\alpha\beta}(t, \tau) = -i\Theta(t - \tau) \left\langle \left[\hat{s}_{i_1}^\alpha(t), \hat{s}_{i_1}^\beta(\tau) \right] \right\rangle_{\hat{\rho}_0} , \tag{3.39}$$

from which we get the following equation for the local magnetic moment:

$$\langle \hat{\boldsymbol{s}}_{i_1} \rangle_t = K \int_0^t d\tau \boldsymbol{\chi}(t,\tau) \boldsymbol{S}_1(\tau) \;, \tag{3.40}$$

where $\boldsymbol{\chi}$ is the matrix built up by the components $(\chi_{\alpha\beta})_{\alpha=x,y,z;\ \beta=x,y,z}$.

Of course, this can also be extended to multiple impurity spins, which we did in [III].

3.5 – Absorbing Boundary Conditions

The dynamics in our systems is focused around the impurities in the system. Typically the host system is initially in its ground state. A dynamics is then initiated by exciting the system locally around the impurities. This is for example done by quenching the system's parameters at the impurities, e.g., the host-impurity interaction. Therefore, the only part of the system, which is excited at $t = 0$, are the impurities or a small area around the impurities. When we then propagate the system in time, only a small part of the system around the impurities is affected at first. The rest of the system away from the impurities does not show any dynamics in the beginning. This, however, changes over time as the excitation around the impurities is slowly dissipated into the bulk. The maximum speed of the propagation of these excitations is roughly limited by the Fermi velocity, which for a simple tight-binding model is given by $v_F \approx \frac{2}{T}$ [17]. This goes on and on until the excitations reach the host system's boundaries after a time of $\approx \frac{L}{2v_F}$ assuming the impurities are located at the center of the host system. The excitations then are reflected at the host system's boundaries and travel back through the host system until they reach the impurities after the same time again. Up until this point the dynamics of the impurities was unperturbed by the finite size of the host system. Now, however, the dynamics of the impurities is disturbed by the reflected excitations. In theory, we could prevent this by making the host system larger, as it would take longer for the excitations to travel back and forth through the host system. Unfortunately the computational effort of the numerical calculations is roughly proportional to L^3. Hence, doubling the system size makes the calculations take eight-times longer. In addition, increasing the system size increases the maximal unperturbed propagation time, which contributes linearly to the total computation time as well. This means, increasing the system size is only feasible up to a certain degree as the numerical calculations would just take too long.

Typically, we want to achieve unperturbed propagation times of at least $10^4 \frac{1}{T}$. The numerical calculations for 10^3 inverse hoppings and a host system size of $L = 10^3$ take around an hour on a standard desktop PC. The numerical calculations for 10^4 inverse hoppings with a system size of $L = 10^4$ would therefore take on the order of 10^4 hours

or around 420 days, which is just too much time. Additionally, note that it is not of much use to perform the calculations on a compute cluster as it is necessary to calculate the previous step of the time propagation before calculating the next step. Ergo, the gains, by parallelizing the numerical calculations, are very limited.

Therefore, we have to come up with a different way other than simply making the system larger. One option would be to use periodic boundary conditions instead of open boundary conditions. So a ring like geometry for the host system instead of a chain geometry. This would weaken the disturbing finite-size effects, but not completely eliminate them and the real-time dynamics of the impurities would still be noticeably different than for an infinitely large host system without finite-size effects.

Hence, we came up with a different kind of boundary conditions, which we call "absorbing boundary conditions" (ABC). The idea is to couple the edge of the host system to an absorbing bath mimicking an infinitely large system. As we have full control over the bath parameters, we have much more control over how the incoming excitations are absorbed compared to just using periodic boundary conditions. To construct the ABC we employ the Lindblad master equation [62,63]:

$$\frac{d}{dt}\hat{\boldsymbol{\rho}}(t) = -i\left[\hat{H}, \hat{\boldsymbol{\rho}}(t)\right] + \sum_{\mu}\left(2\hat{L}_{\mu}\hat{\boldsymbol{\rho}}(t)\hat{L}_{\mu}^{\dagger}\right) - \left\{\hat{L}_{\mu}^{\dagger}\hat{L}_{\mu}, \hat{\boldsymbol{\rho}}(t)\right\}, \qquad (3.41)$$

where $\hat{\boldsymbol{\rho}}(t)$ is the full density operator and the $\hat{L}_{\mu}$ are non-Hermitian and typically local operators, which we will use to construct the absorbing boundaries. The reason we use the Lindblad master equation is that it is the most general form of a master equation, which still ensures that the density operator stays a density operator during time propagation [62,64]. Therefore, we do not have to worry about unphysical effects like negative probabilities in the density operator. This is discussed further in the discussion of [I] in Chapter 4.

The detailed derivation of the exact form of the ABC is shown in [I] and ultimately results in the following equation of motion for the one-particle reduced density matrix:

$$\frac{d}{dt}\boldsymbol{\rho}(t) = -i\left[\boldsymbol{T}_{\text{eff}}(t), \boldsymbol{\rho}(t)\right] - \left\{\boldsymbol{\gamma}, \boldsymbol{\rho}(t) - \boldsymbol{\rho}_0\right\}. \qquad (3.42)$$

There $\boldsymbol{\rho}_0$ is the ground state one-particle reduced density matrix and $\boldsymbol{\gamma}$ is a real diagonal matrix, which defines which sites couple to the bath and how strong this coupling is. As only the few outer most sites couple to the bath, most entries of $\boldsymbol{\gamma}$ are zero and only the first and last (≈ 10) diagonal entries corresponding to these outer most sites are not.

The first term in Eq. (3.42) $-i\left[\boldsymbol{T}_{\text{eff}}(t), \boldsymbol{\rho}(t)\right]$ is just a von Neumann term and is the

same as in Sec. 3.3 and therefore does not lead to a different dynamics. The second term $-\{\boldsymbol{\gamma}, \boldsymbol{\rho}(t) - \boldsymbol{\rho}_0\}$, on the other hand, is new and leads to a non-unitary time propagation. It leads to a damping of the one-particle reduced density matrix to its ground state value $\boldsymbol{\rho}_0$ as the term vanishes there. However, this damping is only happening on the sites at the system's boundaries specified by $\boldsymbol{\gamma}$. Hence, the advantage of Eq. (3.42) is that it induces no dynamics on itself in the beginning of the time propagation, as the elements of $\boldsymbol{\rho}(t = 0)$ and $\boldsymbol{\rho}_0$ corresponding to the boundary sites are approximately the same. Therefore, at $t = 0$ we have $\{\boldsymbol{\gamma}, \boldsymbol{\rho}(t) - \boldsymbol{\rho}_0\} \approx 0$. The result of this is that the bath only initiates the damping process when the first excitations reach the edge of the system. This was a major problem in the first iterations of the ABC, where the bath itself initiated a dynamics at $t = 0$, which is also shown in [I]. Comparing the impurity spin dynamics of a comparatively small system ($L \approx 70$) with ABC to the dynamics of a much larger system ($L \approx 1000$) without ABC shows the effectiveness of the ABC as the impurity spin dynamics looks exactly the same except that there are no finite-size effects disturbing the dynamics for ABC, see Fig. I-6. Due to the much smaller needed system sizes the calculations for ABC only take a fraction of the time and it enables us to calculate long-time dynamics for times $t > 10^4 \frac{1}{T}$.

3.6 – Generalized Gibbs Ensemble and (Non-)Thermalization After a Quantum Quench

One generic problem in theoretical condensed matter physics is: Given a physical system, e.g., some lattice model, how does the dynamics of the system looks like after it is excited out of its ground state. For a macroscopically large system the first expectation would probably be that the system approaches its thermal ground state after some time when all the excitations are fully dissipated (equally) throughout the whole system. Such cases where the system fully relaxes in its thermal equilibrium ground state we call thermalization of the system. Typically, we expect a generic system to thermalize. However, sometimes we find exceptional cases where the system is trapped in a metastable state and only approaches its ground state, if at all, on time scales much larger than the typical intrinsic time scale of the system.

Understanding the (non-)thermalization of generic macroscopically large system was and still is of high interest in research. For example, for quantum systems after a quantum quench, integrability, closeness to integrability, disorder, and interactions are well-known sources for the violation of ergodicity [37, 38, 65–81]. Theories like the eigenstate thermalization hypothesis try to predict when exactly thermalization happens in a system. In classical Hamiltonian dynamics, on the other hand, it is known that the ergodicity of the system is broken for integrable systems or for non-integrable systems close to integrability, as predicted by the KAM theorem [29–31].

Additionally, systems with glassy dynamics are known for violating ergodicity [82,83]. In the following, we will take a closer look at the quantum mechanical case.

Normally, the dynamics of a system can move freely on the given microcanonical energy shell, which leads to the "ergodic exploration" of this very same shell. However, when there are many constants of motion, the free movement on the microcanonical energy shell becomes restricted, which ultimately leads to a break down of ergodicity and thermalization. Most of the time the system then tries to maximize its entropy with respect to the restrictions of the different constants of motion leading to the so-called "generalized thermalization" of the system [84], which is described by the general Gibbs ensemble (GGE) [37, 38, 76, 85].

Suppose some quantum mechanical system with Hamiltonian $\hat{H}_0$ is in its ground state $|\Psi_0\rangle$. We then perform a quantum quench of some parameters of the Hamiltonian $\hat{H}_0 \to \hat{H}$ leading to the now quenched Hamiltonian $\hat{H}$. While the system is still in the same state $|\Psi_0\rangle$ this state is generally no longer a ground state or even an eigenstate of the quenched Hamiltonian $\hat{H}$. Additionally, the time evolution of $|\Psi_0\rangle$ is now also governed by the quenched Hamiltonian $\hat{H}$. For an arbitrary observable $\hat{O}$ the time evolution of its expectation value is consequently given by

$$O(t) := \langle \hat{O}(t) \rangle = \langle \Psi_0| \exp(i\hat{H}t)\hat{O} \exp(-i\hat{H}t)|\Psi_0\rangle \ . \tag{3.43}$$

In the following, we are interested in the fluctuations of these quantum averages as they can give us insight into the thermalization of the system. Non-vanishing fluctuations hint to non-thermalized states as it means there is some kind of dynamics left. For the analysis of these fluctuations we are going to follow [84] for the rest of this section. We can split the quantum average into two parts

$$O(t) = \overline{O} + \delta O(t). \tag{3.44}$$

The first term $\overline{O}$ is constant in time and is given by the long-time average of the observable,

$$\overline{O} = \lim_{t \to \infty} \frac{1}{t} \int_0^t d\tau O(\tau) \ , \tag{3.45}$$

The second term $\delta O(t)$ is time-dependent and has a vanishing long-time average. Therefore, we call it the fluctuating part. This fluctuating part can be quite arbitrary and chaotic and can, therefore, be hard to analyze. It makes it easier for the analysis to consider the long-time average of the absolute square of the fluctuating part

$$\delta_O^2 := \lim_{t \to \infty} \frac{1}{t} \int_0^t d\tau |\delta O(t)|^2 \qquad (3.46)$$

as a measure for the strength of the temporal fluctuations. If $\delta_O^2 \to 0$ we will also have vanishing fluctuations in the long-time limit $\lim_{t \to \infty} |\delta O(t)| = 0$, and consequently the expectation value of the observable would relax to a final value of $\lim_{t \to \infty} O(t) = \overline{O}$. On the other hand, if $\delta_O^2 \nrightarrow 0$ the fluctuations do not vanish over time and the limit $\lim_{\to \infty} O(t)$ is not defined. In particular, this means that the whole system itself did not thermalize fully and is rather stuck in a metastable state or even a completely non-stable state with ongoing dynamics left. Therefore, one can predict whether a system thermalizes by investigating if the strength of the fluctuating parts δ_O^2 vanishes in the long-limit $t \to \infty$.

Returning to the actual problem of the thermalization after a quantum-quench, we consider a non-interacting system of electrons, e.g., the stub impurity model in [III], where we perform a quantum-quench at $t = 0$ by switching on the coupling between the impurities and the host system. For arbitrary one-particle observables the strength of the fluctuations can be easily calculated following [84]. For example, for an element of the one-particle reduces density matrix $O(t) = \rho_{IJ}(t)$ they are given by

$$\delta_{\rho_{IJ}}^2 = \sum_{\mu\nu}^{\mu \neq \nu} |U_{I_\mu}|^2 |U_{J_\nu}|^2 |\rho_{\mu\nu}(t = 0)|^2 \ , \qquad (3.47)$$

where $U_{I\mu}$ is the I-th component of the μ-th eigenvector of the total post-quench hopping matrix and where

$$\rho_{\mu\nu}(t = 0) = (\boldsymbol{U}^\dagger \boldsymbol{\rho}(t = 0) \boldsymbol{U})_{\mu\nu} \qquad (3.48)$$

represents an element of the one-particle reduced density matrix at $t = 0$ in the basis of eigenstates of the total post-quench hopping matrix. Note that Eq. (3.47) assumes no degeneracies and no gap degeneracies in the spectrum of the one-particle eigenenergies ε_μ. A system is gap degenerate when $\varepsilon_\mu - \varepsilon_\nu = \varepsilon_{\mu'} - \varepsilon_{\nu'}$ for $\mu \neq \mu'$ or $\nu \neq \nu'$. More details and how Eq. (3.47) would look like for a system with gap degeneracies can be found in [III].

We can see that the strength of the fluctuating part depends on two different things. Firstly, it depends on the general structure of the whole system, namely on the exact form of the eigenvectors of the full hopping matrix. Secondly, it directly depends on the initial state of the system. In general we choose the initial state of the system as

the ground state of the pre-quench Hamiltonian at a given particle number. However, after the quench this state can look like anything depending on the exact nature of the quench.

Having said this, a generic (one-dimensional) one-particle state is typically extended throughout the whole system with an increasing number of nodes for increasing energies. As the weight of these eigenstates is approximately equally distributed over all sites, its weight at a specific site has to be proportional to $\frac{1}{\sqrt{L}}$. On the other hand, localized eigenstates have significant weight ($\approx \mathcal{O}(10^{-1})$) at some single sites.

Looking at Eq. (3.47), it is easy to see that $U_{I\mu} \propto \frac{1}{\sqrt{L}}$ would only lead to vanishing contributions to the sum in the $L \to \infty$ limit and consequently would result in vanishing fluctuations $\delta^2_{\rho_{IJ}}$ as well[1]. Contrary, a single localized eigenstate with a finite $U_{I\mu}$ independent of L can lead to a non-vanishing contribution in Eq. (3.47) and therefore, to a non-vanishing $\delta^2_{\rho_{IJ}}$. Of course, due to symmetry, it can happen that the contributions from localized eigenstates to Eq. (3.47) cancel each other out, but this is a problem depending on the specific system considered and in general we can conclude that localized eigenstates in the post-quench Hamiltonian lead to non-vanishing fluctuating parts and, therefore, prohibit the relaxation of the system.

3.7 – Classical Heisenberg Impurity Model

In chapter 6 we will compare different kind of impurity models. One of which is the classical Heisenberg model with classical spin impurities. As opposed to the models prior, this model is purely classical.

We replace all electron sites in the host system with classical spins $\boldsymbol{s}_i$ of length $s = |\boldsymbol{s}_i| = \frac{1}{2}$ and replace the hopping of the electrons with an antiferromagnetic exchange interaction J. We still have the classical impurity spins $\boldsymbol{S}_m$ (for us: $m \in \{1,2\}$) of length $S = |\boldsymbol{S}_m| = \frac{1}{2}$, which are coupled to the host spins $\boldsymbol{s}_{i_m}$ respectively with an antiferromagnetic exchange interaction K. Typically, the host-impurity interaction K is much weaker than the inter host interaction J: $K \ll J$.

The Hamiltonian for this classical model reads

$$H = J \sum_{i=1}^{L-1} \boldsymbol{s}_i \boldsymbol{s}_{i+1} + K \sum_{m=1}^{2} \boldsymbol{S}_m \boldsymbol{s}_{i_m} \ . \tag{3.49}$$

The equations of motion are easily derived by using the spin Poisson bracket [59,60] and are of the same Landau-Lifshitz [15] form as the equations of motion for the impurities,

---

[1]Note, when $U_{I\mu} \propto \frac{1}{\sqrt{L}}$, we can approximate Eq. (3.47) with $\delta^2_{\rho_{IJ}} \approx \frac{1}{L^2} \sum_{\mu\nu}^{\mu\neq\nu} |\rho_{\mu\nu}(t=0)|^2$. However, this can be easily estimated by $\delta^2_{\rho_{IJ}} \leq \frac{1}{L^2} \sum_{\mu\nu} |\rho_{\mu\nu}(t=0)|^2 = \frac{N_{\text{tot}}}{L^2} \overset{L\to\infty}{\to} 0$, where N_{tot} is the total number of electrons in the system.

Eq. (3.22), of the quantum-classical model discussed in section 3.3. For the impurities we have

$$\frac{d}{dt}\boldsymbol{S}_m(t) = K\boldsymbol{s}_{i_m}(t) \times \boldsymbol{S}_m(t) \tag{3.50}$$

and for the host spins

$$\frac{d}{dt}\boldsymbol{s}_i(t) = J\left(\boldsymbol{s}_{i-1} + \boldsymbol{s}_{i+1}\right) \times \boldsymbol{s}_i(t) + K\sum_m \left(\delta_{ii_m}\boldsymbol{S}(t) \times \boldsymbol{s}_i(t)\right) , \tag{3.51}$$

where $\boldsymbol{s}_i := 0$ for $i \notin \{1, 2, ..., L\}$. One can easily see that the length of each individual spin is conserved, which constrains the configuration space of the spin dynamics to a manifold given by a $L+2$-fold direct product $\mathcal{S} \equiv S^2 \times S^2 \times ...$ of 2-spheres with radius $\frac{1}{2}$. This makes the system different from the quantum-classical model in Sec. 3.3 as there the local magnetic moments have a variable length with a maximum of length $\frac{1}{2}$. Here, the length of the spins is constant. The ground state of the classical Heisenberg model depends on the exchange interactions J and K. For $J, K > 0$ the ground state is an antiferromagnetic Néel state and for $J, K < 0$ it is a ferromagnet. Due to the rotational symmetry of the system the ground state is also SO(3) degenerate. This distinguishes the classical Heisenberg model from the quantum mechanical model as the ground state of the quantum mechanical antiferromagnetic Heisenberg model is a spin singlet.

There are much fewer degrees of freedom in the classical system than in the quantum-classical model, so we do not need to use tricks like the absorbing boundary conditions from [I] to calculate the complete relaxation dynamics. We can just compute the dynamics for large enough system sizes, such that finite-size effects would only appear after the relaxation dynamics is finished. As the possible configuration space only scales linearly with the number of spins the numerical calculations are not very demanding, which makes increasing the system size feasible.

4 – Accessing Long Timescales in the Relaxation Dynamics of Spins Coupled to a Conduction-Electron System Using Absorbing Boundary Conditions

In this paper, we derive the so-called absorbing boundary conditions (ABC). Shortly summarized, we attach an absorbing bath to the boundaries of a system of non-interacting itinerant electrons, which absorbs outgoing excitations. This suppresses finite-size effects and enables us to simulate the existence of a much larger system without actually having to calculate the full dynamics of such a system.

We derive the absorbing boundary conditions from the Lindblad master equation [62, 63], which, as shown prior in Eq. (3.42), results in an additional term in the equations of motion for the one-particle reduced density matrix of the electron system:

$$\frac{d}{dt}\boldsymbol{\rho}(t) = -i\left[\boldsymbol{T}_{\text{eff}}(t), \boldsymbol{\rho}(t)\right] - \left\{\boldsymbol{\gamma}, \boldsymbol{\rho}(t) - \boldsymbol{\rho}_0\right\} \ , \tag{4.1}$$

where $\boldsymbol{\gamma}$ describes the damping at the boundaries and $\boldsymbol{\rho}_0$ is the ground state one-particle reduced density matrix of the electron system. The additional term $\left\{\boldsymbol{\gamma}, \boldsymbol{\rho}(t) - \boldsymbol{\rho}_0\right\}$ effectively damps the system, described by $\boldsymbol{\rho}(t)$, to $\boldsymbol{\rho}_0$, as the term vanishes for $\boldsymbol{\rho}(t) = \boldsymbol{\rho}_0$.

The exact derivation and discussion can be found in [I]. As we focused on the derivation of the absorbing boundary conditions in the paper and did not really investigate physical phenomena, it does not feature "physical results" per se to discuss. Therefore, in this section we want to discuss some points not covered in [I], and look at a similar work combining spin dynamics with the Lindblad master equation.

Let us consider a physical system built up by two parts. Firstly, a spatially finite central region, where most of the interactions happen, and secondly, a spatially asymptotic outer region, in which just the unbound part of the system travels outwards. When calculating the dynamics of such a system most of the computational capacity is "wasted" on the "uninteresting" outer part of the system. It therefore makes sense to want to cut off this outer part somehow, such that we can focus on the central part. However, doing this recklessly leads to problems in form of finite-size effects like reflections at

the boundaries of the inner part. In order to minimize these unphysical effects, one can impose absorbing boundary conditions, whose task is to absorb the excitations going outwards with the aim to minimize the reflections at the boundaries. One of the more common and simpler ways to impose such absorbing boundary conditions is to add a so-called complex absorbing potential (CAP) to the system and its Hamiltonian [86, 87]. For example, this is common practice in atomic physics [88, 89] or within molecular dynamics [90–92]. The CAP Hamiltonian gains an additional anti-Hermitian term

$$\hat{H}_{\mathrm{CAP}} := \hat{H} - i\hat{\Gamma} \ , \tag{4.2}$$

with Hermitian $\hat{H}$ and $\hat{\Gamma}$ and positive semi definite $\hat{\Gamma}$. The time evolution of the density operator is governed by the von Neumann equation

$$i\frac{d}{dt}\hat{\boldsymbol{\rho}}(t) = [\hat{H}, \hat{\boldsymbol{\rho}}(t)] - i\{\hat{\Gamma}, \hat{\boldsymbol{\rho}}(t)\} \ , \tag{4.3}$$

which features an additional anti-commutator term. This term makes the time evolution non-unitary. So the trace of the density operator is not necessarily conserved and probability can be lost. This ansatz can work quite well, depending on the exact choice of $\hat{\Gamma}$, for reducing the complexity of the system. However, there is a problem with this ansatz when considering multiple particles [87]. The wavefunction of a multi-particle system describes the probability to find each particle at some place inside the system. Due to the non-Hermitian CAP it can happen that a particle leaves the system. When that is the case the original N-particle wavefunction does not go to an $(N-1)$-particle wavefunction, instead it goes to zero. It also turns out that it is not possible to construct a formalism, in which every time a particle leaves the N-particle system a new $(N-1)$-particle wavefunction is created, as the process of losing a particle is irreversible and information is irretrievably lost [87].

Hence, instead of such a pure state approach, it might be better to start from a Markovian master equation [87]. One example for that is the Lindblad master equation, which we also used in our work [I]. The Lindblad master equation Eq. (3.41) looks very similar to the CAP-von Neumann equation Eq. (4.3), however, the non-unitary part is chosen slightly differently. Additionally, the Lindblad master equation ensures that the density operator stays a density operator over time. This means the density operator is positive semi-definite at all times and its trace is conserved. In fact, it can be proven that the Lindblad master equation is the most general form of a Markovian master equation, which ensures positivity and conservation of the trace of the density operator [62, 64] and every Markovian master equation with theses properties can be written in the form of the Lindblad master equation. All of that makes the Lindblad

master equation a good starting point for the investigation of non-unitary dynamics of different systems.

For example, recently the Lindblad formalism was used to analyze the relaxation dynamics of spin systems [93]. There, the well known LLG equation governing the effective spin dynamics of such a system was derived from a Lindblad master equation approach. The theory uses quantum spins and is spin-only. Hence, there is no electron host system as in our approach. By just assuming a minimal relaxation channel, where the Lindblad operators are given by the raising operators of the spins $\hat{L} = \hat{S}^+$, it is possible to derive an effective equation of motion. Using a standard mean-field approach, this equation of motion can then be simplified to the LLG equation in the weak-field limit. This shows on one hand that the Lindblad master equation is a suitable tool for analyzing spin dynamics and can be used on different ways, and on the other hand, it shows that the dynamics of the phenomenological LLG equation can be rooted in a more fundamental approach.

However, while this treatment of the spin relaxation dynamics via the Lindblad master equation is instructive, it is also restricted to macrospins only as no host system or similar is considered. Therefore, there is a difference between this approach and our treatment, where we consider additional degrees of freedom in form of the host system. While our treatment is more complicated, it is able to capture more intricate effects caused by the host system, for example the relaxation dynamics of a spin coupled to a topological insulator in the next chapter.

Accessing long timescales in the relaxation dynamics of spins coupled to a conduction-electron system using absorbing boundary conditions

Michael Elbracht[1] and Michael Potthoff ●[1,2]

[1]*I. Institute of Theoretical Physics, Department of Physics, University of Hamburg, Jungiusstraße 9, 20355 Hamburg, Germany*
[2]*The Hamburg Centre for Ultrafast Imaging, Luruper Chaussee 149, 22761 Hamburg, Germany*

The relaxation time of a classical spin interacting with a large conduction-electron system is computed for a weak magnetic field, which initially drives the spin out of equilibrium. We trace the spin and the conduction-electron dynamics on a timescale which exceeds the characteristic electronic scale that is set by the inverse nearest-neighbor hopping by more than five orders of magnitude. This is achieved with a construction of absorbing boundary conditions, which employs a generalized Lindblad master-equation approach to couple the edge sites of the conduction-electron tight-binding model to an external bath. The failure of the standard Lindblad approach to absorbing boundaries is traced back to artificial excitations initially generated due to the coupling to the bath. This can be cured by introducing Lindblad parameter matrices and by fixing those matrices to perfectly suppress initial-state artifacts as well as reflections of physical excitations propagating to the system boundaries. Numerical results are presented and discussed for generic one-dimensional models of the electronic structure.

I. INTRODUCTION

The relaxation of a nonequilibrium state of a single or several local magnetic moments is one of the central issues in various atomistic spin-dynamics theories [1–5]. In many cases the local moments are treated as classical spins and the relaxation process is covered by an atomistic version of the Landau-Lifshitz-Gilbert (LLG) equation [6]. Such effective spin-only theories are extremely effective and have proven to be very successful.

In many cases, however, an explicit treatment of the coupling of the spins to the conduction-electron system is necessary and can be described, e.g., with *s-d*-type models [7]. Those approaches comprise the effective spin-only theories and can rederive the LLG equation and the Gilbert-damping parameter using, e.g., perturbative techniques [8–11], or perturbative or other downfolding approaches within a first-principles framework [12–16].

An explicit and nonperturbative treatment of the full problem of coupled spin and electron dynamics on equal footing becomes necessary, if the exchange interaction J between the spin and the conduction-electron system is strong, if the spins are driven fast compared to typical electronic timescales, or, generally speaking, if the coupled dynamics of spin and electron degrees of freedom is intricate and cannot be separated easily. Examples comprise one-dimensional systems, where the perturbative derivation of Gilbert damping breaks down [17], or spin prerelaxation effects due to electronic correlations [18], or the feedback of local topological properties of the fast electron system to the slow spin dynamics [19–21]. Certainly, another general motivation to address the full problem is the discovery of new physical phenomena.

With the present paper we would like to focus on the technical aspects and the numerical feasibility of a full, combined treatment of spin and electron degrees of freedom for a particular class of problems, as sketched in Fig. 1. We consider a single classical spin (or a few spins) coupled to a finite but large system of noninteracting electrons described by a tight-binding model with nearest-neighbor (NN) hopping on a lattice of L sites. A one-dimensional geometry is assumed for simplicity but the discussion will be general. The coupling is given by a local exchange interaction J at a site i_0 of the lattice, and the system is assumed to be instantaneously kicked out of its ground state by some strong but local perturbation at the same site. There is a closed system of equations of motion [17] determining the real-time dynamics such that, in principle, this type of problem can be solved (numerically) exactly. One expects that locally the system decays to its ground state, i.e., that all local observables in the vicinity of i_0 converge to their ground-state values as time $t \mapsto \infty$. For a single classical spin, the timescale required for the completion of this process defines the spin-relaxation time τ. Our goal is the numerically exact computation of τ and of other local observables in the interaction region close to i_0 by solving the equations of motion for coupled spin and electron dynamics explicitly.

While this type of calculation provides the maximum information on the system, it runs into computational troubles, when the relevant timescale, e.g., the spin-relaxation time, becomes large compared to L/v, where v is the characteristic velocity, at which energy- and spin-carrying excitations propagate through the electron system. Namely, since energy and spin are conserved quantities, the excitation energy and the excess spin must be completely transported away from
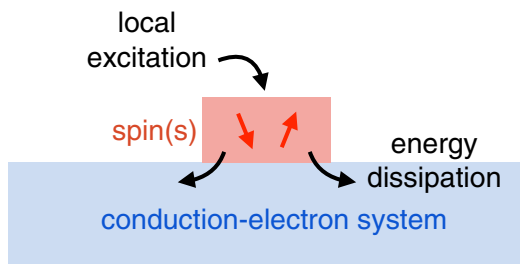
FIG. 1. Relaxation of a single spin or a few spins interacting with a large conduction-electron system after an initial local excitation. In the long-time limit, the spin-electron system is expected to reach its ground state locally, i.e., in the vicinity of the impurity spin(s), since the excitation energy is completely dissipated to the bulk.

i_0 during the relaxation process and must be fully dissipated into the macroscopically large electron system. Thus, the dissipation rate sets a bound on τ. As the computational effort scales about cubic with the system size L, long-time relaxation processes cannot be treated exactly.

Calculations are spoiled by unwanted reflections of excitations, which backpropagate and interfere with the system dynamics in the interaction region. This type of problem is well known in atomic, molecular, and optical physics, where an unbound quantum system under study is conceptually decomposed into an interaction region of finite spatial extent and an asymptotic region where the (single-particle) wave function has some asymptotic form, and where it is desirable to focus on the dynamics in the interaction region only. This can be achieved by imposing absorbing boundary conditions (absorbing BCs), which minimize reflections from the edge of the core physical system represented on a numerical grid [22]. In most cases, one uses a complex absorbing potential (CAP) as an additional non-Hermitian term in the Hamiltonian, which is optimized with respect to its reflection properties [23]. In the context of wave equations this is also known as perfectly matched layers [24]. Such techniques are widely used but become problematic for systems with more than a single quantum particle [25] since, if particles are lost, the Schrödinger equation with a CAP is not able to consistently describe the remainder of the system.

A consistent formalism can be based on Markovian quantum master equations of the Lindblad type [26,27], which focus on the many-body statistical operator $\hat{\rho}(t)$ rather than on the single-particle wave function of the quantum system and which preserve the trace, Hermiticity, and positivity of $\hat{\rho}(t)$ and thus respect the usual probability interpretation. In derivations of the Lindblad equation a couple of approximations must be made, such as assuming a weak system-bath interaction or the Born-Markov approximation (see, e.g., Refs. [28–30]).

Hence, we will merely use the master-equation approach to construct absorbing BCs, i.e., the different approximations are controlled by choosing a setup where the central region of interest, which is initially excited by a local perturbation, is surrounded by a sufficiently large core region and finally by a boundary region where local Lindblad operators couple to the bath degrees of freedom and which must be large enough

to fully absorb excitations emitted from the central part. If perfectly absorbing BCs can be constructed, one may in fact obtain the exact relaxation dynamics in the central part.

A similar idea has been applied recently [31] to compute the steady-state properties of strongly correlated electron systems out of equilibrium. The required numerical solution of the Lindblad equation for interacting impurity systems can be carried out, e.g., with an exact-diagonalization approach in the superfermion representation of the Lindbladian [32]. This requires auxiliary degrees of freedom and thus enlarges the Hilbert space, which, due to the two-body (Coulomb) interaction terms, is large anyway, such that the numerical implementation of Lindblad-type absorbing BCs can become quite demanding in practice. For one-dimensional and impurity systems, density-matrix renormalization-group techniques are very powerful [33–35].

Actually, the Lindblad approach to absorbing BCs appears to be perfectly suited for impurity models, where classical degrees of freedom are coupled to an *uncorrelated* electron system. With the present study we focus on a system consisting of a single classical spin coupled to noninteracting conduction electrons with the goal to further develop the idea of absorbing BCs. We will demonstrate that the Lindblad approach can straightforwardly be adapted to the noninteracting case. Surprisingly, however, we find that the resulting absorbing BCs are not useful as demonstrated by comparing with results for open BCs obtained for short propagation times. While the coupling to the bath is found to almost perfectly suppress the unwanted reflections from the system boundaries, standard choices for the Lindblad parameters also *induce* unwanted artifacts, namely excitations *generated* initially at the boundaries, which are then propagating towards the core system and interfering with the physical dynamics. We therefore suggest to extend the Lindblad theory by considering Lindblad parameter *matrices* and by fixing those parameters such that a perfect suppression of the mentioned artificial initial excitations is achieved. This requires one to adapt the parameters to the system's initial state. It is demonstrated that this approach leads to convincing results.

The paper is organized as follows: Section II introduces the model and the fundamental equations of motion. Section III discusses the standard Lindblad approach to absorbing BCs and demonstrates its limitations. These are overcome with the BCs introduced in Sec. IV. In Sec. V we discuss results demonstrating the progress made, and the conclusions are given in Sec. VI.

II. MODEL AND EQUATIONS OF MOTION

The generic model to discuss spin-relaxation dynamics is the s-d exchange model [7] where the spin $\boldsymbol{S} = (S_x, S_y, S_z) = \boldsymbol{S}(t)$ is treated as a classical dynamical variable, i.e., as a classical vector of fixed length $S = \frac{1}{2}$. The spin is coupled to a system of noninteracting conduction electrons via a local antiferromagnetic exchange interaction. The electron system serves as a large reservoir for the dissipation of energy and spin. It is specified by the hopping T_{ij} between the sites $i, j = 1, \ldots, L$ of a chain consisting of L sites. Throughout the study we consider hopping $T_{ij} = -T$ with $T > 0$ between nearest neighbors i and j only. We assume half filling with
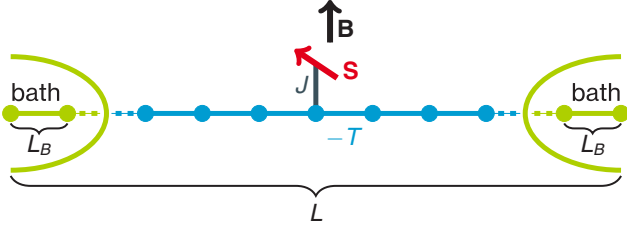
FIG. 2. Sketch of the system geometry: A classical spin S of length $|S| = \frac{1}{2}$ is coupled via a local antiferromagnetic exchange interaction J to a noninteracting system of electrons on a chain of L sites. The hopping between nearest-neighboring sites is $-T$. L_B sites on the left and L_B sites on the right edge are coupled to a bath. The spin is located at the chain center and subjected to a local magnetic field B. Suddenly flipping the field direction induces the real-time dynamics.

$N = L$ electrons in an isolated system with open boundary conditions (open BCs). Half filling is also maintained when introducing a coupling of the sites close to the chain edges to an external bath in Sec. III. Figure 2 provides a sketch of the system. The corresponding Hamiltonian (with open BCs) reads

$$H = \sum_{ij\sigma} T_{ij} c_{i\sigma}^\dagger c_{j\sigma} + J S s_{i_0} - S B. \tag{1}$$

Here, $c_{j\sigma}$ annihilates an electron at site j with spin projection $\sigma = \uparrow, \downarrow$. The classical spin couples locally with strength $J > 0$ to the local spin of the electron system, $s_{i_0} = \frac{1}{2} \sum_{\sigma\sigma'} c_{i_0\sigma}^\dagger \tau_{\sigma\sigma'} c_{i_0\sigma'}$, at site i_0 of the chain, where $\tau = (\tau_x, \tau_y, \tau_z)$ is a vector whose components are the Pauli spin matrices. Furthermore, the model includes an external local magnetic field B, which can be used to drive the classical spin. Note that this does not couple to the electronic degrees for freedom. The energy scale and (with $\hbar \equiv 1$) the timescale is set by choosing $T = 1$.

Since the electron system is noninteracting, Wick's theorem applies, and all correlation functions factorize into one-particle correlations. A closed system of equations of motion,

$$\frac{d}{dt} S(t) = J \langle s_{i_0} \rangle_t \times S(t) - B \times S(t) \tag{2}$$

and

$$i \frac{d}{dt} \rho(t) = [T_{\text{eff}}(t), \rho(t)], \tag{3}$$

can be obtained for the classical spin $S = S(t)$ and for the one-particle reduced density matrix $\rho = \rho(t)$ with elements

$$\rho_{i\sigma i'\sigma'}(t) = \langle \Psi(t)|c_{i'\sigma'}^\dagger c_{i\sigma}|\Psi(t)\rangle, \tag{4}$$

where $|\Psi(t)\rangle$ is the many-body quantum state of the electron system, where $\langle s_{i_0} \rangle_t = \langle \Psi(t)|s_{i_0}|\Psi(t)\rangle = \frac{1}{2} \sum_{\sigma\sigma'} \tau_{\sigma\sigma'} \rho_{i_0\sigma' i_0\sigma}$, and where the effective hopping matrix T_{eff} in Eq. (3) is given by the elements

$$T_{i\sigma i'\sigma'}^{(\text{eff})}(t) = T_{ii'} \delta_{\sigma\sigma'} + \delta_{ii'} \frac{J}{2} S(t) \tau_{\sigma\sigma'} \tag{5}$$

(see Refs. [17,36] for a derivation and further details).

Suppose that initially the system is in its ground state for a given external field direction B_0. The formal purpose of the field is twofold: First, it breaks the SO(3) degeneracy of the ground state. Second, it will be employed to initiate the real-time dynamics at time $t = 0$, namely by suddenly switching the field direction: $B_0 \to B$. This sudden switch causes a local excitation of the system in the vicinity of site i_0. In the course of time, the system is expected to relax such that the ground state will be restored locally. This requires that conserved quantities, i.e., energy and spin, must be transported away from i_0 and is in fact seen in the numerical solution of the equations of motion (2) and (3): Excitations are emitted from i_0 and propagate ballistically at a velocity $v = \mathcal{O}(T)$ set by the nearest-neighbor hopping. Assuming that the spin couples to the middle of the chain, i.e.,

$$i_0 = (L+1)/2, \tag{6}$$

for odd L, this implies that after a time $\sim L/v$, the emitted excitations have reached the system boundaries, have been reflected, and, after backpropagation, interfere with the local dynamics in the vicinity of site i_0.

To avoid this unwanted finite-size effect in a practical calculation, a sufficiently large system is required. If one is interested in tracing the time evolution of the spin from the instant of the initial excitation to the fully relaxed final state, a system size $L \sim v\tau = \mathcal{O}(T\tau)$ is required. Here, τ is the spin-relaxation time. For a metallic state with $v \approx 2T$ [17], complete spin relaxation could be observed in computations for chains as long as $L = \mathcal{O}(10^3)$ sites, but only at comparatively strong fields $B = \mathcal{O}(T)$. At weaker B or for insulating states, however, the spin-relaxation time is expected to be possibly several order of magnitudes longer. Since the computational effort for the numerical solution of the equations of motion scales as L^3 for large systems, such timescales $\gg 10^3/T$ cannot be reached in practice with the present theoretical setup.

III. CONSTRUCTION OF ABSORBING BOUNDARIES

A major goal of this paper is to construct system boundaries, which absorb the outgoing excitations emitted from the chain center. The boundaries shall prevent any reflections to avoid the unwanted interference with the time evolution of local observables close to the central site i_0, such that their real-time dynamics in a sufficiently large environment of i_0 is practically indistinguishable from the dynamics of an infinite system ($L \to \infty$). To this end we couple the outermost L_B sites on the left and on the right edge of the chain to a suitable bath, while the remaining $L - 2L_B$ sites are left untouched. Typically we take $L_B \ll L$. The model is displayed schematically in Fig. 2.

As a suitable framework for the construction of the absorbing boundaries, we consider the Lindblad master equation [26,27]

$$\frac{d}{dt} \hat{\rho}(t) = -i[H, \hat{\rho}(t)] + \sum_\mu (2 L_\mu \hat{\rho}(t) L_\mu^\dagger - \{L_\mu^\dagger L_\mu, \hat{\rho}(t)\}) \tag{7}$$

for the many-body statistical operator $\hat{\rho}(t)$. This appears as an attractive approach to construct absorbing boundaries as it preserves fundamental properties of the statistical operator, namely for all times t we have $\mathrm{tr}\,\hat{\rho}(t) = 1$, $\hat{\rho}(t)^\dagger = \hat{\rho}(t)$, and $\hat{\rho}(t) \geqslant 0$. In Eq. (7) the first term on the right-hand side is the von Neumann term describing the system's unperturbed dynamics while the second one models the coupling to an external bath via Lindblad operators L_μ. Here, $\{\cdot, \cdot\}$ stands for the anticommutator.

Typically, the Lindblad operators are non-Hermitian and local. Here, we choose $L_\mu = L_{i\sigma}^{(r)}$ with $r = 1, 2$ and furthermore

$$L_{i\sigma}^{(1)} = \sum_{i'\sigma'} \alpha_{i\sigma i'\sigma'}^{(1)} c_{i'\sigma'}, \quad L_{i\sigma}^{(2)} = \sum_{i'\sigma'} \alpha_{i\sigma i'\sigma'}^{(2)*} c_{i'\sigma'}^\dagger, \quad (8)$$

i.e., we consider arbitrary linear combinations of annihilators or creators, respectively. With this choice, one introduces a large number of unknown parameters to the theory, even if one takes into account that the sums over i' are restricted to those sites coupling to the bath. We will later see how these parameters are fixed in a satisfactory way. In standard calculations one typically employs r-independent and diagonal matrices $\alpha_{i\sigma i'\sigma'}^{(r)} \propto \delta_{ii'}\delta_{\sigma\sigma'}$ to keep the number of parameters at a reasonable level.

For the present case of a noninteracting electron system, the Lindblad equation (7) for the statistical operator $\hat{\rho}(t)$ can be strongly simplified and reformulated as a $2L \times 2L$ matrix equation for the one-particle reduced density matrix $\rho(t)$ [see Eq. (4)]. This is easily achieved by multiplying Eq. (7) with $c_{i'\sigma'}^\dagger c_{i\sigma}$ from the right, by taking the trace, and using that $\mathrm{tr}[\hat{\rho}(t)c_{i'\sigma'}^\dagger c_{i\sigma}] = \rho_{i\sigma i'\sigma'}(t)$. We first get

$$\frac{d}{dt}\rho_{i\sigma i'\sigma'}(t) = -i\,\mathrm{tr}([H, \hat{\rho}(t)]\,c_{i'\sigma'}^\dagger c_{i\sigma}) + \sum_{j\tau j'\tau' j''\tau''} \alpha_{j\tau j'\tau'}^{(1)}\,\mathrm{tr}\,(2c_{j'\tau'}\hat{\rho}(t)c_{j''\tau''}^\dagger c_{i'\sigma'}^\dagger c_{i\sigma} - \{c_{j''\tau''}^\dagger c_{j'\tau'}, \hat{\rho}(t)\}c_{i'\sigma'}^\dagger c_{i\sigma})\alpha_{j\tau j''\tau''}^{(1)*}$$

$$+ \sum_{j\tau j'\tau' j''\tau''} \alpha_{j\tau j'\tau'}^{(2)*}\,\mathrm{tr}\,(2c_{j'\tau'}^\dagger\hat{\rho}(t)c_{j''\tau''}c_{i'\sigma'}^\dagger c_{i\sigma} - \{c_{j''\tau''}c_{j'\tau'}^\dagger, \hat{\rho}(t)\}c_{i'\sigma'}^\dagger c_{i\sigma})\alpha_{j\tau j''\tau''}^{(2)}. \quad (9)$$

Exploiting the cyclic invariance of the trace and using $\mathrm{tr}[\hat{\rho}(t)O] = \langle O\rangle_t$ for an operator O, we find

$$\frac{d}{dt}\rho_{i\sigma i'\sigma'}(t) = -i\sum_{j\tau}\left(T_{i\sigma j\tau}^{(\mathrm{eff})}(t)\rho_{j\tau i'\sigma'}(t) - \rho_{i\sigma j\tau}(t)T_{j\tau i'\sigma'}^{(\mathrm{eff})}(t)\right)$$

$$+ \sum_{j\tau j'\tau' j''\tau''} \alpha_{j\tau j'\tau'}^{(1)}(2\langle c_{j''\tau''}^\dagger c_{i'\sigma'}^\dagger c_{i\sigma} c_{j'\tau'}\rangle - \langle c_{j''\tau''}^\dagger c_{j'\tau'} c_{i'\sigma'}^\dagger c_{i\sigma}\rangle - \langle c_{i'\sigma'}^\dagger c_{i\sigma} c_{j''\tau''}^\dagger c_{j'\tau'}\rangle)\alpha_{j\tau j''\tau''}^{(1)*}$$

$$+ \sum_{j\tau j'\tau' j''\tau''} \alpha_{j\tau j'\tau'}^{(2)*}(2\langle c_{j''\tau''} c_{i'\sigma'}^\dagger c_{i\sigma} c_{j'\tau'}^\dagger\rangle - \langle c_{j''\tau''} c_{j'\tau'}^\dagger c_{i'\sigma'}^\dagger c_{i\sigma}\rangle - \langle c_{i'\sigma'}^\dagger c_{i\sigma} c_{j''\tau''} c_{j'\tau'}^\dagger\rangle)\alpha_{j\tau j''\tau''}^{(2)}. \quad (10)$$

The first term on the right-hand side reproduces the equation of motion (3), while the remaining ones can be simplified using the standard Fermi anticommutator rules. This results in the following equation of motion,

$$\frac{d}{dt}\rho_{i\sigma i'\sigma'}(t) = -i\sum_{j\tau}\left(T_{i\sigma j\tau}^{(\mathrm{eff})}(t)\rho_{j\tau i'\sigma'}(t) - \rho_{i\sigma j\tau}(t)T_{j\tau i'\sigma'}^{(\mathrm{eff})}(t)\right) - \sum_{j\tau j'\tau'} \alpha_{j\tau i'\sigma'}^{(1)}\rho_{i\sigma j'\tau'}\alpha_{j\tau j'\tau'}^{(1)*} - \sum_{j\tau j'\tau'} \alpha_{j\tau j'\tau'}^{(1)}\rho_{j'\tau' i'\sigma'}\alpha_{j\tau i\sigma}^{(1)*}$$

$$- \sum_{j\tau j'\tau'} \alpha_{j\tau i\sigma}^{(2)*}\rho_{j'\tau' i'\sigma'}\alpha_{j\tau j'\tau'}^{(2)} - \sum_{j\tau j'\tau'} \alpha_{j\tau j'\tau'}^{(2)*}\rho_{i\sigma j'\tau'}\alpha_{j\tau i'\sigma'}^{(2)} + 2\sum_{j\tau} \alpha_{j\tau i\sigma}^{(2)*}\alpha_{j\tau i'\sigma'}^{(2)}, \quad (11)$$

which can be written in matrix form:

$$\frac{d}{dt}\rho(t) = -i[T_{\mathrm{eff}}(t), \rho(t)] - \rho(t)\alpha_1^\dagger\alpha_1 - \alpha_1^\dagger\alpha_1\rho(t) - \alpha_2^\dagger\alpha_2\rho(t) - \rho(t)\alpha_2^\dagger\alpha_2 + 2\alpha_2^\dagger\alpha_2. \quad (12)$$

We define the Hermitian and non-negative matrices

$$\gamma = \alpha_1^\dagger\alpha_1 + \alpha_2^\dagger\alpha_2, \quad \Gamma = \alpha_2^\dagger\alpha_2, \quad (13)$$

such that the equation reads as

$$\frac{d}{dt}\rho(t) = -i[T_{\mathrm{eff}}(t), \rho(t)] - \{\gamma, \rho(t)\} + 2\Gamma. \quad (14)$$

This replaces Eq. (3). Note that the effective hopping matrix depends on $S(t)$, and thus Eq. (14) must still be supplemented by the equation of motion (2) for the classical spin.

Equations (2) and (14) describe the relaxation of the system after an initial excitation of the localized spin. In the core system, i.e., for $L_B < i < L + 1 - L_B$, conservation laws hold locally. Hence, energy, spin, and particles are transported to the chain edges and dissipated to the external baths for finite Lindblad coupling parameters Γ, γ. The Lindblad parameters are taken to be nonzero at the boundaries only.

To test the quality of the absorbing boundaries implemented with the standard Lindblad equation and generic Lindblad parameters, we consider a manifestly particle-hole symmetric electron system at half filling, i.e., $\sum_\sigma \rho_{i\sigma i\sigma}(t) = 1$. For the sake of simplicity, we assume diagonal coefficient matrices α_r with real spin- and r-independent diagonal elements,

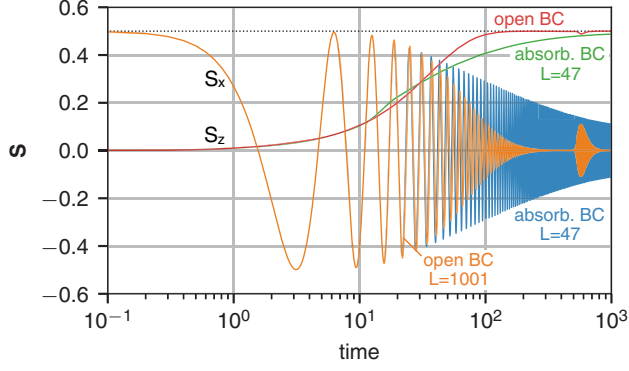$$\alpha_{i\sigma i'\sigma'}^{(r)} = \delta_{ii'}\delta_{\sigma\sigma'}\alpha_i. \quad (15)$$

FIG. 3. Time evolution of the z and the x component of the classical spin coupled to an electron system with NN hopping $-T$ at half filling after a sudden switch of the local magnetic field from the x to z direction (see text for details). Red/orange lines: Standard theory for a chain with open boundary conditions (open BCs) with $L = 1001$ sites ($i_0 = 501$, $J = 1$, $B = 1$). Green/blue lines: Calculation with absorbing boundaries (absorbing BCs) [Eqs. (2), (14), (15), and (17)] for $L = 47$ ($i_0 = 24$, $J = 1$, $B = 1$, $L_B = 5$, $\Gamma_{\min} = 0.2$). Energy and timescales set by $T = 1$, $\hbar = 1$.

This implies $\boldsymbol{\gamma} = 2\boldsymbol{\Gamma}$ and $\Gamma_{i\sigma i'\sigma'} = \delta_{ii'}\delta_{\sigma\sigma'}\Gamma_i$. With this standard choice, particle-number conservation is maintained as is easily verified by taking the trace of both sides of Eq. (14) and noting that $\langle N \rangle = \mathrm{tr}\,\boldsymbol{\rho}(t)$. We furthermore set the parameters either as constant,

$$\Gamma_i = \Gamma > 0, \tag{16}$$

for all sites coupling to the external bath, or choose them to increase linearly with increasing distance to the outermost sites of the core system,

$$\Gamma_i = \begin{cases} (L_B + 1 - i)\Gamma_{\min}, & i \leqslant L_B, \\ 0, & L_B < i < L + 1 - L_B, \\ [i - (L - L_B)]\Gamma_{\min}, & i \geqslant L + 1 - L_B, \end{cases} \tag{17}$$

with $\Gamma_{\min} > 0$, and use Γ or $\Gamma_{\min}$ to optimize the absorbing properties of the coupling to the bath.

To check the effect of absorbing boundaries, we compare numerical results obtained with the standard theory for a large system ($L = 1001$) and open BCs to results obtained with Eq. (14) for a much smaller system ($L = 47$) and absorbing BCs (see Fig. 3). For the integration of the equations of motion a high-order Runge-Kutta technique with variable step size is employed. We set $J = 1$ and $B = 1$, as we expect a comparatively short spin-relaxation time τ for this choice of model parameters. The local magnetic field is suddenly switched from the x to z direction to initiate the dynamics, i.e., we prepare the system in its ground state for $\boldsymbol{B}_0$ pointing in the x direction by diagonalization of the effective hopping matrix and by filling the effective one-particle eigenstates up to the Fermi level to reach half filling. For the subsequent dynamics starting at $t = 0$, the field $\boldsymbol{B}$ points into the z direction.

In the case of open BCs, the x component of the classical spin immediately starts to oscillate (see Fig. 3). Together with the y component (not displayed), this just reflects the Larmor precession of the spin around the field direction. The

precession frequency is $\omega \approx B$. Looking at the z component we see that the spin relaxes to the new field direction on a timescale of $t \approx 200$. Our physical expectation is that after reaching its new ground-state direction, the spin dynamics should basically stop. As can be seen in Fig. 3, however, there is an unphysical revival of the dynamics for $t \gtrsim 500$. Further revivals at still later times are expected as well. These are in fact caused by the effect of excitations reaching the site i_0 after back reflection from the system boundaries. The timescale for this unwanted artifact is approximately given by twice the distance of i_0 to the edges of the system size, $2 \times L/2 \approx 1000$, divided by the Fermi velocity $v_{\rm F} = 2$.

Let us now compare with the results obtained for the small system ($L = 47$) with absorbing BCs. We employ the model with linearly increasing coupling parameters, Eq. (17), starting with $\Gamma_{\min} = 0.2$ and use $L_B = 5$ absorbing sites on each edge, such that the core system has $L - 2L_B = 37$ sites. We find that, initially, up to about $t = 10$, the dynamics is reproduced more or less correctly. For $t < 10$, there are tiny deviations, which are most clearly seen in the z component of the spin. These could be attributed, e.g., to the coarser description of the initial Fermi-sea ground state. The main effect for $t \gtrsim 10$, however, appears to be again related to the presence of the boundaries as becomes obvious when comparing calculations for different system sizes L (not displayed). Compared to the results for open BCs, these deviations must obviously show up much earlier, at about $t = 23$, due to the much shorter distance to the edges ($L = 47$ vs $L = 1001$). We find, however, that they come even earlier by about a factor of 2.

At later times $t \gtrsim 100$, the predicted dynamics deviates strongly and full spin relaxation, if present at all, is massively delayed with $\tau \gg 1000$. We conclude that absorbing BCs, naively derived from the Lindblad approach with a standard parameter choice, lead to an unacceptable impact on the spin (and electron) dynamics. Note, however, that there are in fact no visible effects, which hint to *reflections* from the boundaries. Hence, the presently discussed absorbing BCs do absorb the outgoing excitations, but at the same time strongly disturb the time evolution. Let us point out that this does not depend very much on the parameter choice as has been checked by varying $\Gamma_{\min}$ and L_B. Also for spatially constant parameters [see Eq. (16)], the results do not improve or get worse significantly.

Our strategy in the following is to find the cause of the problem and to modify the absorbing boundary conditions accordingly. Figure 4 displays the initial one-particle reduced density matrix at time $t = 0$. The density matrix at time $t = 0$ is constructed as the ground-state density matrix for $\boldsymbol{B}_0 = \boldsymbol{e}_x$, i.e., for the classical spin pointing in the x direction. Since $J > 0$, the electron magnetic moment at i_0 is antiferromagnetically oriented. We see that $\rho_{i\sigma i\sigma} = 0.5$ for all sites, corresponding to half filling. Further, $\rho_{i\uparrow i\downarrow} = \rho_{i\downarrow i\uparrow}$ for an x-polarized state. The site off-diagonal elements $\rho_{i\sigma i'\sigma}$ with $i \neq i'$ show a damped oscillation with increasing distance $|i - i'|$. Close to i_0 and particularly close to the chain edges, there are some Friedel-like oscillations of the diagonal elements $\rho_{i\sigma i\sigma}$ as a function of i. The oscillations induced by the edges are strongly damped, such that the density-matrix elements close to the center are essentially unaffected.
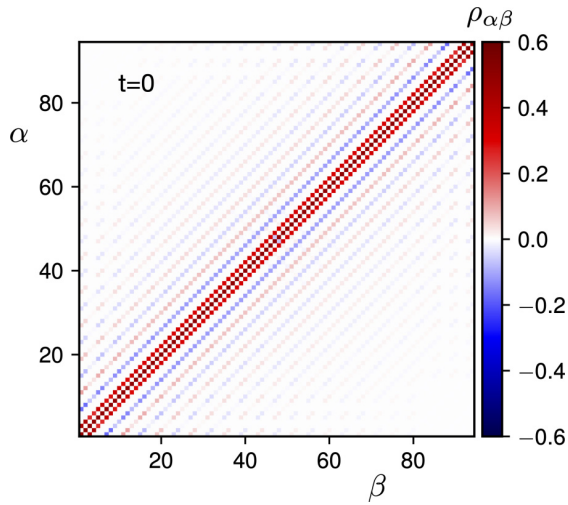
FIG. 4. Initial one-particle reduced density matrix at time $t = 0$ for a system with $L = 47$ sites, open BCs, and the impurity spin at the central site $i_0 = (L + 1)/2$ pointing in the x direction. The color coding is indicated by the bar on the right side. Exchange coupling $J = 1$. We display the elements $\rho_{\alpha\beta}$ of $\boldsymbol{\rho}$ using the combined site-spin ("orbital") index $\alpha \equiv 2i - \frac{1}{2}(1 + z_\sigma) = 1, \ldots, 2L$ with $z_\uparrow = +1, z_\downarrow = -1$.

Figure 5 shows the time evolution of the density-matrix elements for a system with $L = 47$ sites. As compared to the initial density matrix $\boldsymbol{\rho}(0)$ the time-dependent *deviations* of the matrix elements, $\boldsymbol{\rho}(t) - \boldsymbol{\rho}(0)$, are typically smaller by more than an order of magnitude (note the different scales encoded with the color plots in Figs. 4 and 5). Hence, only (the real part of) the difference is plotted. For open BCs (middle panel of Fig. 5) we see an overall oscillation of elements $\rho_{i\sigma i'\sigma'}$ with i, i' close to i_0 (central site) with a period approximately given by $2\pi/\omega_L$, where $\omega_L = B = 1$ is the Larmor frequency. More important, however, one finds spin-dependent excitations being emitted from the central region. These oscillate with the same frequency but are phase shifted depending on the distance to i_0, i.e., we see a propagation of a wave packet through the lattice. This propagation is found to be equally pronounced for the spatially diagonal ($i = i'$) elements of $\rho_{i\sigma i'\sigma'}$ as well as for the off-diagonal ones. At later times t, approximately given by the distance $L/2$ divided by the Fermi velocity $v_F = 2$, i.e., $t \gtrsim 10$, the excitations reach the edges, are back reflected and, for still later times, lead to the unwanted interference with the relaxation dynamics close to i_0.

For the same system but with absorbing BCs based on the Lindblad approach with a standard parameter choice, Eqs. (14), (15), and (17), there are several defects that are uncovered with the upper panel of Fig. 5. First, the comparison of results for open and absorbing BCs at early times shows that the presence of the coupling to the bath *induces* artificial excitations, which *start* close to the edges and propagate to the central region with Fermi velocity and finally, at times
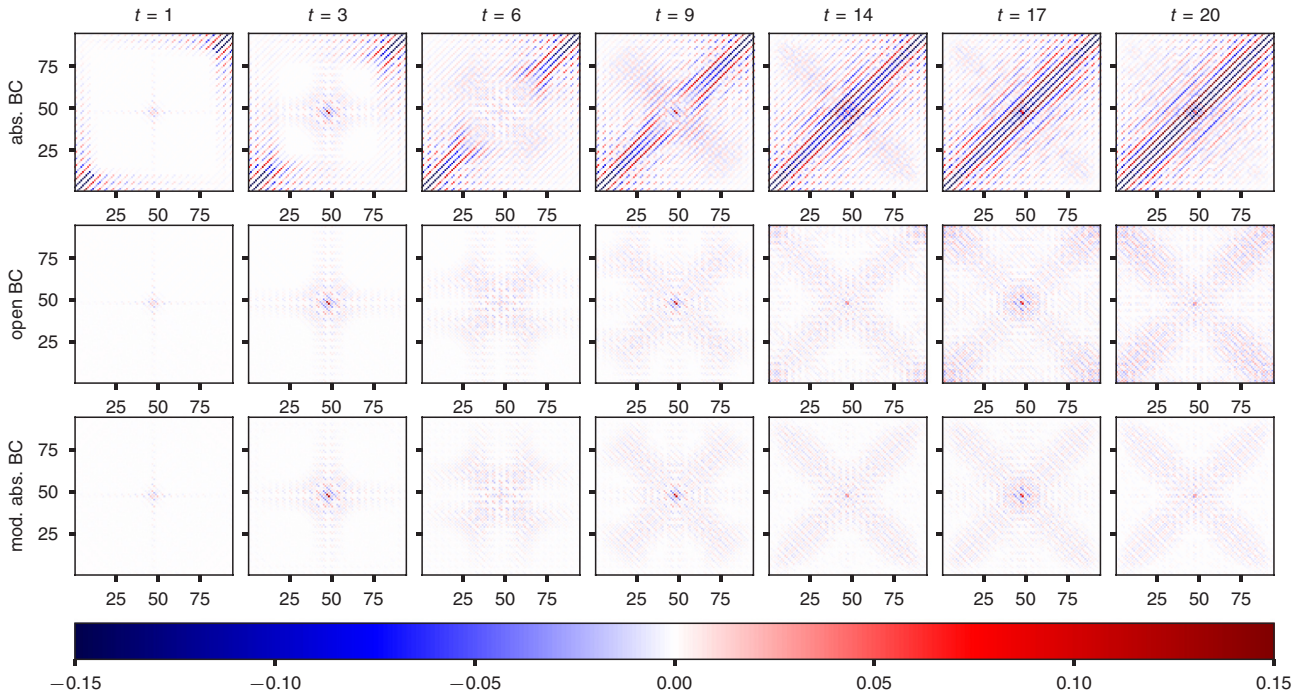

FIG. 5. Time dependence of the one-particle reduced density matrix for a system of $L = 47$ sites. The color code (see bottom) quantifies the real part of the difference to the initial density matrix, $\text{Re}[\boldsymbol{\rho}(t) - \boldsymbol{\rho}(0)]$, at selected instants of time (see the time labels at the top). Representation of the elements $\rho_{\alpha\beta}$ as in Fig. 4 using the orbital index $\alpha = 2i - \frac{1}{2}(1 + z_\sigma) = 1, \ldots, 2L$. Middle panel: System with open BCs. Upper panel: Same system but with absorbing BCs based on the standard Lindblad approach [Eqs. (14), (15), and (17)]. Lower panel: Same system but with modified absorbing BCs (see text). Other parameters as in Figs. 3 or 6, respectively.

$\approx (L/2)/v_{\mathrm{F}}$, interfere with the spin-relaxation dynamics close to i_0. This actually explains the different time evolution of the classical spin in Fig. 3 for times $t \gtrsim (L/2)/v_{\mathrm{F}} \approx 12$. This artifact stems from bath contributions to the equations of motion, which are nonzero in the initial state at $t = 0$ and must be avoided by an improved model for the coupling to the bath.

Second, as a consequence of the damping terms in the equation of motion (14) for the one-particle reduced density matrix, we see that all its nondiagonal elements $i \neq i'$ are exponentially approaching zero. In the full dynamics, on the other hand, this is not the case at all. Especially the elements with $i' = i \pm 1$, have a considerable absolute magnitude at $t = 0$ (Fig. 4), and essentially do not decrease in the course of time.

Finally, absorbing BCs based on the standard Lindblad approach do not introduce absorption of excitations propagating along the antidiagonal of the density matrix. Such excitations on the antidiagonal, however, are clearly seen in the middle panel of Fig. 5 and are actually of the same order of magnitude as compared to the diagonal. Hence, absorption of both diagonal and antidiagonal excitations reaching the edges must be included in a modified coupling to the bath.

IV. IMPROVED ABSORBING BOUNDARIES

To analyze their origin and to remove the artifacts, we first consider the equation of motion (14) at time $t = 0$. For a quench of the magnetic field direction, the density matrix $\boldsymbol{\rho}(t)$ commutes with the effective hopping matrix $\boldsymbol{T}_{\mathrm{eff}}(t)$ at $t = 0$. For an infinite system or for a system with open boundaries, this would imply $d\boldsymbol{\rho}(t)/dt|_{t=0} = 0$. Note that there is a finite torque on the local impurity spin that initiates the dynamics, and the updated impurity-spin direction will impact $\boldsymbol{\rho}(t)$ for $t > 0$. With standard Lindblad boundaries, however, there is a nonzero time derivative of $\boldsymbol{\rho}(t)$ already at $t = 0$,

$$\frac{d}{dt}\boldsymbol{\rho}(t)|_{t=0} = -\{\boldsymbol{\gamma}, \boldsymbol{\rho}(0)\} + 2\boldsymbol{\Gamma}, \tag{18}$$

which gives rise to dynamics due to the mere presence of the bath and which starts from the system boundaries. Avoiding this artificial cause of dynamics implies the following condition on the Lindblad parameters,

$$\boldsymbol{\Gamma} = \tfrac{1}{2}\{\boldsymbol{\gamma}, \boldsymbol{\rho}(0)\}, \tag{19}$$

i.e., we must necessarily choose the parameters dependent on the initial system state. Furthermore, this condition also implies an r-dependent choice of the coefficient matrices $\boldsymbol{\alpha}_r$ [see Eq. (13)]. Using Eq. (19) to eliminate $\boldsymbol{\Gamma}$, the resulting equation of motion reads

$$\frac{d}{dt}\boldsymbol{\rho}(t) = -i[\boldsymbol{T}_{\mathrm{eff}}(t), \boldsymbol{\rho}(t)] - \{\boldsymbol{\gamma}, \boldsymbol{\rho}(t) - \boldsymbol{\rho}(0)\}. \tag{20}$$

We emphasize that all properties that are constitutive for the general Lindblad approach apply to this equation as well, as it exactly derives from the fundamental Lindblad equation (7) by merely specializing to a noninteracting electron system and by a special parameter choice only. Particularly, Eq. (20) therefore respects the Hermiticity and the non-negativity of $\boldsymbol{\rho}(t)$ at all times t.

However, there are restrictions for the choice of the parameter $\boldsymbol{\gamma}$, which must be taken care of. To discuss this, let us first construct the general formal solution of Eq. (20), assuming that the impurity spin $\boldsymbol{S}(t)$ and thus the time dependence of $\boldsymbol{T}_{\mathrm{eff}}(t)$ is given. Equation (20) represents a linear inhomogeneous system of first-order ordinary differential equations. The corresponding homogeneous system, $\frac{d}{dt}\boldsymbol{\rho}(t) = -i[\boldsymbol{T}_{\mathrm{eff}}(t), \boldsymbol{\rho}(t)] - \{\boldsymbol{\gamma}, \boldsymbol{\rho}(t)\}$, can be written as $i(d/dt)\boldsymbol{\rho} = \boldsymbol{\Theta}\boldsymbol{\rho} - \boldsymbol{\rho}\boldsymbol{\Theta}^{\dagger}$ with $\boldsymbol{\Theta} \equiv \boldsymbol{T} - i\boldsymbol{\gamma}$ and is thus solved by $\boldsymbol{\rho} = \boldsymbol{U}\boldsymbol{\rho}_0\boldsymbol{U}^{\dagger}$ for the initial condition $\boldsymbol{\rho}(t = 0) = \boldsymbol{\rho}_0$. Here, $\boldsymbol{U} = \boldsymbol{U}(t) = \boldsymbol{U}(t, 0)$ with $\boldsymbol{U}(t, t') = \mathcal{T}\exp[-i\int_{t'}^{t} d\tau\,\boldsymbol{\Theta}(\tau)]$ (for $t > t'$) is a *nonunitary* time-evolution matrix formally constructed with the help of the time-ordering operation $\mathcal{T}$. A special solution of the inhomogeneous system is easily obtained with the ansatz $\boldsymbol{\rho} = \boldsymbol{U}\widetilde{\boldsymbol{\rho}}\boldsymbol{U}^{\dagger}$. We find $\dot{\widetilde{\boldsymbol{\rho}}} = \boldsymbol{U}^{-1}\{\boldsymbol{\gamma}, \boldsymbol{\rho}_0\}\boldsymbol{U}^{\dagger -1}$. The desired special solution with initial condition $\widetilde{\boldsymbol{\rho}}(t = 0) = 0$ is obtained by integration and back transformation from $\widetilde{\boldsymbol{\rho}}$ to $\boldsymbol{\rho}$. Adding the solution of the homogeneous system, we finally obtain

$$\boldsymbol{\rho}(t) = \boldsymbol{U}(t, 0)\boldsymbol{\rho}(0)\boldsymbol{U}(t, 0)^{\dagger} + \int_0^t d\tau\,\boldsymbol{U}(t, \tau)\{\boldsymbol{\gamma}, \boldsymbol{\rho}(0)\}\boldsymbol{U}(t, \tau)^{\dagger}. \tag{21}$$

Note that for finite damping $\boldsymbol{\gamma}$ the backwards time evolution $\boldsymbol{U}(t, t')^{-1} = \boldsymbol{U}(t', t) = \widetilde{\mathcal{T}}\exp[-i\int_t^{t'} d\tau\,\boldsymbol{\Theta}(\tau)]$ (for $t > t'$ and with the antichronological ordering $\widetilde{\mathcal{T}}$) is generally different from the adjoint of the time evolution $\boldsymbol{U}(t, t')^{\dagger} \neq \boldsymbol{U}(t', t)$. Due to the nonunitarity of $\boldsymbol{U}$, damping is not only described by the second term including a memory effect but also by the first one.

One immediately sees that $\boldsymbol{\rho}(t)$ is Hermitian and non-negative for all t, if (i) the anticommutator $\{\boldsymbol{\gamma}, \boldsymbol{\rho}(0)\}$ is non-negative, and if (ii) $\boldsymbol{\gamma}$ is Hermitian. Furthermore, we must have (iii) $\boldsymbol{\gamma} \geqslant 0$ to ensure that the first "homogeneous" term remains bounded for $t \rightarrow \infty$. The conditions (i) and (iii) are also obvious from Eqs. (13) and (19).

All conditions (i)–(iii) can be satisfied as follows: We diagonalize the initial density matrix, $\boldsymbol{\rho}(0) = \boldsymbol{V}^{\dagger}\boldsymbol{n}\boldsymbol{V}$, with a unitary matrix $\boldsymbol{V}$. The elements of the diagonal matrix $\boldsymbol{n}$, the natural occupations, are non-negative since $\boldsymbol{\rho}(0) \geqslant 0$. The rows of $\boldsymbol{V}$ are the corresponding natural orbitals. Note that, for an infinite and translationally invariant system, the natural orbitals are delocalized states and labeled by a wave vector. Hence, for a finite but large L we expect them to be rather delocalized as well. Using $\boldsymbol{V}$, we can now define $\boldsymbol{\gamma} \equiv \boldsymbol{V}^{\dagger}\boldsymbol{g}\boldsymbol{V}$, where $\boldsymbol{g}$ is a real, non-negative, and diagonal matrix. With this choice, we immediately have $\boldsymbol{\gamma}^{\dagger} = \boldsymbol{\gamma}$ and $\boldsymbol{\gamma} \geqslant 0$, i.e., conditions (ii) and (iii) are satisfied. Furthermore, since $\boldsymbol{\gamma}$ and $\boldsymbol{\rho}(0)$ are, by construction, simultaneously diagonalized by the same unitary transformation $\boldsymbol{V}$, they must commute. This immediately implies condition (i). The remaining degrees of freedom, the elements of the diagonal matrix $\boldsymbol{g}$, should be used to localize $\boldsymbol{\gamma}$ close to the system boundary. Strictly speaking, we need to satisfy $\mathcal{O}[(L - L_B)^2]$ conditions of the form $\gamma_{ii'\sigma\sigma'} = 0$ for i, i' in the core system, having only $\mathcal{O}(L)$ parameters at our disposal. While this is not an obstacle in principle, it would imply that the boundary region with finite coupling to the bath extends over almost the whole system and

that the remaining core system is comparatively small. From a computational point of view this is highly inconvenient.

In practice, it has turned out, however, that a more pragmatic and much simpler procedure is fully satisfying. We take γ as diagonal right from the start and set $\gamma_{i\sigma} = \gamma$ with $\gamma > 0$ for a small number of sites $2L_B$ coupling to the external bath and $\gamma_{i\sigma} = 0$ else. Alternatively, a linear γ profile, analogous to Eq. (17), may be employed. This implies that generically γ does not commute with $\rho(0)$, and hence $2\Gamma = \{\gamma, \rho(0)\}$ [see Eq. (19)] may develop negative eigenvalues. While there are negative eigenvalues of 2Γ indeed, as is easily seen numerically, these have a small modulus for all cases studied and particularly for setups with a small boundary and a large core region, i.e., for the conceptually and computationally attractive case. Causality problems, such as negative densities $\rho_{i\sigma i\sigma} < 0$, have not been observed. One may also relax the condition (19) and replace the initial density matrix by the $J = 0$ density matrix for the computation of Γ, with the idea to work with a spin-independent Γ matrix. Again, this is unproblematic in practice, as the finite coupling to the classical spin does not affect the density-matrix elements in the boundary region substantially if L is reasonably large.

To test the construction of absorbing BCs, we solve the coupled system of Eqs. (2) and (20) for the comparatively small system with $L = 47$ sites. The lower panel of Fig. 5 displays the time evolution of the one-particle reduced density matrix as obtained with the modified absorbing BCs. Comparing with the results obtained for open BCs (middle panel) at early instants of time ($t \leqslant 9$) and in the central region for i, i' close to i_0, only marginal differences are found, which are by far too small to be visible in the figure. In particular, all fine details of the spatial structure of the density matrix are reproduced correctly.

For later times (see $t = 20$, for example) there are still no deviations in the central region. This is as desired. In the calculation with open boundaries, we expect unphysical interference effects only for times $t \gtrsim 2i_0/v_F \approx 23$. Off the central region, however, artifacts start for $t = 20$ and also for earlier times, e.g., $t = 14$, but only for sites i and i' far from the central site i_0, both on the diagonal and the antidiagonal (see, e.g., the middle panel for $t = 14$, around $i = 1$, $i' = 1$ and around $i = 1$, $i' = L$). On the other hand, the calculations with modified absorbing BCs are entirely free from those artifacts. Comparing with the simple absorbing BCs based on the naive application of the Lindblad approach (upper panel), demonstrates the progress made, in particular if one takes into account the fact the small scale of *differences* to the initial-state ($t = 0$) density matrix.

We conclude that the absorption of the outgoing excitations is perfectly accomplished with our approach [Eq. (20)] and that therefore the temporal development of the density matrix in the physical core of the system indeed reflects the temporal development of the infinite system very accurately.

This is also nicely seen in the resulting relaxation dynamics of the classical spin. In Fig. 6 we compare $S(t)$ as obtained from the calculation for the small system with $L = 47$ sites and with the new absorbing BCs to corresponding results of a calculation with open BCs but for a much larger system ($L = 1001$). For the chosen system parameters the spin-relaxation time amounts to $\tau \approx 200$ inverse hoppings.
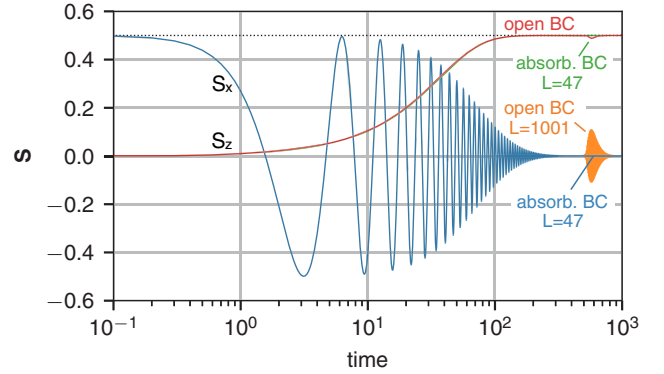

FIG. 6. Time evolution of the z and the x component of the classical spin as in Fig. 3 but here the results of the standard theory (red/orange lines) for open BCs and $L = 1001$ are compared to those obtained for $L = 47$ sites (green/blue lines) with modified BCs (linear profile and $\gamma_{\min} = 0.2$). Other parameters as in Fig. 3.

We note that for $t \gtrsim \tau$ artificial interference with excitations back reflected from the edges manifests itself in an unphysical revival of the dynamics starting at $t \approx 500$ inverse hoppings in the calculation done for open BCs, while there is no such effect visible for modified absorbing BCs. For times shorter than $t \approx 500$, the agreement between the results obtained for $L = 1001$ (open BCs) and for $L = 47$ sites (absorbing BCs) is not perfect but extremely good, such that deviations are more or less invisible on the scale of the figure. Remaining discrepancies can be eliminated systematically by increasing the core system size.

V. ACCESSING LONG TIMESCALES

The benefit of the absorbing BCs is that much longer timescales are accessible. This is demonstrated with Fig. 7, which displays the relaxation time τ as a function of the magnetic field strength B. For convenience the classical spin is
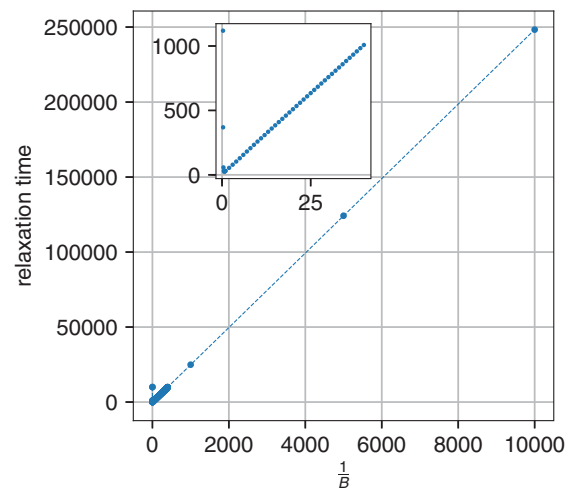

FIG. 7. Relaxation time τ as a function of $1/B$. Calculations for $i_0 = 1$ (spin couples to the "left" edge), $L = 46$, $J = 1$, and modified BCs for the "right" edge (linear profile, $\gamma_{\min} = 0.2$, $L_B = 5$).

coupled to the first site of the chain, $i_0 = 1$, and the absorbing BCs are implemented, with $L_B = 5$ sites coupling to the bath, for the opposite edge. We define τ pragmatically as the time required for $S_z(t)$ to reach 95% of its fully relaxed value $S_z(t \to \infty) = 0.5$. As can be seen in the figure, for very weak fields, down to $B = 1 \times 10^{-4}$, the relaxation time approaches $\tau \approx 250\,000$ in units of the inverse hopping parameter, i.e., the coupled microscopic real-time dynamics of the spin and the conduction-electron system can be traced on a timescale, which is by more than five orders of magnitude longer than the intrinsic bare timescale of the electron system that is set by the inverse hopping $1/T = 1$. This is way beyond what can be reached with conventional calculations using open BCs.

It is instructive to compare the results with the prediction of the Landau-Lifshitz-Gilbert (LLG) approach [6],

$$\tau \propto \frac{1 + \alpha^2}{\alpha} \frac{1}{B}, \tag{22}$$

where α is the Gilbert damping parameter (see Ref. [37]). Starting from the simplified model considered here, the LLG equation can be derived by lowest-order perturbation theory in J and by a Markov approximation assuming that the spin dynamics is much slower than the electron dynamics, i.e., by assuming that the strength of the local field B is weak on the scale given by the nearest-neighbor hopping (see, e.g., Ref. [17] for a detailed discussion).

Thus, in the present context, Eq. (22) is not expected to capture the case of very strong fields. For strong B, the field term will eventually dominate and only the precessional motion will survive. This means that τ should increase with increasing B and diverge for $B \to \infty$. In fact, as is seen in Fig. 7 for field strengths exceeding a critical strength of the order of the bandwidth, the computed relaxation time diverges.

On the other hand, Eq. (22) should well describe the physics at weak B. It is satisfying to note that our approach, based on microscopic calculations including the details of the electronic structure, perfectly agrees with the prediction of the spin-only LLG theory. As is seen in the figure, the relaxation time is proportional to $1/B$ for weak fields down to $B = 0.0001$. We conclude that even for very moderate system sizes L and even for timescales of the order of 10^5 inverse hoppings, the absorbing BCs do not lead to any observable artifacts.

The predictive power can be exploited to study spin relaxation in cases where lowest-order perturbation theory in J and the Markov approximation do not apply. One important example to be discussed here is the case of a system with a gapped electronic structure. Even for a conventional band insulator, perturbation theory must break down, as this predicts the Gilbert damping constant to be given by [9,17,38]

$$\alpha = J^2 \frac{\partial}{\partial \omega} \text{Im} \, \chi^{(\text{ret})}(\omega)|_{\omega=0}. \tag{23}$$

For an insulator with a gapped electronic structure, the imaginary part of the retarded magnetic susceptibility $\chi^{(\text{ret})}(\omega)$ must vanish in a finite range of excitation energies ω around $\omega = 0$, which immediately implies $\alpha = 0$. Hence, perturbation theory predicts the absence of damping, i.e., an infinite spin-relaxation time, independent of the field strength. However, this is unphysical since relaxation should be possible, if
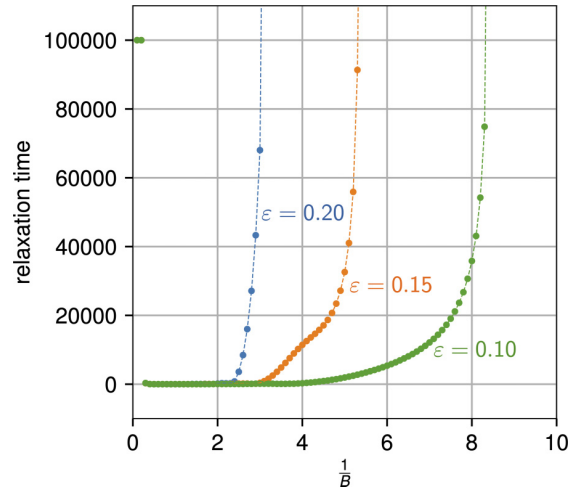

FIG. 8. Relaxation time τ as function of $1/B$ as in Fig. 7 but for an insulator [see Eq. (24)] and for different values of the on-site potential ε as indicated.

the initially induced Larmor precession with frequency $\omega \approx B$ can couple to the magnetic modes in the electron system. This is the case when $\text{Im} \, \chi^{(\text{ret})}(\omega = B) \neq 0$, i.e., for field strengths of the order of the fundamental gap or larger. Hence, a more elaborate effective theory would be necessary to cover this case.

The microscopic theory that includes the electronic degrees of freedom explicitly, on the other hand, perfectly complies with the expectation of a critical field strength: Fig. 8 displays results for the spin-relaxation time τ as obtained for a simple one-dimensional model of a band insulator, which is constructed by replacing

$$T_{ii'} \mapsto T_{ii'} + \varepsilon_0 (-1)^i \delta_{ii'} \tag{24}$$

in the Hamiltonian, Eq. (1), or, equivalently, in the effective hopping matrix, Eq. (5). The staggered on-site potential of strength $\varepsilon_0 > 0$ leads to a doubling of the unit cell and opens a gap of size $\Delta E = 2\varepsilon_0$ in the bulk band structure at the edges of the reduced Brillouin zone. Here, for a finite system, the gap is $\Delta E \gtrsim 2\varepsilon_0$. For $L = 46$ sites, however, the difference is small, and we have checked that the results do not change significantly when increasing L. Figure 8 indeed shows that complete spin relaxation is possible if the spin is driven with a sufficiently strong field. A divergent spin-relaxation time ($\tau > 100\,000$) is only found for field strengths weaker than a certain critical value related to the gap size.

Finally, we would like to stress that our approach is a systematic one, as the reliability of the approximations involved is fully controlled by the choice for the size of the system L. For $L \to \infty$, one trivially recovers the exact dynamics of a spin and of the coupled electron degrees of freedom, since the Lindblad-type boundaries become meaningless and since the construction of the boundaries is the only approximative element of the theory. Thus, varying the system size gives a good impression on the quality of results.

To give an example, we display in Fig. 9 the spin-relaxation time τ at a fixed field strength $B = 0.001$ but as a function of L for the metallic case. This corresponds to Fig. 7 where
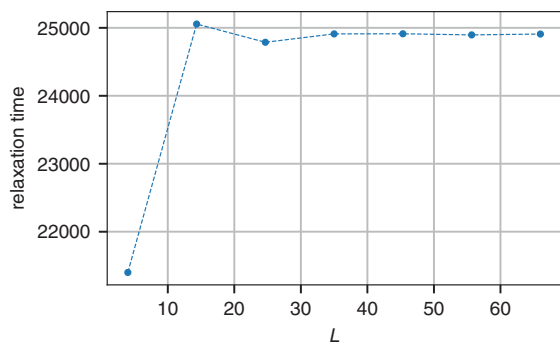
FIG. 9. Relaxation time τ as function of the system size $L = 6$, 16, 26, 36, 46, 56, 66 and $L_B = 5 = $ const as in Fig. 7 for $B = 0.001$.

$L = 46$ was chosen to represent converged results. Figure 9 demonstrates that this is in fact the case: We have $\tau \approx 25\,000$ for $L = 46$, and this value is not significantly changing when larger system sizes are considered. For $L = 56$ and $L = 66$, we get the same value from the numerical calculation within an error of less than 0.1%. It is very satisfying to see that already $L = 16$ sites are actually quite sufficient, and only with $L = 6$, which means one site that is left unchanged plus five sites coupling to the bath, the deviation of about 15% is clearly beyond what should be tolerated.

VI. CONCLUSIONS

The real-time dynamics of local magnetic moments interacting with a large conduction-electron system is in most cases much slower than the bare electronic timescales. One general reason is the weakness of magnetic interactions compared to the conduction-band width or to the Fermi energy. Moreover, spin dynamics can be slowed down by missing phase space for magnetic scattering or by strongly anisotropic magnetic interactions and by other effects. The strong separation of energy and timescales makes the theoretical description a challenging task. For the study of relaxation phenomena, for example, it is the long-time limit that is of primary interest, but this cannot be treated independently from and is actually governed by the fast electronic processes.

On short timescales, perturbation theory, exploiting the separation of energy scales, can be very helpful. Master-equation approaches, including the Landau-Lifshitz-Gilbert approach, Redfield, and other more sophisticated theories, are quite powerful but are necessarily based on approximations, which in most cases are of *ad hoc* character and can be controlled *a posteriori* only. For complex dynamics with phase-space bottlenecks, prerelaxation phenomena, or emergent symmetries, there is clearly an urgent need for a fully atomistic modeling, which covers timescales spanning several orders of magnitude and which is controlled *systematically*.

Here, we have presented some steps towards such an approach. The main idea is that relaxation processes are unidirectional, i.e., they are characterized by dissipation of energy and other conserved quantities due to flows of energy, spin, etc., away from the initially excited core system to the electronic bulk but not vice versa. The fast processes in the core system, consisting of the local magnetic moments and the immediate surrounding, lead to the emission of wave packets carrying energy and spin, which implies that the core region must approach its ground state in the course of time. Hence, the theory must (i) treat this spatial region exactly and (ii) must ensure that the processes within the core region and the excitations leaving the core region are not disturbed by artificial excitations backpropagating from the bulk to the core. Those backpropagating modes, however, are typically produced by reflections of outgoing wave packets from the edges of a system of finite extent, i.e., they result from the use of open or periodic boundary conditions.

Boundary conditions, which fully absorb the outgoing excitations, solve the problem. We found that those can be realized with coupling the sites that are close to the edges of the finite system to an external bath as described by the Lindblad equation for the one-particle reduced density matrix. The important point is that the master-equation approach is merely employed as a technical tool to realize the absorbing boundaries while the quality of the approximation is solely controlled by the size of the core region, and thus we get a systematic approach.

It has turned out that the Lindblad coupling to the bath does a perfect job inasmuch as the absorption is concerned. However, the naive implementation of Lindblad boundaries also *generates* excitations propagating from the edges to the core right at the start of the dynamics. Fortunately, this problem could be solved completely by using a Lindblad approach with matrix-valued Lindblad parameters that are fixed to perfectly suppress the mentioned initial-state artifacts.

This type of absorbing boundaries has been tested in detail. For a single classical spin coupled to a one-dimensional system of conduction electrons we were easily able to trace the atomistic real-time dynamics on a timescale longer than 10^5 inverse hoppings without any noticeable problem. The computational limitation is solely given by the necessary size L of the core system. For the currently studied case, we find that $L \lesssim 50$ is fully sufficient for convergence of the results.

Future applications will address systems with several spins, coupled to electron systems in two and three dimensions, and including anisotropic interactions. The role of lattice degrees of freedom could be investigated as well. For quantitative and realistic studies, relaxation mediated also via phonons is an important aspect. Work along these lines is in progress. An open question is whether correlated electron systems might be treated within a similar framework on a level beyond standard Hartree-Fock theory.

[1] G. Tatara, H. Kohno, and J. Shibata, Phys. Rep. **468**, 213 (2008).

[2] B. Skubic, J. Hellsvik, L. Nordström, and O. Eriksson, J. Phys.: Condens. Matter **20**, 315203 (2008).

[3] G. Bertotti, I. D. Mayergoyz, and C. Serpico, *Nonlinear Magnetization Dynamics in Nanosystems* (Elsevier, Amsterdam, 2009).

[4] M. Fähnle and C. Illg, J. Phys.: Condens. Matter **23**, 493201 (2011).

[5] R. F. L. Evans, W. J. Fan, P. Chureemart, T. A. Ostler, M. O. A. Ellis, and R. W. Chantrell, J. Phys.: Condens. Matter **26**, 103202 (2014).

[6] L. D. Landau and E. M. Lifshitz, Phys. Z. Sowjetunion **8**, 153 (1935); T. Gilbert, Phys. Rev. **100**, 1243 (1955); IEEE Trans. Magn. **40**, 3443 (2004).

[7] S. V. Vonsovsky, Zh. Eksp. Teor. Fiz. **16**, 981 (1946); C. Zener, Phys. Rev. **81**, 440 (1951); S. V. Vonsovsky and E. A. Turov, Zh. Eksp. Teor. Fiz. **24**, 419 (1953).

[8] M. Onoda and N. Nagaosa, Phys. Rev. Lett. **96**, 066603 (2006).

[9] S. Bhattacharjee, L. Nordström, and J. Fransson, Phys. Rev. Lett. **108**, 057204 (2012).

[10] N. Umetsu, D. Miura, and A. Sakuma, J. Appl. Phys. **111**, 073909 (2012).

[11] U. Bajpai and B. K. Nikolic, Phys. Rev. B **99**, 134409 (2019).

[12] V. P. Antropov, M. I. Katsnelson, M. van Schilfgaarde, and B. N. Harmon, Phys. Rev. Lett. **75**, 729 (1995).

[13] J. Kuneš and V. Kamberský, Phys. Rev. B **65**, 212411 (2002).

[14] K. Capelle and B. L. Gyorffy, Europhys. Lett. **61**, 354 (2003).

[15] H. Ebert, S. Mankovsky, D. Ködderitzsch, and P. J. Kelly, Phys. Rev. Lett. **107**, 066603 (2011).

[16] A. Sakuma, J. Phys. Soc. Jpn. **81**, 084701 (2012).

[17] M. Sayad and M. Potthoff, New J. Phys. **17**, 113058 (2015).

[18] M. Sayad, R. Rausch, and M. Potthoff, Phys. Rev. Lett. **117**, 127201 (2016).

[19] C. Stahl and M. Potthoff, Phys. Rev. Lett. **119**, 227203 (2017).

[20] M. Elbracht, S. Michel, and M. Potthoff, Phys. Rev. Lett. **124**, 197202 (2020).

[21] U. Bajpai and B. K. Nikolic, arXiv:2005.14153.

[22] X. Antoine, A. Arnold, C. Besse, M. Ehrhardt, and A. Schadle, Commun. Comput. Phys. **4**, 729 (2008).

[23] D. E. Manolopoulos, J. Chem. Phys. **117**, 9552 (2002).

[24] J. Berenger, J. Comput. Phys. **114**, 185 (1994).

[25] S. Selstø and S. Kvaal, J. Phys. B **43**, 065004 (2010).

[26] G. Lindblad, Commun. Math. Phys. **48**, 119 (1976).

[27] P. Pearle, Eur. J. Phys. **33**, 805 (2012).

[28] H. Carmichael, *An Open Systems Approach to Quantum Optics* (Springer, Berlin, 1993).

[29] H.-P. Breuer and F. Petruccione, *The Theory of Open Quantum Systems* (Oxford University Press, Oxford, U.K., 2010).

[30] X. Xu, J. Thingna, C. Guo, and D. Poletti, Phys. Rev. A **99**, 012106 (2019).

[31] E. Arrigoni, M. Knap, and W. von der Linden, Phys. Rev. Lett. **110**, 086403 (2013).

[32] A. A. Dzhioev and D. S. Kosov, J. Chem. Phys. **134**, 044121 (2011).

[33] F. Verstraete, J. J. García-Ripoll, and J. I. Cirac, Phys. Rev. Lett. **93**, 207204 (2004).

[34] M. Zwolak and G. Vidal, Phys. Rev. Lett. **93**, 207205 (2004).

[35] T. Prosen and M. Znidari, J. Stat. Mech. (2009) P02035.

[36] H. Elze, Phys. Rev. A **85**, 052109 (2012).

[37] R. Kikuchi, J. Appl. Phys. **27**, 1352 (1956).

[38] E. Simanek and B. Heinrich, Phys. Rev. B **67**, 144418 (2003).

5 – Long-Time Relaxation Dynamics of a Spin Coupled to a Chern Insulator

In this paper we investigated the relaxation dynamics of a single classical spin coupled to a one-dimensional topological insulator in form of a spinful Su–Schrieffer–Heeger (SSH) model. The theoretical background for this model was already discussed above in Sec. 3.2, so in this section we will give a short summary of the scientific results, discuss them, and at the end go a bit beyond the scope of the paper and shortly analyze what happens if the topological edge states are pushed out of the band gap.

5.1 – Results

The SSH model features a band gap $\Delta = 4|\delta T|$ with its size depending on the strength of the staggered hopping δT. Depending on whether the SSH chain starts with the stronger or weaker hopping at the edge there also may be edge states, with spin $\uparrow, \downarrow$, inside the band gap. These states are exponentially localized at the edge and do not reach into the bulk of the SSH chain. This means we have three different options on how to couple the classical spin to the SSH chain. Firstly, it can be coupled to a electron site somewhere in the bulk of the chain. There, it does not matter whether there are edge states inside the band gap or not as they have no weight at the bulk electron sites. Secondly, the spin can be coupled to the edge of the SSH chain without any edge states present. This should all in all be very similar to the bulk case, but there might be some effects due to the closeness to the boundary of the system. Thirdly, we can couple the spin to the edge of the SSH chain with edge states present. As the spin is then coupled to a electron site majorly influenced and dominated by the edge states, we can expect some influence of them on the dynamics of the classical spin.

Let us discuss the first case of a classical spin coupled to the bulk of the SSH chain. As the system is at half-filling and all states up to the band gap are filled, the band gap needs to be bridged to make non-trivial dynamics possible. A strong enough magnetic field should intuitively be sufficient to do exactly this. The question, however, is what exactly is a strong enough magnetic field in this context?

Initially, at $t = 0$ we perform a sudden flip of the magnetic field from $\boldsymbol{B}_{\mathrm{ini}} \parallel \boldsymbol{S}(t = 0)$ to some $\boldsymbol{B}_{\mathrm{fin}} \perp \boldsymbol{S}(t = 0)$. It is tempting to assume that as long as the excitation energy $E_{\mathrm{ex}} = -\boldsymbol{B}_{\mathrm{fin}}\boldsymbol{S}(t = 0) - (-\boldsymbol{B}_{\mathrm{ini}}\boldsymbol{S}(t = 0)) = \frac{B}{2}$ of the system at $t = 0$ is larger

than the size of the band gap, relaxation is possible, so $B > 8|\delta T|$. However, this is not what we see in the numerical calculations in Fig. II-3. We rather get a clear cut line defined by $B = 4|\delta T|$ separating the regime of relaxation and non-relaxation. In fact, we even find that whether the system relaxes or not does not depend on the exact initial spin position (with the exception of singular points, where the system starts in an (un)stable equilibrium and no dynamics is initiated).

Hence, more intricate methods for analysis are needed like time-dependent perturbation or linear-response theory. The latter enables us to calculate the spin susceptibility, which tells us to which excitation energies ω the system is susceptible. In [II] formulas are given for the spin susceptibility in time and frequency space. For a system of non-interacting electrons, the susceptibility $\chi_{\mathrm{loc}}(\omega)$ can be expressed as a convolution of the occupied with the unoccupied part of the local density of states. The most important part, however, is that we get a criterion for whether the system relaxes, namely

$$\mathrm{Im}\chi_{\mathrm{loc}}(\omega = B) \neq 0 \ . \tag{5.1}$$

This also explains why the exact initial position of the impurity spin does not play a role as only the excitation frequency matters, which is solely given by the strength of the magnetic field. An example of a spin susceptibility is plotted in Fig. II-4. As its imaginary part is given by the convolution of the occupied with the unoccupied part of the density of states, it is antisymmetric around $\omega = 0$ and features two non-zero regions starting at $\omega = \pm\Delta$ and reaching up to $\omega \approx \pm 4T$. Hence, the relaxation criterion Eq. (5.1) can be rewritten as

$$2\delta T = \Delta \leq |B| \leq 4T \ . \tag{5.2}$$

We can transfer these findings to the topologically non-trivial case, where there are now two topological edge states with zero energy inside the band gap. At half-filling they are also partially occupied with one electron splitted between the two edge states. Hence, when we calculate the spin susceptibility the non-zero areas of the imaginary part move closer together and reach now from $-\frac{\Delta}{2}$ to $\frac{\Delta}{2}$. This is shown in Fig. II-7. Hence, if we apply our criterion for relaxation we expect relaxation for $\frac{\Delta}{2} \leq |B| \leq 4T$. However, if we do calculate the relaxation time of the classical spin numerically, see Fig. II-6, we find that the spin still relaxes for magnetic field strengths not covered by our relaxation criterion as the classical impurity spin already relaxes for some $|B| \leq \frac{\Delta}{2}$. We find that this is because of a Zeeman spin-splitting of the edge states caused by coupling the classical impurity spin to the electron system. The energy of the edge states is exactly zero only in the SSH model without an attached classical impurity spin. With the classical impurity spin attached the edge states are at energies $\pm\epsilon_0$,

which can be computed in first order perturbation theory as

$$\epsilon_0 = \frac{1}{2} J S \left(1 - \left(\frac{T - \delta T}{T + \delta T} \right)^2 \right) . \tag{5.3}$$

But alone, this is not enough to explain the relaxation behavior, as after the splitting of the edge states at half-filling, the lower energy edge state is occupied while the higher energy is not. This leads to a spin susceptibility, for which the imaginary part is zero for $-\frac{\Delta}{2} - \epsilon_0 \leq \omega \leq \frac{\Delta}{2} + \epsilon_0$, which is a larger interval than before the splitting of the edge states. That would mean that larger B are necessary for the relaxation of the system; however, that is not what we see in the phase diagram Fig. II-6, where the system still relaxes for smaller B.

Hence, something is still missing to explain the relaxation behavior. We call this missing piece a "dynamic relaxation mechanism". The classical impurity spin influences the electron states of the host system. While the bulk states are not significantly affected by the spin impurity, the edge states, on the other hand, are greatly affected. Suppose at some point the classical spin points in $-z$-direction, then it would be energetically optimal that the ↑-spin edge state is occupied while the ↓-spin edge state is not. During the dynamics, the classical spin constantly changes its direction while it precesses in the magnetic field. The electron system follows the classical spin and thereby changes over time which edge state is the most favorable. Hence, the occupation of the ↑,↓-spin edge states also changes. As this process is not fully adiabatic in nature and the electron system always lags somewhat behind the classical spin, this leads to a partial occupation of the energetically higher edge state. But a non-vanishing occupation of the energetically higher edge state would also lead to a different spin susceptibility, where the non-zero imaginary part would already start at $\omega = \pm(\frac{\Delta}{2} - \epsilon_0)$, which would result in a relaxation criterion of

$$\frac{\Delta}{2} - \epsilon_0 \leq |B| \leq 4T . \tag{5.4}$$

As it can be seen in the phase diagram Fig. II-6 this criterion fits the numerical calculations quite well.

5.2 – Edge States Outside the Gap

We found out that the edge states help the relaxation process by bridging the gap, which is even further amplified by the Zeeman spin-splitting of the edge states. The strength of this splitting depends on the impurity-host interaction J and the length S
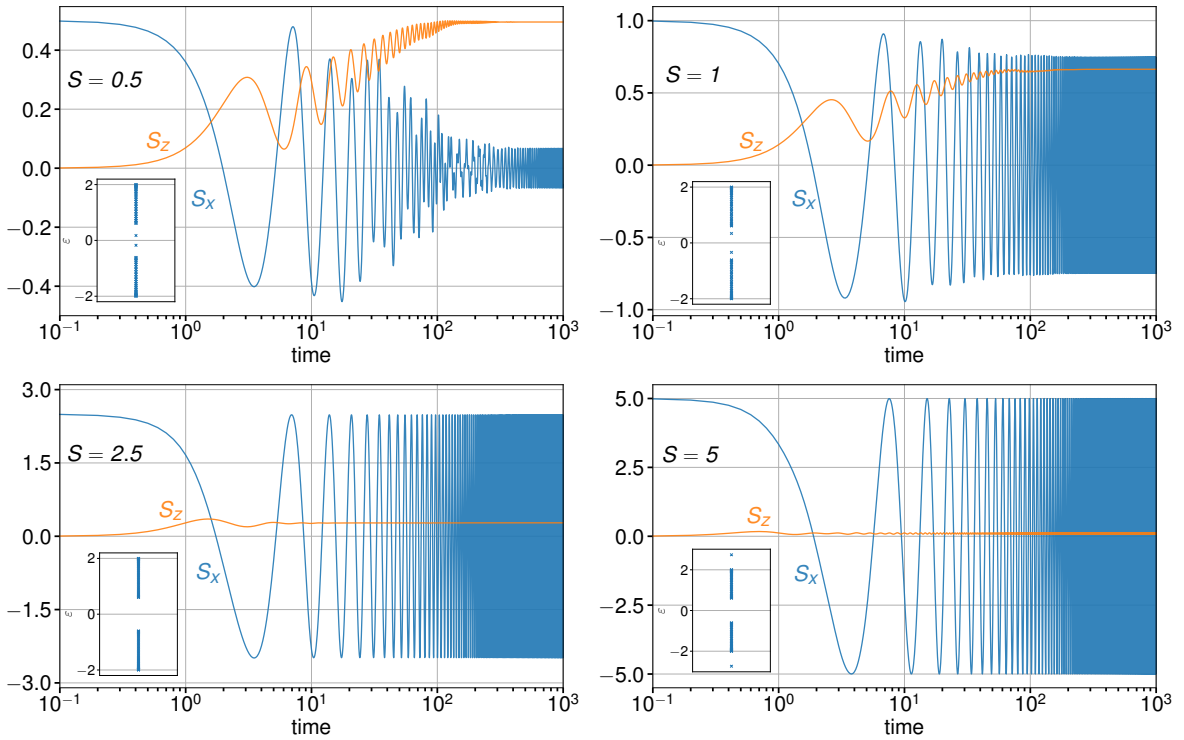
Figure 5.1: *Impurity spin dynamics for four different lengths of the impurity spin after a sudden flip of the local magnetic field from the x to z direction at time $t = 0$. The spin lengths are from left to right and top to bottom: $S = 0.5$, $S = 1$, $S = 2.5$, and $S = 5$. The insets in the bottom-left of the plots show the spectrum of the one-particle eigenenergies in units of the average hopping $T = 1$. Calculations for $L = 47$, $B = 0.75$, $\delta T = 0.3$. Absorbing boundary conditions with $L_B = 5$ and $\gamma_{min} = 0.2$.*

of the impurity spin. If J and/or S are large enough, the splitting of the edge states can push the edge states out of the gap into the bulk of the bands and even further. On first thought, the edge states should not be able to support the relaxation process if they are no longer inside the band gap. In the following, we, therefore, will analyze how the relaxation behavior changes when we increase the length of the impurity spin. In Fig. 5.1 the impurity spin dynamics for four different lengths of the impurity spin is depicted with parameters corresponding to the dynamics shown in Fig. II-5. Additionally, a small inset shows the spectrum of one-particle eigenenergies. We can see that for $S = 0.5$ and $S = 1$, the edge states are still inside the gap. For $S = 2.5$, they are inside the bulk of the bands and no longer inside the gap. For $S = 5$, they are pushed so far that they are even no longer inside the bulk of the band. The dynamics for $S = 0.5$ is thoroughly discussed in [II]. Shortly summarized, it shows a nearly full ($\approx 95\%$) relaxation of the impurity spin to the direction of the magnetic field $\boldsymbol{B}$. At that point, the dynamics of the impurity spin is dominated by the local magnetic moment $\boldsymbol{s}_{i_0}$ of the host system rather than by the magnetic field $\boldsymbol{B}$. As $s_{i_0} < B$ the excitation frequency is no longer large enough to bridge the gap (even with the help of the edge states) and the system becomes stuck in a pre-relaxed state.

For $S = 1$, we see a similar story. The edge states are still inside the gap, however, there are further apart than for $S = 0.5$. Also, due to the larger S the electron system is stronger polarized and the local magnetic moment s_{i_0} is larger than for $S = 0.5$. All this leads to an earlier completion of the pre-relaxation process, as the impurity spin stops relaxing further after reaching $S_z \approx 0.66$.

For $S = 2.5$, the edge states are no longer inside the gap and vanish somewhere in the bulk of the bands. In general, it is also probably no longer right to speak about edge states, as when we calculate the localization of the eigenstates, we do not find any distinguished localized states anymore. As the gap is now too large, the dynamics basically shows no relaxation. The impurity spin shifts only a small amount in z-direction, but not by any significant amount.

For $S = 5$, the edge states are pushed so far out that they are no longer inside the bulk of the bands anymore. These states are now again extremely localized, but as they are decoupled from the rest of the system, they do not aid the relaxation in any way. We do not see any relaxation, since the band gap is too large. All we see, is a precession of the impurity spin around the magnetic field $\boldsymbol{B}$ and the local magnetic moment $\boldsymbol{s}_{i_0}$ in the host system.

So concluding we find, that for not too large impurity spins the dynamics is the same as discussed in [II]. For too large impurity spins, however, the edge states are no longer inside the gap and the dynamics looks like the dynamics of a classical spin coupled to a trivial insulator.

Long-time relaxation dynamics of a spin coupled to a Chern insulator

Michael Elbracht [1] and Michael Potthoff [1,2]

[1] *I. Institute of Theoretical Physics, Department of Physics, University of Hamburg, Jungiusstraße 9, 20355 Hamburg, Germany*
[2] *The Hamburg Centre for Ultrafast Imaging, Luruper Chaussee 149, 22761 Hamburg, Germany*

The relaxation of a classical spin, exchange coupled to the local magnetic moment at an edge site of the one-dimensional spinful Su-Schrieffer-Heeger model, is studied numerically by solving the full set of equations of motion. A Lindblad coupling of a few sites at the opposite edge to an absorbing bath ensures that convergence with respect to the system size is achieved with only a moderate number of core sites. This allows us to numerically exactly study the long-time limit and to determine the parameter regimes where spin relaxation takes place. Corresponding dynamical phase diagrams for the topologically trivial and the nontrivial cases are constructed. The dynamical phase boundaries, the role of the topological edge state, and its internal Zeeman splitting for the spin-relaxation process, as well as incomplete spin relaxation on long time scales can be explained within the framework of a renormalized linear-response approach when explicitly taking retardation effects and nonequilibrium spin-exchange processes into account.

I. INTRODUCTION

Novel concepts [1] to achieve ever smaller magnetic bits and thus higher data storage continue to drive research of systems of magnetic atoms on nonmagnetic surfaces [2]. Since the manipulation of magnetic bits requires external time-dependent fields, there is a strong interest in the stability of excitations of single magnetic atoms. Such spin excitations of single absorbed magnetic atoms can be probed experimentally, e.g., via inelastic scanning tunneling spectroscopy [3–7].

Surfaces of topological insulators [8,9] are particularly interesting in this context since a magnetic impurity atom located at the surface is expected to predominantly interact with the conducting surface state and since the existence of this surface state and its robustness against weak perturbations is ensured by the topological properties of the bulk band structure and the bulk-boundary correspondence principle [10–13]. The *static* properties of magnetic impurities at the surface of topological insulators have been studied extensively, both experimentally and theoretically [14–26].

Recently, also *dynamical* properties of impurities at surfaces of topological insulators have been investigated theoretically, based on the linear-response approach within time-dependent density-functional theory [27] and on Floquet theory applied to a periodically driven (nonmagnetic) impurity coupled to a two-dimensional topological insulator [28]. Earlier theoretical studies have considered the effect of the surface state of a topological insulator on the magnetization dynamics of a coupled ferromagnetic system [29–32]. An array of magnetic adatoms interacting with the electronic surface states was investigated in Ref. [33]. A large single-atom anisotropic magnetoresistance on a surface of a three-dimensional topological insulator (Bi_2Se_3) decorated with magnetic adatoms (Mn) has been found in

first-principles transport calculations [34]. Beyond the level of linear-response theory, however, the full microscopic real-time dynamics of a single magnetic atom coupled to the electronic structure of the topological substrate has not been addressed so far.

Clearly, for real systems, the application of nonperturbative time-dependent *ab initio* methods is extremely demanding. The situation is different, however, in the case of strongly simplified model systems, where one can address the full real-time dynamics of an initial magnetic excitation beyond the linear-response approach. Here, we consider the one-dimensional spinful Su-Schrieffer-Heeger (SSH) model [35–37] as a prototypical system, which, depending on the ratio of the hopping parameters, hosts a Kramers-degenerate edge state at each of the boundaries. Coupling a classical spin to one of the edge sites locally destroys time-reversal symmetry, which leads to a spin splitting of the edge state. There is a closed system of equations of motions such that, in principle, the full coupled real-time dynamics [38–43] of the electronic structure and the classical spin is accessible by numerical means beyond the linear-response theory [44–46].

However, even in this comparatively simple case, calculations based on the full set of equations of motion are demanding since relaxation times typically exceed the bare electronic time scale by several orders of magnitudes [38,41]. We note that estimates for lifetimes of excitations of $3d$ and $4d$ magnetic impurities embedded in Bi_2Te_3 and Bi_2Se_3 range from the pico- to the microsecond regime [27]. Let us also mention that simulations of real-time dynamics based on classical *spin-only models*, see Refs. [47,48] for example, are much simpler and can be performed for large two- or three-dimensional systems approaching the thermodynamic limit [49] or coupling the spin system to classical lattice degrees of freedom in addition [50].

Here, on the other hand, we are interested in the dynamic relaxation process of a classical spin coupled to a topologically nontrivial electronic structure. The necessity to explicitly account for the time dependence of the electronic structure complicates the computations. Due to spin and energy conservation, the relaxation of an initial magnetic excitation requires the transport of spin and energy away from the magnetic impurity and dissipation into the bulk of the system. An exact treatment of the equations of motion, however, can only be done for a finite, comparatively small system size in practice. This implies that excitations of the electronic system that are emitted by the impurity will eventually reach the boundaries of the system. Reflections at the boundaries, back propagation, and interference with the dynamics close to the impurity will severely spoil the computation of the spin-relaxation time.

Recently, we have constructed [51] a novel type of absorbing boundary conditions, which employs a generalized Lindblad master-equation approach to couple the edge sites of the conduction-electron tight-binding model to an external bath. With these boundary conditions, outgoing excitations resulting from an initial excitation of a classical spin exchange-coupled to the conduction-electron system can be absorbed completely without disturbing the dynamics close to the impurity spin. It has been demonstrated that this allows us to trace the spin and the conduction-electron dynamics on a time scale, which exceeds the characteristic electronic scale that is set by the inverse nearest-neighbor hopping by more than five orders of magnitude.

Here, we will employ these absorbing boundary conditions to microscopically trace the coupled time evolution of spin and electron degrees of freedom for a single classical spin coupled to one of the edges of an SSH model on long time scales. In particular, we study the impact of the electronic edge state on the spin relaxation time. Lowest-order time-dependent perturbation theory in the exchange coupling is expected to break down in the long-time regime. We therefore carefully check the validity of the linear-response approach and head for possible new nonperturbative phenomena.

II. CLASSICAL SPIN COUPLED TO THE SPINFUL SSH MODEL

Figure 1 presents a sketch of the setup considered here. The corresponding Hamiltonian is given by $H = H_0 + H_{\text{imp}}$, where

$$H_0 = -\sum_{i=1}^{L-1} \sum_{\sigma=\uparrow,\downarrow} [(T + (-1)^i \delta T) c_{i\sigma}^\dagger c_{i+1\sigma} + \text{H.c.}] \quad (1)$$

is the spinful SSH model [35–37]. An electron at site i with spin projection $\sigma = \uparrow, \downarrow$ is created or annihilated by $c_{i\sigma}^\dagger$ or $c_{i\sigma}$, respectively. The nearest-neighbor hopping amplitudes alternate between

$$T_1 \equiv T - \delta T \quad \text{and} \quad T_2 \equiv T + \delta T. \quad (2)$$

We set $T = 1$ to fix the energy unit and (with $\hbar \equiv 1$) the time unit. Furthermore, the chemical potential is set to $\mu = 0$ such that the system is at half filling with $N = L$ electrons. For $\delta T = 0$, the system is in a metallic state, while for any nonzero
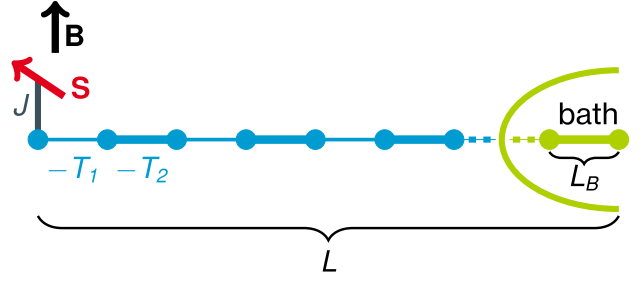

FIG. 1. Sketch of the system geometry: A classical spin S of length $|S| = \frac{1}{2}$ is coupled via a local antiferromagnetic exchange interaction J to the first site of a spinful SSH model consisting of L sites. The nearest-neighbor hopping alternates between $-T_1$ and $-T_2$. To construct absorbing boundary conditions at the opposite edge, the last L_B sites of the chain are coupled to a Lindblad bath [51]. The classical spin is subjected to a local magnetic field B. At time $t = 0$, real-time dynamics is initiated by a sudden flip of the field direction.

δT there is a finite bulk band gap

$$\Delta = 4|\delta T| = 2|T_1 - T_2| \quad (3)$$

between the highest occupied and the lowest unoccupied state. For even L and for $\delta T < 0$, i.e., for $T_1 > T_2$, the system is in a topologically trivial insulating state. If $\delta T > 0$, on the other hand, the system is topologically nontrivial, and two spin-degenerate edge states appear at zero energy. These are exponentially localized close to each of the two edges $i = 1$ and $i = L$. We will couple the sites close to the $i = L$ edge to an absorbing bath. When studying the topologically nontrivial case, we will therefore consider a chain with an odd number of sites L and $\delta T > 0$. In this case there is a spin-degenerate edge state localized close to the $i = 1$ edge only. This is a convenient choice which does not affect the physics close to the $i = 1$ edge.

The impurity part of the Hamiltonian is given by

$$H_{\text{imp}} = J s_{i_0} S - B S. \quad (4)$$

Here, $S = (S_x, S_y, S_z)$ denotes classical spin of length $S = \frac{1}{2}$. This is coupled via a local antiferromagnetic ($J > 0$) exchange to the local spin of the electron system $s_{i_0} = \frac{1}{2} \sum_{\sigma\sigma'} c_{i_0\sigma}^\dagger \tau_{\sigma\sigma'} c_{i_0\sigma'}$ at site i_0. Here, τ is the vector of Pauli spin matrices. Throughout the study, we will couple the classical spin to the edge site $i_0 = 1$. Furthermore, the model includes an external local magnetic field B which is used to drive the classical spin.

III. EQUATIONS OF MOTION AND ABSORBING BOUNDARIES

The motion of the classical spin is driven by the torque that is generated by the external local field B and by the torque due to the local magnetic moment $\langle s_{i_0} \rangle = \langle \Psi(t) | s_{i_0} | \Psi(t) \rangle$ of the electron system. Here, $|\Psi(t)\rangle$ is the N-electron state at time t. With the help of the one-particle reduced density matrix $\rho(t)$ defined as

$$\rho_{i\sigma i'\sigma'}(t) = \langle \Psi(t) | c_{i'\sigma'}^\dagger c_{i\sigma} | \Psi(t) \rangle, \quad (5)$$

the equation of motion for the classical spin can be written as:

$$\frac{d}{dt}\mathbf{S}(t) = J\langle \mathbf{s}_{i_0}\rangle_t \times \mathbf{S}(t) - \mathbf{B} \times \mathbf{S}(t). \qquad (6)$$

The one-particle reduced density matrix satisfies a von Neumann-type equation of motion,

$$i\frac{d}{dt}\boldsymbol{\rho}(t) = [\mathbf{T}^{(\mathrm{eff})}(t), \boldsymbol{\rho}(t)], \qquad (7)$$

where $\mathbf{T}^{(\mathrm{eff})}(t)$ is an effective, time-dependent hopping matrix with the elements

$$T^{(\mathrm{eff})}_{i\sigma i'\sigma'}(t) = T_{ii'}\delta_{\sigma\sigma'} + \delta_{ii'}\frac{J}{2}\mathbf{S}(t)\boldsymbol{\tau}_{\sigma\sigma'}, \qquad (8)$$

and where $T_{ii'}$ are the elements of the standard hopping matrix $\mathbf{T}$. Its nonzero elements are given by $T_{i,i+1} = -(T + (-1)^i\delta T) = T_{i+1,i}$ for $i = 1, ..., L - 1$. Let us emphasize that we do not have to construct the N-electron state $|\Psi(t)\rangle$ explicitly, since Eqs. (6) and (7) form a closed nonlinear set of ordinary differential equations. This is due to the fact that the electron system is effectively noninteracting such that $|\Psi(t)\rangle$ is a simple Slater determinant at any point of time t. In Refs. [41,52] the foundations of the dynamics of quantum-classical hybrid systems and the concrete derivation of the equations of motion are discussed in detail. We note that the equations of motion (6) and (7) imply the conservation of the total energy $\langle H\rangle$, the total particle number $N = \sum_{i\sigma}\langle c^{\dagger}_{i\sigma}c_{i\sigma}\rangle$, and (for $B = 0$) the total spin $\mathbf{S} + \sum_i\langle\mathbf{s}_i\rangle$.

At time $t = 0$ the system is prepared in the ground state for a field pointing in the x direction. This aligns the classical spin, $\mathbf{S}(t = 0) \propto \mathbf{e}_x$. We set the according effective hopping matrix $\mathbf{T}^{(\mathrm{eff})}(t = 0)$ for the given spin direction, and, via numerical diagonalization of $\mathbf{T}^{(\mathrm{eff})}(0)$, compute the initial density matrix as the corresponding ground-state density matrix: $\boldsymbol{\rho}(t = 0) = \Theta(\mu\mathbf{1} - \mathbf{T}^{(\mathrm{eff})}(0))$. Here, Θ is the Heaviside step function and $\mu = 0$. To initiate the dynamics, we then suddenly flip the field to the z direction and hold the field direction and strength constant for $t > 0$.

We are interested in tracing the time evolution up to the point, where the system is fully relaxed, i.e., where locally, close to i_0, the system reaches its ground state. This defines the spin relaxation time τ. As the computational effort for solving the equations of motion scales as L^3 for large L, one is in practice limited to a system size of $L \lesssim 1000$. For gapped systems discussed below, the relaxation time is typically large (up to 10^5 inverse hoppings). This implies that one cannot avoid unwanted finite-size effects due to reflection of the excitations initiated at i_0 from the opposite system edge simply by taking a sufficiently large system.

The problem can be solved, however, by using absorbing boundary conditions. As is discussed in detail in Ref. [51], these can be realized within the framework of the Lindblad master equation, i.e., by coupling the outmost $L_B \ll L$ sites $i = L - L_B + 1, ..., L$ of the system to a bath that fully absorbs the spin and energy of any excitations emitted from the spatial region close to the edge at $i = 1$, where the classical spin is coupled. A naive application of the Lindblad equation, however, has been demonstrated as being inadequate. One must in fact carefully exclude artifacts that could be introduced at $t = 0$ and early times due to the coupling to the bath itself.

This can be taken care of with a matrix formulation of the Lindblad equation which still respects the Hermiticity and the non-negativity of $\boldsymbol{\rho}(t)$ at all times t and by a special choice of the (matrix) Lindblad parameters. Following our previous work [51] this results in replacing Eq. (7) by

$$i\frac{d}{dt}\boldsymbol{\rho}(t) = [\mathbf{T}^{(\mathrm{eff})}(t), \boldsymbol{\rho}(t)] - i\{\boldsymbol{\gamma}, \boldsymbol{\rho}(t) - \boldsymbol{\rho}(0)\}. \qquad (9)$$

The coupling of the outermost L_B sites to the bath is regulated by the diagonal matrix $\boldsymbol{\gamma}$ with diagonal elements $\gamma_{i\sigma,i\sigma} = \gamma_i$ for $i = L - L_B + 1, ..., L$ and $\gamma_{i\sigma,i\sigma} = 0$ else. The precise site dependence of γ_i is not very important. Here, we employ a linear profile: $\gamma_i = (i - (L - L_B))\gamma_{\min}$ for $i = L - L_B + 1, ..., L$ with a single parameter $\gamma_{\min}$. Clearly, when employing absorbing boundary conditions, energy and spin conservation only holds locally, for $i < L - L_B$. Due to manifest particle-hole symmetry, on the other hand, conservation of the total particle number still holds.

IV. TOPOLOGICALLY TRIVIAL CASE

Numerical results will be discussed for the topologically trivial case $\delta T < 0$ first. The upper panel of Fig. 2 displays the
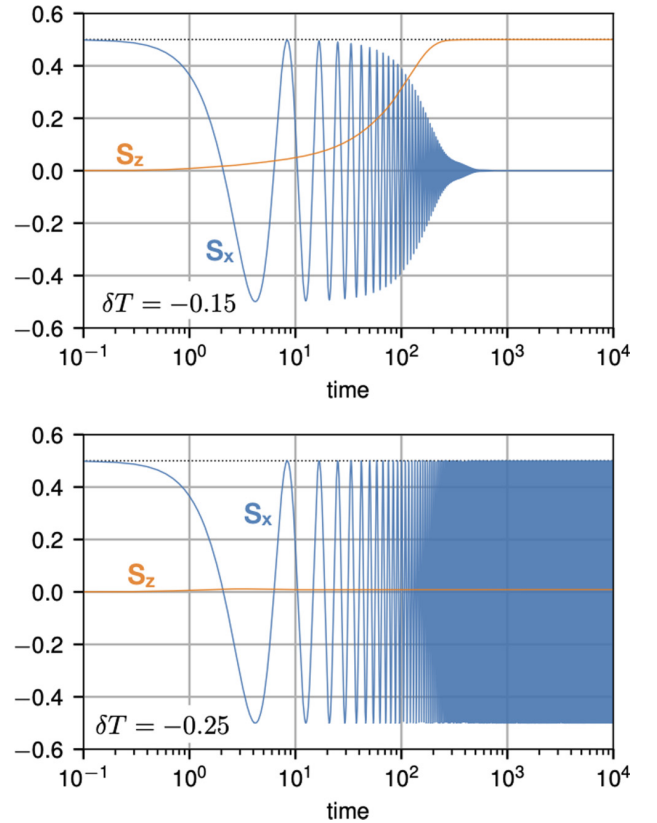

FIG. 2. Real-time dynamics of the impurity spin after a sudden flip of the local magnetic field from the x to z direction at time $t = 0$. Calculations for a system with $L = 46$ sites, exchange interaction $J = 1$, field strength $B = 0.75$. Upper panel: $\delta T = -0.15$, lower panel: $\delta T = -0.25$. Absorbing boundary conditions with $L_B = 4$ and $\gamma_{\min} = 0.2$. Energy and time units are set by the hopping integral $T \equiv 1$.
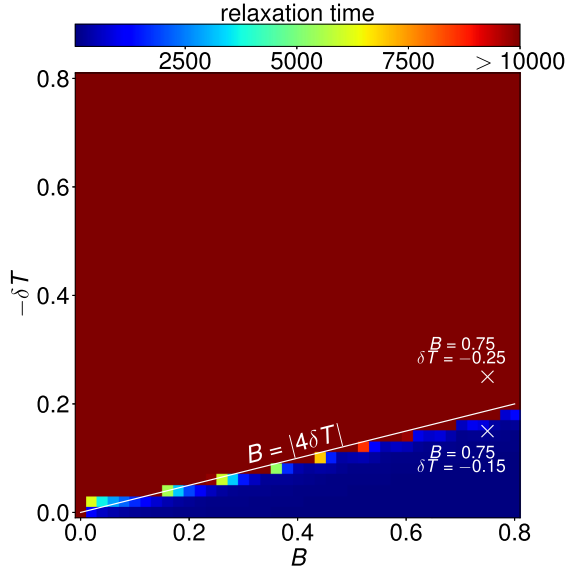
FIG. 3. Relaxation time τ (see color code) as a function of $-\delta T$ and B. Note that the dark red region filling most of the phase diagram indicates relaxation times $\tau > 10^4$. Other parameters as in Fig. 2. White line: $B = 4|\delta T|$. White crosses: parameter sets used in Fig. 2.

time evolution of the x and z component of the impurity spin for $\delta T = -0.15$. After the sudden flip of the field $\boldsymbol{B} = Be_x \mapsto Be_z$, the spin immediately starts to precess around the z axis, as can be seen in the x and y component (not shown) of $\boldsymbol{S}(t)$. The precession frequency is approximately given by the Larmor frequency $\omega_p \approx B$. Additionally, there is a damping effect due to the coupling of the spin to the electron system. This is seen in the z component of $\boldsymbol{S}(t)$, which steadily increases with time until at $\tau \approx 500$ the system is fully relaxed and the spin is aligned to the new field direction. This is a plausible result which is qualitatively similar to the spin dynamics seen in the case of a metallic electron system [41,51].

We have regularly checked the reliability of the calculations. Results obtained with absorbing boundary conditions for system size L are compared with those for much larger systems with open boundary conditions on the short time scale before reflections from the edge opposite to the impurity spin set in. We also compare calculations performed with absorbing boundary conditions for different system sizes and have checked that results do not depend on L. Systems as small as $L = 46$ turn out as fully sufficient for convergence. The parameters L_B and γ_{min} are optimized to suppress backscattering of excitations from the opposite edge of the system. This is in fact the case for the parameter choices made here. A detailed discussion is given in Ref. [51].

In the lower panel of Fig. 2 the result of a calculation with the same parameters but for $\delta T = -0.25$ is shown. Here, we see the same precessional motion but there is almost no damping of the spin up to a propagation time $t = 10^4$. We conclude that the relaxation time crucially depends on the hopping parameters and thus on the size of the gap $\Delta = 4|\delta T|$.

An overview is given with Fig. 3. Here we display the spin relaxation time τ as a function of $-\delta T > 0$ and B. Each point in the phase diagram is obtained from an independent

calculation solving the full set of equations of motion (6) and (7). For a definitive pragmatic definition, we fix τ as the shortest time for which the z component of $\boldsymbol{S}$ is larger than 95% of its fully relaxed value, i.e., $S_z(t > \tau) > 0.475$. Other choices would not significantly affect the phase diagram and the interpretation. There is a relatively clear separation between parameter sets for which spin relaxation is seen and those where the spin is not relaxed on the maximum propagation time scale $t = 10^4$ considered. For fixed δT and with decreasing field strength B, the spin-relaxation time diverges at a critical field. This is quite precisely given by $B = 4|\delta T|$, i.e., we find that the system relaxes, if $B > \Delta = 4|\delta T|$. We have also checked that this result does not depend on the initial direction of the classical spin. Calculations with initial directions $\boldsymbol{S}(t = 0) = \frac{1}{2}(\cos\varphi, 0, \sin\varphi)$ for various angles φ yield essentially the same phase diagrams and, in particular, the same phase boundary separating parameter regions leading to full spin relaxation or not.

To understand the phase boundary, we first consider the excitation energy, which is pumped into the system at $t = 0$ due to the sudden field switch. This is given by $E_{ex} = E_{fin} - E_{ini}$, where E_{ini} is the ground-state energy of the whole system and where E_{fin} is the energy right after the sudden flip of the field direction. Note that, due to total energy conservation, $E_{fin} = \text{const.}$ for early times until excitations of the electron system are absorbed at the opposite boundary. Right after the switch of the field, the energy of the Fermi sea $\langle H_0 \rangle$ and the exchange-coupling energy $J\langle s_{i_0}\rangle\boldsymbol{S}$ are unchanged. Hence, $E_{ex} = -\boldsymbol{B}_{fin}\boldsymbol{S} - (-\boldsymbol{B}_{ini}\boldsymbol{S}) = \boldsymbol{B}_{ini}\boldsymbol{S} = B/2$, since $\boldsymbol{B}_{fin} \perp \boldsymbol{S}$ and $|\boldsymbol{S}| = 1/2$. This energy must be dissipated to the bulk to achieve complete spin relaxation.

Since the lowest excitation energy of the electron system is given by the gap $\Delta = 4|\delta T|$, it is tempting to assume that spin relaxation is possible if $E_{ex} > \Delta$, i.e., if $B > 8|\delta T|$. Obviously, however, this argument cannot explain the different spin dynamics seen in the upper and the lower panel of Fig. 2— it would predict absence of spin relaxation for both cases, $\delta T = -0.15$ and $\delta T = -0.25$ at $B = 0.75$. It is at variance with the phase boundary displayed in Fig. 3 by a factor of two. In fact, the argument misses that the exchange coupling $Js_{i_0}\boldsymbol{S}$ mediates virtual processes at order J^2. Such processes can slightly tilt the classical spin and reduce its potential energy in the external field by an arbitrarily small amount.

This can be formalized by time-dependent perturbation or linear-response theory, see Refs. [41,44–46,53], for example: In first order in J, the response of the local magnetic moment $\langle s_{i_0}\rangle_t$ at time t due to the classical spin $\boldsymbol{S}(t)$ is given via the Kubo formula as

$$\langle s_{i_0}\rangle_t = J \int_0^t dt' \chi_{loc}(t - t')\boldsymbol{S}(t') , \qquad (10)$$

where $\chi_{loc}(t) \equiv \chi_{loc,\alpha\alpha}(t)$ $(\alpha = x, y, z)$ is the retarded isotropic local magnetic susceptibility $\chi_{loc,\alpha\beta}(t - t') = -\Theta(t - t')\langle[s_{i_0}^\alpha(t), s_{i_0}^\beta(t')]\rangle$. Inserting Eq. (10) in the equation of motion (6) for $\boldsymbol{S}(t)$ yields an integrodifferential equation

$$\frac{d}{dt}\boldsymbol{S}(t) = \boldsymbol{S}(t) \times \boldsymbol{B} - J^2\boldsymbol{S}(t) \times \int_0^t dt' \chi_{loc}(t - t')\boldsymbol{S}(t'). \quad (11)$$

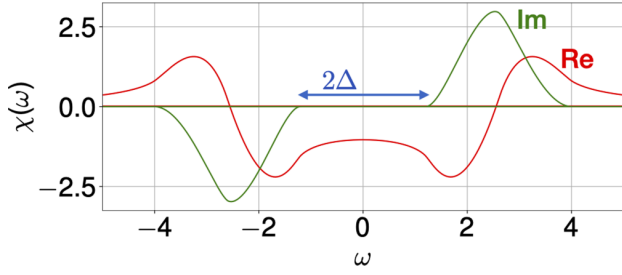This shows that spin damping originates from the second term as a memory effect. Furthermore, with Eq. (11) it is

FIG. 4. Imaginary and real part of the local retarded spin susceptibility χ_{loc} as a function of the excitation energy ω at the edge site $i = 1$ of the SSH model. Calculation for the topologically trivial case $\delta T = -0.3$.

straightforward to see that, disregarding a transient effect at early t, a precessional motion of the x, y components of $\boldsymbol{S}$ with frequency $\omega_{\mathrm{p}} = B$ induces a change of its z component $\dot{S}_z \propto J^2 \mathrm{Im}\,\chi_{\mathrm{loc}}(\omega = B)$, where $\chi_{\mathrm{loc}}(\omega) = \int d\tau\,\chi_{\mathrm{loc}}(\tau)e^{i\omega\tau}/2\pi$ is the frequency-dependent susceptibility. This implies that spin damping is obtained if

$$\mathrm{Im}\,\chi_{\mathrm{loc}}(\omega = B) \neq 0. \qquad (12)$$

For a noninteracting system of electrons, the susceptibility $\chi_{\mathrm{loc}}(\omega)$ is given by a convolution of the occupied with the unoccupied part of the local density of states $\rho_{\mathrm{loc}}(\omega)$ (LDOS). Hence, one finds that spin excitations are gapped and that the spin gap is twice the one-particle excitation gap. This can also be demonstrated explicitly by computing (see Ref. [41])

$$\chi_{\mathrm{loc}}(t) = \Theta(t)\mathrm{Im}[(e^{-i\boldsymbol{T}t}\Theta(\boldsymbol{T}-\mu))_{i_0 i_0}(e^{i\boldsymbol{T}t}\Theta(\mu-\boldsymbol{T}))_{i_0 i_0}] \qquad (13)$$

via numerical diagonalization of the unperturbed ($J = 0$) hopping matrix $\boldsymbol{T}$ of the SSH model. The Fourier transform is easily obtained numerically and shown in Fig. 4. We see that the imaginary part vanishes for frequencies with $-\Delta < \omega < \Delta$, where $\Delta = 4|\delta T|$ is the one-particle excitation gap. There­with, the condition (12) for spin damping reads as $B > \Delta = 4|\delta T|$. This nicely fits with the boundary in the dynamical phase diagram, see the white line in Fig. 3. We conclude that linear-response theory well describes the topologically trivial case.

V. TOPOLOGICALLY NONTRIVIAL CASE

When the spin is coupled to a site $i_0 \approx L/2$ in the bulk of the system, its relaxation behavior is fully determined by the bulk electronic structure and by the bulk band gap in particular. This means that there is no difference in the spin dynamics upon a sign change of δT, cf. Eq. (3). This has been checked and verified numerically.

However, in the topologically nontrivial case for $\delta T > 0$, there is a protected edge state localized around $i = 1$. Its spin degeneracy is lifted due to the exchange coupling to the classical spin, which is coupled to the electron system at site $i_0 = 1$, and in the ground state at half filling ($\mu = 0$) the state of the spin doublet with lower eigenenergy is fully occupied. The presence of this polarized edge state is expected to affect the mechanism for the relaxation of the classical impurity
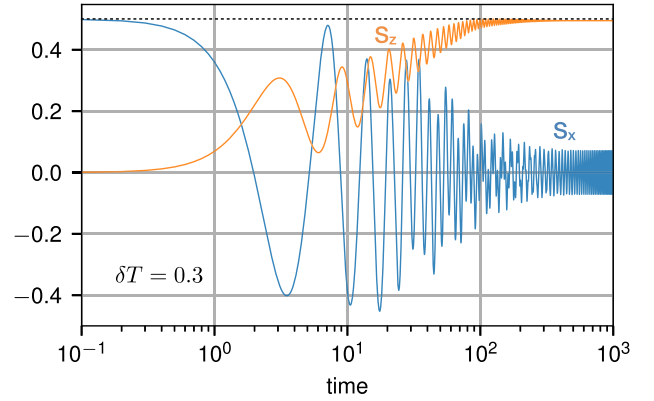

FIG. 5. Impurity spin dynamics for $\delta T = 0.3 > 0$ after a sudden flip of the local magnetic field from the x to z direction at time $t = 0$. Calculations for $L = 47$, $J = 1$, $B = 0.75$. Absorbing boundary conditions with $L_B = 5$ and $\gamma_{\min} = 0.2$.

spin. We consider systems with an odd number of sites L such that there is no edge state at the opposite edge, where a few sites are coupled to the absorbing bath.

A. Pre-relaxation

An example for the impurity-spin dynamics is given with Fig. 5. Compared to the topologically trivial case, see Fig. 2, the result is qualitatively different. Overall, the time evolution is somewhat more complicated and composed of at least two oscillations with different frequencies, rather than one major oscillation as in the absence of the edge state.

At early times $t \lesssim 100$, a simple precessional dynamics is seen with only slight irregularities and with a well defined precession frequency which is close to but somewhat higher than the Larmor frequency B. At later times the spin starts to relax and to align to the new field direction $\boldsymbol{B} = B\boldsymbol{e}_z$. In a temporal transition regime around $t = 100$, the dynamics is less simple.

For $t \gg 100$, however, a quite regular dynamics is seen again. Here, S_z approaches as a constant. We find $S_z/S > 95\%$, i.e., spin relaxation according to our pragmatic definition above, but clearly S_z stays smaller than its fully relaxed value $S_z = S$. In fact, up to a time scale of $\tau = 1 \times 10^5$, we do not see any indication for a complete relaxation of the spin. S_z rather saturates at a value $S_z \approx 0.495 < S$. We refer to this behavior as "pre-relaxation." Accordingly, the transversal x and y components undergo a precessional motion. The corresponding frequency is $\omega_{\mathrm{p}} \approx 0.285$, i.e., much smaller than the Larmor frequency $\omega_{\mathrm{p}} = B = 0.75$. The cause of the incomplete relaxation is discussed below in Sec. V D.

The pre-relaxation process in fact takes place in a large parameter range of the dynamical phase diagram. This is quantified in Fig. 6, where the relaxation time τ is again pragmatically defined as the shortest time for which $S_z/S > 95\%$. This is the same criterion used for the topologically trivial case. We see that the phase diagram is roughly similar to the one obtained in the absence of the edge state, cf. Fig. 3. The parameter range, where (pre-)relaxation is observed, however, considerably extends beyond the $B = 4|\delta T|$ line, which, for
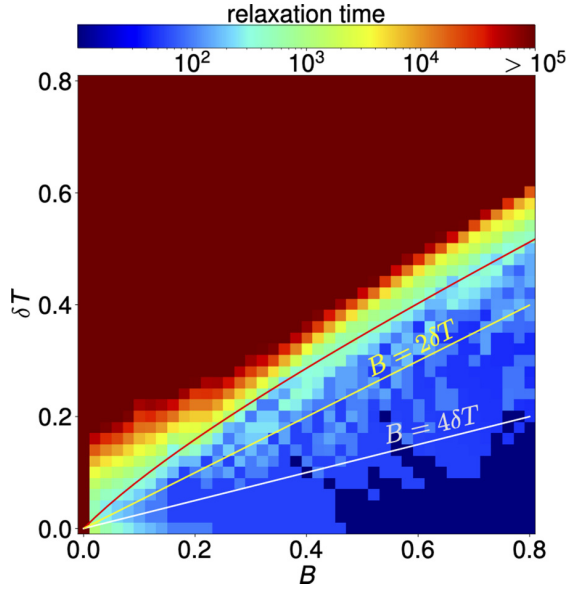
FIG. 6. Dynamical phase diagram as in Fig. 3 but for the topologically nontrivial case with $\delta T > 0$ and $L = 47$. τ (color code): shortest time for which $S_z/S > 95\%$. Dark red: $\tau > 10^5$. White line: $B = 4|\delta T|$. Yellow line: $B = 2|\delta T|$. Curved red line: see text.

the topologically trivial case, was obtained from the linear-response approach. Furthermore, the relaxation time no longer increases monotonically with δT in general, and we observe certain narrow parameter ranges with comparatively fast pre-relaxation. We also note that the numerical determination of the pre-relaxation time becomes difficult for very weak $B \lesssim 0.01$.

In an attempt to understand the phase boundary of the (pre-) relaxation regime we consider linear-response theory again. The $J = 0$ retarded local magnetic susceptibility at $i_0 = 1$ is shown in Fig. 7. However, as compared to the topologically trivial case, Fig. 4, there are important differences. First, the edge state at $\omega = 0$ in the LDOS gives rise to a δ peak in the imaginary part of $\chi_{\text{loc}}(\omega)$. We note that this cannot contribute to the spin damping since, according to the
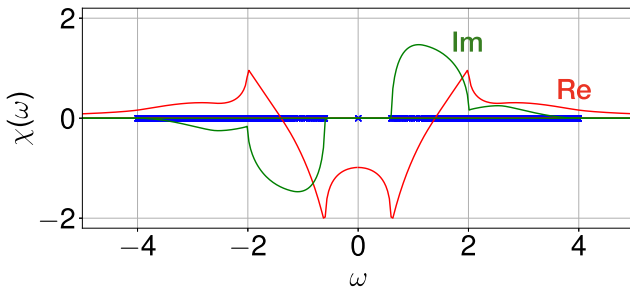

FIG. 7. Imaginary and real part of the local retarded spin susceptibility $\chi_{\text{loc}}(\omega)$ of the SSH model at site $i_0 = 1$. Results for the topologically nontrivial case $\delta T = 0.3$. Blue crosses indicate the positions of the poles of $\chi_{\text{loc}}(\omega)$. Note that there is a pole at $\omega = 0$ lying in the spin gap and that the resulting δ-like peak in the imaginary part of $\chi_{\text{loc}}(\omega)$ is not shown. At $\delta T = 0.3$, the spin gap is given by $\Delta = 4\delta T = 1.2$.

condition Eq. (12), it corresponds to the static case $B = 0$. Second, however, as the spin-degenerate edge state is filled by exactly one electron, it also mediates additional particle-hole excitations with finite excitation energy. Single-particle excitations from the highest occupied states of the lower band to the edge state and from the edge state to the lowest unoccupied states of the upper band have an energy of $\omega = 2\delta T = \Delta/2$, where Δ is the bulk band gap.

The susceptibility shown in Fig. 7 can be understood as the convolution of the occupied with the unoccupied part of the LDOS at $i_0 = 1$. Hence, due to the presence of the edge state, there are additional contributions to $\chi_{\text{loc}}(\omega)$ due to the convolution of the δ peak, resulting from the edge state, with the occupied and with the unoccupied parts of the local density of extended band states. This explains the additional broad peaks in Im $\chi_{\text{loc}}(\omega)$ around $\omega = \pm 1.2$, see Fig. 7. It also explains that the spin gap in $\chi_{\text{loc}}(\omega)$ equals the bulk band gap Δ, i.e., exactly half of the spin gap present in the topologically trivial case.

Figure 8 provides a schematic overview. Panel (a) of the figure, referring to the topologically trivial case, demonstrates that the LDOS with single-particle excitation gap Δ results in a spin gap of 2Δ. In the topologically nontrivial case, panel (b), the additional contributions to $\chi_{\text{loc}}(\omega)$ resulting from convolutions with the δ-like edge-state peak in the LDOS (yellow peaks), lead to a shrinking of the spin gap by the mentioned factor two.

We infer that, on the basis of standard linear-response theory, spin damping is expected to take place for $B > \Delta/2 = 2\delta T$. As is seen in Fig. 6, however, this prediction is still by far too restrictive. Pre-relaxation is found in a much larger parameter range. We conclude that linear-response theory cannot adequately explain the dynamical phase diagram and that the full theory is necessary to account for the effects of the edge mode on spin relaxation.

B. Spin splitting of the edge state

As it derives from lowest-order perturbation theory in J, the linear-response approach is based on the $J = 0$ spin susceptibility of the unperturbed SSH model. This misses at least two effects.

First of all, at finite J, the exchange coupling induces an internal Zeeman-like spin splitting of the edge state. Panel (c) of Fig. 8 indicates two spin-split localized edge states at energies $\omega = \pm\varepsilon_0$ (with $\varepsilon_0 > 0$) in the LDOS. The spin splitting of the edge state should have an impact on the relaxation dynamics.

In an *ad hoc* extension of the linear-response theory, it is tempting to employ the resulting $J > 0$ spin susceptibility in the criterion (12) to determine the phase boundary for (pre-) relaxation in the dynamical phase diagram Fig. 6, i.e., we replace the bare hopping matrix T by $T^{(\text{eff})}(t = 0)$. We refer to this approach as "renormalized" linear-response theory.

For weak J, the splitting can be calculated approximately by using first-order perturbation theory in J, i.e., we treat $\delta T = T^{(\text{eff})}(t = 0) - T$ as a perturbation of the bare hopping matrix T. Without loss of generality, we can assume that $S(0) = Se_z$ for the moment being. This implies that $\delta T = \text{diag}(\frac{1}{2}JS, -\frac{1}{2}JS, 0, 0, 0, ...)$ is diagonal in the basis of one-particle states $\{|i, \sigma\rangle\}$. We pick the unperturbed eigenvector
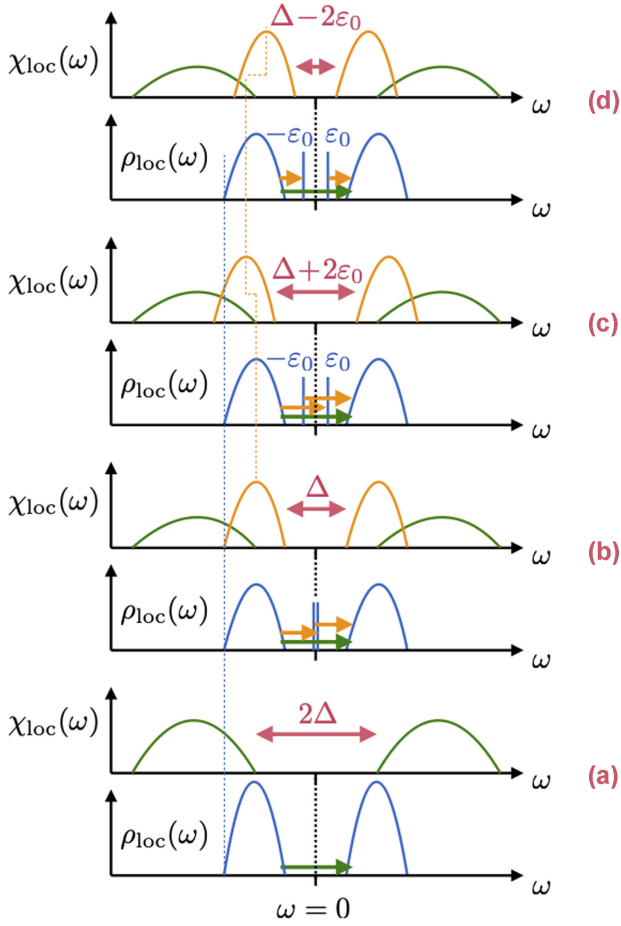
FIG. 8. Sketch of the the local density of states $\rho_{\text{loc}}(\omega)$ and (absolute value of the) imaginary part of the local spin susceptibility $|\text{Im}\chi_{\text{loc}}(\omega)|$ at site $i_0 = 1$. (a) Topologically trivial case, no edge state. (b) Topologically nontrivial case, $J = 0$, spin-degenerate edge state. (c) $J > 0$, spin-split edge state. (d) $J > 0$, spin-split edge state, nonequilibrium contributions to $\chi_{\text{loc}}(\omega)$. Δ is the bulk band gap of the density of states. Green: particle-hole excitations between occupied/unoccupied extended band states and resulting contributions to $\chi_{\text{loc}}(\omega)$. Yellow: particle-hole excitations involving the localized edge states and resulting contributions to $\chi_{\text{loc}}(\omega)$. Red: resulting spin gap.

$|\text{edge}, \uparrow\rangle$ of $\boldsymbol{T}$ corresponding to the eigenvalue zero in the spin-$\uparrow$ channel, i.e., the spin-$\uparrow$ edge state. Then,

$$\varepsilon_0 = \langle \text{edge}, \uparrow |\delta\boldsymbol{T}|\text{edge}, \uparrow\rangle > 0. \tag{14}$$

For the (spinful) SSH model (with $\sigma = \uparrow$) and in the limit $L \to \infty$, the expansion of the edge state in the one-particle basis states $|i, \sigma\rangle$ is given by [37]

$$|\text{edge}, \uparrow\rangle = \sum_{i=0}^{\infty} c_i |i, \uparrow\rangle, \tag{15}$$

where the coefficients $c_i = 0$ for even site index i and $c_i = (-T_1/T_2)^{(i-1)/2}c_1$ for odd i, and with T_1, T_2 given by Eq. (2). The modulus of c_1 is obtained from the normalization condition $\langle \text{edge}, \uparrow |\text{edge}, \uparrow\rangle = 1$ as $|c_1|^2 = 1 - (T_1/T_2)^2$. With
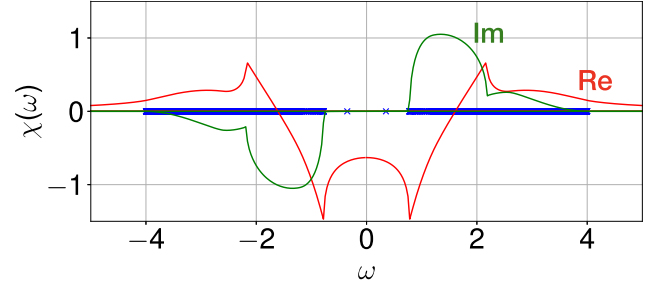

FIG. 9. Spin susceptibility $\chi_{\text{loc}}^{(xx)}(\omega)$ as in Fig. 7 but calculated with the effective hopping matrix at $J = 1$ for $\boldsymbol{S} = S\boldsymbol{e}_x$. Note that there are two poles at $\omega = \pm 2\varepsilon_0 \approx \pm 0.351$ lying in the spin gap and that the resulting δ-like peaks in the imaginary part of $\chi_{\text{loc}}(\omega)$ are not shown. At $\delta T = 0.3$, the spin gap is $1.55 \approx \Delta + 2\varepsilon_0 > \Delta = 4\delta T = 1.2$.

Eq. (14) this yields:

$$\varepsilon_0 = \frac{1}{2}JS\left(1 - \left(\frac{T - \delta T}{T + \delta T}\right)^2\right). \tag{16}$$

For $J = 1$ and $\delta T = 0.3$ we get $\varepsilon_0 \approx 0.178$.

We have numerically computed the xx component of the spin-susceptibility tensor $\chi_{\text{loc}}^{(xx)}(\omega)$ for $\boldsymbol{S}(t = 0) = S\boldsymbol{e}_x$ at $J = 1$ and $\delta T = 0.3$. The result is shown in Fig. 9. Opposed to Fig. 7, there are *two* isolated poles of the susceptibility $\omega = \pm 2\varepsilon_0$ resulting from the spin-split edge state. The numerical calculation yields $\varepsilon_0 \approx 0.176$, which is in fact very close to the perturbative result discussed above.

As visualized by panel (c) of Fig. 8, the spin splitting of the edge state yields a spin gap $\Delta + 2\varepsilon_0$ which is *larger* than the spin gap Δ obtained with the unrenormalized theory. This is due to the fact that an additional energy ε_0 is necessary to make transitions from occupied bulk states to the unoccupied edge state with energy $+\varepsilon_0$ possible, and vice versa for transitions from the occupied edge state with energy $-\varepsilon_0$ to unoccupied bulk states. This implies that the parameter region, where spin pre-relaxation is predicted, actually *shrinks* when taking into account that spin excitations are also mediated via the spin-split edge state, and that, therefore, the renormalized linear-response theory does *not* lead to an improved description.

C. Dynamic relaxation mechanism

A second effect missing in the standard linear-response approach is the dynamic occupation of states above and the depopulation of states below the Fermi energy. This nonequilibrium effect provides an additional important mechanism for spin relaxation.

Let us assume for a moment that the electron system follows the spin dynamics in a perfectly adiabatic way, i.e., that the state of the electron system at time t is given by the ground state of the system for the current direction of the classical spin at time t. The Hamiltonian of the spinful SSH model is invariant under global SU(2) spin rotations. This symmetry reduces to a U(1) rotation symmetry around the axis defined by the classical spin in case of a finite coupling $J > 0$. The local ground-state magnetic moment $\langle s_{i_0}\rangle_t$ of the electron
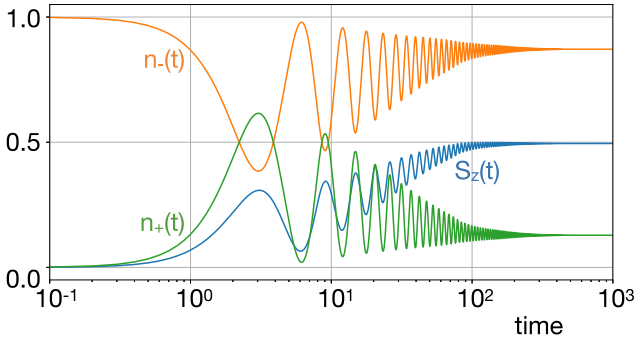
FIG. 10. Time evolution of the spin-dependent occupation $n_{\pm}(t)$ of the momentary spin-split edge state, compared to the z component of the classical spin. Calculation for $L = 47$, $L_B = 5$, $\gamma_{\min} = 0.2$, $J = 1$, $\delta T = 0.3$, and $B = 0.75$.

system at site i_0 must therefore align to $\boldsymbol{S}(t)$, such that the torque of the electron system on the classical spin [see Eq. (6)] vanishes at any instant of time, if the dynamics was perfectly adiabatic. This would imply that there is no spin damping at all. As this is not the case, we can thus safely assume that the dynamics is nonadiabatic. In fact, the numerical solution of the equations of motion shows that the local magnetic moment $\langle \boldsymbol{s}_{i_0} \rangle_t$ is always somewhat *behind* the motion of the classical spin $\boldsymbol{S}(t)$. This has already been noticed earlier in the context of a topologically trivial model [41].

Generally, a nonadiabatic time evolution does not make a big difference as long as bulk states are concerned, as these are barely affected by the impurity spin anyway. The spin-dependent occupation of the edge state, on the other hand, is greatly affected by the retardation effect. If, at a certain instant of time t, the edge state $|\text{edge}, \sigma\rangle$ is fully polarized, i.e., $n_{\uparrow}(t) = 1$ and $n_{\downarrow}(t) = 0$, where $\uparrow, \downarrow$ refers to the momentary quantization axis defined by the direction of $\boldsymbol{S}(t)$, it will stay at least partially polarized with respect to the same direction in space also at a slightly later time $t + \Delta t$. At time $t + \Delta t$, this represents a nonequilibrium configuration.

This effect leads to a *partial* occupation of the upper edge state while the lower edge state becomes less occupied. At time t we obtain the momentary spin-split edge states $|\text{edge}, \pm\rangle_t$ as those eigenstates of the effective hopping matrix $\boldsymbol{T}^{(\text{eff})}(t)$ that are localized close to $i_0 = 1$. Their occupation is obtained as $n_{\pm}(t) \equiv {}_t\langle \text{edge}, \pm | \boldsymbol{\rho}(t) | \text{edge}, \pm \rangle_t$, where $\boldsymbol{\rho}(t)$ is the one-particle reduced density matrix at time t.

Figure 10 displays the time dependence of $n_{\pm}(t)$. While at $t = 0$, the edge state is fully polarized, there is a partial polarization $n_+(t) - n_-(t) < 1$ for all $t > 0$. It oscillates with the frequency of the (damped) precessional motion of the classical spin. In the long-time limit, a partial polarization survives. This again reflects the fact that the spin relaxation is not complete, as has been noted earlier.

As visualized by panel (d) of Fig. 8, the nonequilibrium occupation of the spin-split edge state induces additional transitions, namely from the upper edge of the lower bulk band at $-\Delta/2$ to the *lower* edge state at $-\epsilon_0$, and from the *upper* edge state at ϵ_0 to the lower edge of the upper bulk band at $\Delta/2$. Within the renormalized linear-response theory this results in a nonequilibrium spin gap of $\Delta - 2\epsilon_0$, which in fact is

smaller than the spin gap Δ obtained with the unrenormalized theory. This implies that the parameter region, where spin pre-relaxation is expected, *extends*.

Using Eq. (12) again, but with the susceptibility of the nonequilibrium state, we can equate B with half of the spin gap and thus get $B = 2\delta T - \epsilon_0$ as our improved criterion for pre-relaxation. This is indicated in the dynamical phase diagram Fig. 6 by the red solid line. We note that this prediction quite convincingly describes the numerical data.

D. Incomplete spin relaxation

An explanation for the incomplete spin relaxation seen in Fig. 5 is still missing and shall be discussed here. Figure 5 shows that most of the energy pumped into the system via the sudden flip of the field direction is dissipated to the bulk. However, the dissipation process is not complete. For times later than the pre-relaxation time scale τ, the impurity spin is close to full alignment with the field $\boldsymbol{B}$ but it is trapped in a state where it steadily precesses around $\boldsymbol{B}$ without any further relaxation.

We note that the increase of the z component of the impurity spin has stopped at $S_z \approx 0.495 < 0.5 = S$ which implies that $\boldsymbol{S}$ encloses a small angle of $\gamma \approx 0.01$ with the field direction. In this pre-relaxed state the contribution $\boldsymbol{B} \times \boldsymbol{S}$ to the total torque on $\boldsymbol{S}$ can be neglected safely. The total torque is then dominated by the torque resulting from the local moment at $i_0 = 1$, i.e., by $J\langle \boldsymbol{s}_{i_0} \rangle_t \times \boldsymbol{S}(t)$.

As can be read off from Fig. 10, there is a contribution of about $(0.75$–$0.25)/2 = 0.25$ to the size of the local moment $|\langle \boldsymbol{s}_{i_0} \rangle_t|$ due to the polarization of the edge state. We assume that this is the dominant contribution to the moment $|\langle \boldsymbol{s}_{i_0} \rangle_t|$ at site i_0. This implies that, at $J = 1$, the precession frequency is $\omega_p \approx 0.25$. In fact, we can read off $\omega = 0.285$ from the numerical calculation, see Fig. 5, supporting this assumption.

Varying parameters, we first of all find that ω_p is almost independent of B, which again reflects that the field contribution to the torque is negligible. Furthermore, the edge-state polarization can be increased when increasing δT since this increases the spin splitting of the edge state according to Eq. (16), and thus $|\langle \boldsymbol{s}_{i_0} \rangle_t|$ and therewith ω_p should increase with increasing δT. This is verified numerically as well. As a function of J, the precession frequency ω_p increases approximately linearly with J in the range $0 < J \lesssim 1$. Also this trend is easily explained since, apart from the retardation effect discussed in Sec. V C, the edge state is strongly polarized at $\delta T = 0.3$, so that the J dependence of ω_p is almost exclusively due to bare coupling constant itself. All in all these considerations explain the transition from a precessional motion with Larmor frequency $\omega_p \approx B$ at early times to a frequency $\omega_p \approx J|\langle \boldsymbol{s}_{i_0} \rangle_t|$ in the pre-relaxed state at late times.

They also explain that the relaxation process must stop at some point. Recall that the basic argument explaining the dynamic phase boundary for spin relaxation fundamentally builds on the assumption that the impurity spin dynamics can be described, to a good approximation, by a precessional motion with a well-defined precession frequency. At early times this is in fact given by the Larmor frequency $\omega_p = B$. At late times, however, the field contribution is negligible, so that we have to apply our basic criterion for spin relaxation with

B replaced by the actual precession frequency $\omega_p \approx J|\langle s_{i_0}\rangle_t|$ in the pre-relaxed state. This yields $\omega_p > 4\delta T$ as a condition for spin damping, and with $\omega_p = 0.285$ at late times and $4\delta T = 1.2$, this condition is clearly violated.

We conclude that the observed spin pre-relaxation scenario first of all requires that the field B is sufficiently strong, compared to the band gap, to get initial spin relaxation, and that, at early times, the contribution of $\boldsymbol{B} \times \boldsymbol{S}$ to the total torque on $\boldsymbol{S}$ is dominating. As the initial relaxation proceeds, the further and further alignment of $\boldsymbol{S}$ and $\boldsymbol{B}$ just implies that this contribution diminishes. In the course of time there may be a gradual transition to a regime where the electronic contribution $J\langle s_{i_0}\rangle \times \boldsymbol{S}$ to the total torque on $\boldsymbol{S}$ becomes dominant. In such a case, even if B would be strong enough to feature relaxation, only the relation between the precession frequency at late times $J|\langle s_{i_0}\rangle|$ and the gap size decides whether or not there is full relaxation or whether the system dynamics is finally trapped in a pre-relaxed steady state.

A dominating electronic contribution is not so much favored by a strong coupling constant J since this suppresses the retardation effect and enforces alignment of $\langle s_{i_0}\rangle$ and $\boldsymbol{S}$. Strong J thus rather leads to a small electronic contribution to the total torque. Much more important is a strong polarizability of the local electronic moment $\langle s_{i_0}\rangle$ at site i_0 due to the classical spin $\boldsymbol{S}$ at intermediate J. The presence of the topological edge state very much enhances this polarizability as it is precisely half filled. However, the polarizability also crucially depends on the spatial extension of the edge state and is at a maximum for an edge state that is completely localized at i_0. Hence, one may argue that a late transition to a pre-relaxed steady state is more characteristic for a one-dimensional system opposed, e.g., to a topological surface state at the boundary of a two-dimensional topological insulator which has a finite one-dimensional dispersion and extends along a one-dimensional boundary, such that the local polarization at i_0 will be much weaker.

E. Direct comparison with linear-response theory

Our arguments explaining the absence or the occurrence of spin relaxation are built on the framework of linear-response theory, and we have already seen that various inconsistencies show up when naively applying this approach and that refined considerations are necessary for the correct physical picture. Therefore, a *direct* comparison of linear-response theory with the full spin-dynamics theory should be instructive. Figure 11 displays the predictions of linear-response (LR) and full theory for the impurity-spin dynamics in various parameter regimes. Panel (a) gives an example for the topologically trivial case ($\delta T = -0.3$), similar to the upper panel in Fig. 2. The field $B = 1.75$ is larger than the gap $4|\delta T| = 1.2$ and, therefore, we expect complete relaxation of the impurity spin. This is in fact found by LR theory when numerically solving the integrodifferential equation (11), see blue lines in (a). However, when compared with the full theory, either for a larger system with $L = 200$ and open boundaries, or for a smaller system with $L = 46$ and an absorbing boundary (on the edge opposite to the impurity spin), see green and orange lines, respectively, strong differences are visible. Most notably, the LR approach significantly overestimates the spin-
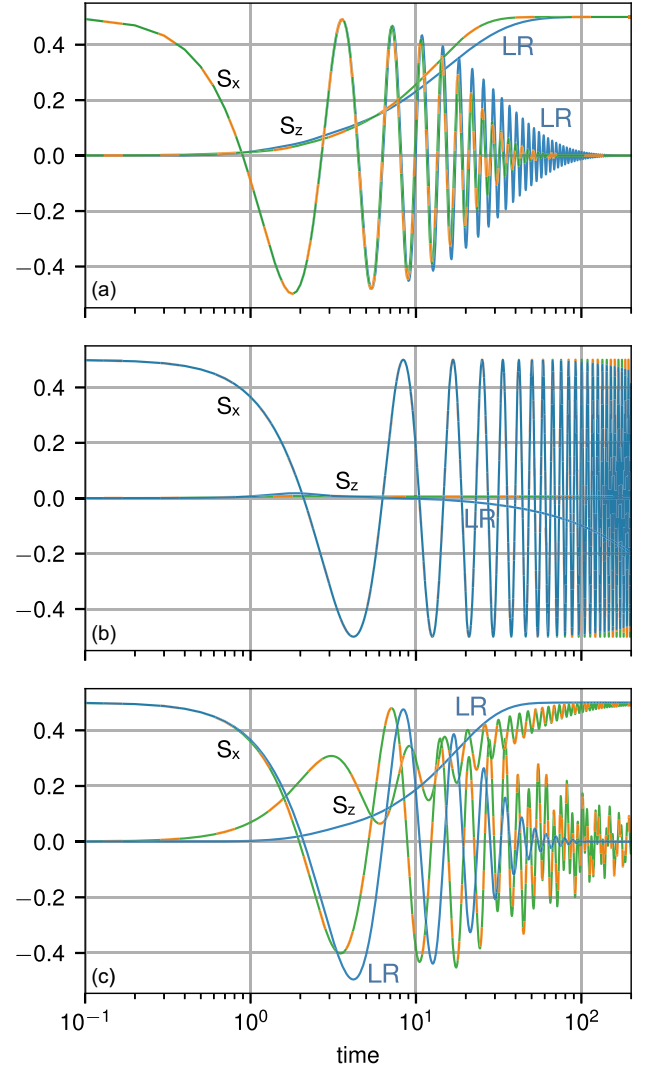

FIG. 11. Real-time dynamics of the impurity spin after a sudden flip of the local field from the x to z direction. Panels (a),(b): $\delta T = -0.3$ (topologically trivial) with $B = 1.75 > 4\delta T$ (a) and $B = 0.75 < 4\delta T$ (b). Panel (c): $\delta T = +0.3$ (nontrivial), $B = 0.75 < 4\delta T$. Results as obtained from three different approaches. Blue lines: linear-response theory (LR) for $L = 500$ [panels (a),(b)] and $L = 501$ [panel (c)]. Green lines: spin-dynamics theory for $L = 200$ [(a),(b)] and $L = 201$ (c) with open boundaries. Orange lines: spin-dynamics theory for $L = 46$ [(a),(b)] and $L = 47$ (c) and absorbing boundaries [with $L_B = 20$, $\gamma_{min} = 0.05$ in (a), and $L_B = 5$, $\gamma_{min} = 0.2$ in (b),(c)]. In all cases $J = 1$. Note the logarithmic time scale.

relaxation time, by about a factor of two. On the other hand, there is no visible discrepancy between the calculations with open and with absorbing boundaries.

In panel (b) the field $B = 0.75$ is smaller than the gap $4|\delta T| = 1.2$, and hence relaxation is not expected to take place (cf. the lower panel of Fig. 2). Full spin-dynamics theory with open and with absorbing boundary do not differ visibly. In both cases, the impurity spin shows an undamped precessional motion on the time interval displayed. Calculations with absorbing boundaries can be performed for much longer

MICHAEL ELBRACHT AND MICHAEL POTTHOFF

time scales and in fact do not show any relaxation effect at all (not shown). The numerical evaluation of linear-response theory is much more involved, such that we are basically restricted to the shorter time scale displayed in the figure. We note that already at early times, $t \approx 10$, the impurity spin starts to "relax," i.e., it develops a finite and even *negative z* component. This is not only at variance with the full spin-dynamics theory but also unphysical.

Finally, in panel (c) we compare the three approaches for the topologically nontrivial case. The real-time dynamics is more complicated in this case. The calculations performed with open and with absorbing boundary conditions match perfectly and show the pre-relaxation behavior as discussed above (cf. Fig. 5). Linear-response theory, on the other hand, still predicts *complete* spin relaxation, and the LR results look more similar to those obtained for the topologically trivial case in panel (a). We conclude that linear-response theory is not able to reproduce the correct physics quantitatively but also qualitatively. A deeper analysis of the causes of the difficulties of LR theory does not seem worthwhile, since spin-dynamics calculations with absorbing edges are numerically much easier and faster. Still, the criterion for spin relaxation, Eq. (12), derived within the linear-response theory, has proven as a rough but valuable guide for the understanding of the dynamical relaxation phase diagrams.

VI. CONCLUSIONS

The spinful SSH model with a classical impurity spin exchange coupled to the local magnetic moment of the electron system at one of the edge sites probably represents the simplest system which allows us to study the effect of a topological edge mode on the relaxation of the impurity spin. Using an absorbing boundary at the opposite edge, we have demonstrated that the coupled dynamics of impurity spin and electron system can be treated numerically exactly. We have used this approach to study the spin relaxation time.

The most obvious effect is the presence or absence of spin relaxation in certain parameter regimes. One can in fact construct a dynamical phase diagram with a rather sharp phase boundary. Comparing the phase diagrams for topologically trivial and nontrivial bulk electronic structures reveals significant differences which must be attributed to the absence or the presence of the topologically protected edge state, respectively.

For a qualitative understanding of the various dependencies on the relevant model parameters, however, a simplified framework is needed. We have argued that this is basically provided by the linear-response theory, i.e., by lowest-order perturbation theory in the coupling strength J.

Admittedly, the linear-response approach can dramatically fail in predicting the microscopic real-time dynamics, as has been demonstrated by direct comparison with the results of the full spin-dynamics theory. Furthermore, its numerical evaluation requires the solution of an integrodifferential equation and is thus much more costly compared to the full theory which must take the time-dependent electronic degrees of freedom into account explicitly but, thanks to the absorbing boundary, can be restricted to small system sizes. On the other hand, the linear-response theory provides an extremely handy and physically appealing criterion for spin relaxation based on the gap size of magnetic excitations.

We have shown that the naive application of this condition for spin relaxation works in the topologically trivial case but must be corrected in the nontrivial case. The most important mechanisms affecting the spin relaxation in the nontrivial case are the following: The presence of the edge state mediates additional spin-exchange processes and thus leads to a strong extension of the parameter regime where relaxation is possible. A renormalized linear-response theory is necessary to account for the effects of the spin splitting of the edge state. In a static picture, however, the spin splitting tends to suppress spin relaxation since the energy of the lowest-energy spin excitations involving the spin-split edge mode increases. We find that this is not the correct point of view and that one must apply a dynamical picture beyond the adiabatic approximation. Namely, the time evolution of the electronic structure and of the edge state in particular is considerably retarded and does not instantaneously follow the motion of the impurity spin. This causes a partial occupation of the upper edge state with energy above the Fermi energy, and vice versa some depopulation of the lower state of the spin-split Kramers pair, which in turn opens another lowest-energy channel for relaxation and in fact finally correctly describes the additional extension of the parameter regime for spin relaxation.

At late times where spin relaxation is almost completed, the magnetic-field term can be disregarded and the spin torque due to the local magnetic moment of the electron system may dominate. It then leads to a precessional motion which can be slowed down decisively due to the mentioned dynamical partial polarization of the edge mode such that the criterion for spin relaxation gets violated and the relaxation process comes to a halt. The resulting pre-relaxation or incomplete spin-relaxation phenomenon is frequently found in the numerical solution of the full set of equations of motion. However, it might represent an effect that is characteristic for one-dimensional systems only.

The present study has paved the way for investigations of the dynamics of individual spins or of spin arrays on two-dimensional Chern or Z_2 insulators, where new phenomena but also additional complications are expected. Some important differences will be due to the delocalization of the topological edge state along an extended one-dimensional edge such that its spin polarization will diminish, or additional features brought in by spin-momentum locking. Work along these lines is in progress.

ACKNOWLEDGMENTS

[1] F. D. Natterer, K. Yang, W. Paul, P. Willke, T. Choi, T. Greber, A. J. Heinrich, and C. P. Lutz, Nature (London) **543**, 226 (2017).

[2] R. Wiesendanger, Rev. Mod. Phys. **81**, 1495 (2009).

[3] A. J. Heinrich, J. A. Gupta, C. P. Lutz, and D. M. Eigler, Science **306**, 466 (2004).

[4] C. Hirjibehedin, C. Lutz, and A. Heinrich, Science **312**, 1021 (2006).

[5] J. Fransson, Nano Lett. **9**, 2414 (2009).

[6] J. Fernández-Rossier, Phys. Rev. Lett. **102**, 256802 (2009).

[7] J.-P. Gauyacq, N. Lorente, and F. D. Novaes, Prog. Surf. Sci. **87**, 63 (2012).

[8] M. Z. Hasan and C. L. Kane, Rev. Mod. Phys. **82**, 3045 (2010).

[9] X.-L. Qi and S.-C. Zhang, Rev. Mod. Phys. **83**, 1057 (2011).

[10] L. Fidkowski, T. S. Jackson, and I. Klich, Phys. Rev. Lett. **107**, 036601 (2011).

[11] R. S. K. Mong and V. Shivamoggi, Phys. Rev. B **83**, 125109 (2011).

[12] T. Fukui, K. Shiozaki, T. Fujiwara, and S. Fujimoto, J. Phys. Soc. Jpn. **81**, 114602 (2012).

[13] E. Prodan and H. Schulz-Baldes, *Bulk and Boundary Invariants for Complex Topological Insulators: From K-Theory to Physics* (Springer, Basel, 2016).

[14] L. A. Wray, S.-Y. Xu, Y. Xia, D. Hsieh, A. V. Fedorov, Y. S. Hor, R. J. Cava, A. Bansil, H. Lin, and M. Z. Hasan, Nat. Phys. **7**, 32 (2011).

[15] J. Honolka, A. A. Khajetoorians, V. Sessi, T. O. Wehling, S. Stepanow, J.-L. Mi, B. B. Iversen, T. Schlenk, J. Wiebe, N. B. Brookes, A. I. Lichtenstein, P. Hofmann, K. Kern, and R. Wiesendanger, Phys. Rev. Lett. **108**, 256811 (2012).

[16] M. R. Scholz, J. Sánchez-Barriga, D. Marchenko, A. Varykhalov, A. Volykhov, L. V. Yashina, and O. Rader, Phys. Rev. Lett. **108**, 256810 (2012).

[17] T. Valla, Z.-H. Pan, D. Gardner, Y. S. Lee, and S. Chu, Phys. Rev. Lett. **108**, 117601 (2012).

[18] F. Goth, D. J. Luitz, and F. F. Assaad, Phys. Rev. B **88**, 075110 (2013).

[19] T. Schlenk, M. Bianchi, M. Koleini, A. Eich, O. Pietzsch, T. O. Wehling, T. Frauenheim, A. Balatsky, J.-L. Mi, B. B. Iversen, J. Wiebe, A. A. Khajetoorians, P. Hofmann, and R. Wiesendanger, Phys. Rev. Lett. **110**, 126804 (2013).

[20] T. Eelbo, M. Waśniowska, M. Sikora, M. Dobrzański, A. Kozłowski, A. Pulkin, G. Autès, I. Miotkowski, O. V. Yazyev, and R. Wiesendanger, Phys. Rev. B **89**, 104424 (2014).

[21] Y. Li, X. Zou, J. Li, and G. Zhou, J. Chem. Phys. **140**, 124704 (2014).

[22] Y. Jiang, C. Song, Z. Li, M. Chen, R. L. Greene, K. He, L. Wang, X. Chen, X. Ma, and Q.-K. Xue, Phys. Rev. B **92**, 195418 (2015).

[23] C.-C. Chen, M. L. Teague, L. He, X. Kou, M. Lang, W. Fan, N. Woodward, K.-L. Wang, and N.-C. Yeh, New J. Phys. **17**, 113042 (2015).

[24] A. Pieper and H. Fehske, Phys. Rev. B **93**, 035123 (2016).

[25] P. Rüßmann, S. K. Mahatha, P. Sessi, M. A. Valbuena, T. Bathon, K. Fauth, S. Godey, A. Mugarza, K. A. Kokh, O. E. Tereshchenko, P. Gargiani, M. Valvidares, E. Jimenez, N. B. Brookes, M. Bode, G. Bihlmayer, S. Blügel, P. Mavropoulos, C. Carbone, and A. Barla, J. Phys. Mater. **1**, 015002 (2018).

[26] K. Sumida, M. Kakoki, J. Reimann, M. Nurmamat, S. Goto, Y. Takeda, Y. Saitoh, K. A. Kokh, O. E. Tereshchenko, J. Güdde, U. Höfer, and A. Kimura, New J. Phys. **21**, 093006 (2019).

[27] J. Bouaziz, M. S. Dias, F. S. M. Guimaraes, and S. Lounis, Phys. Rev. Mater. **3**, 054201 (2019).

[28] S. Pradhan and J. Fransson, Phys. Rev. B **100**, 125163 (2019).

[29] I. Garate and M. Franz, Phys. Rev. Lett. **104**, 146802 (2010).

[30] T. Yokoyama, J. Zang, and N. Nagaosa, Phys. Rev. B **81**, 241410(R) (2010).

[31] H. T. Ueda, A. Takeuchi, G. Tatara, and T. Yokoyama, Phys. Rev. B **85**, 115110 (2012).

[32] Y. Tserkovnyak and D. Loss, Phys. Rev. Lett. **108**, 187201 (2012).

[33] L. Chotorlishvili, A. Ernst, V. K. Dugaev, A. Komnik, M. G. Vergniory, E. V. Chulkov, and J. Berakdar, Phys. Rev. B **89**, 075103 (2014).

[34] A. Narayan, I. Rungger, and D. Sanvito, New J. Phys. **17**, 033021 (2015).

[35] W. P. Su, J. R. Schrieffer, and A. J. Heeger, Phys. Rev. B **22**, 2099 (1980).

[36] A. J. Heeger, S. Kivelson, J. R. Schrieffer, and W. P. Su, Rev. Mod. Phys. **60**, 781 (1988).

[37] J. Asbóth, L. Oroszlány, and A. Pályi, The Su-Schrieffer-Heeger (SSH) model, in *A Short Course on Topological Insulators*, Lecture Notes in Physics Vol. 919 (Springer, Cham, 2016).

[38] V. P. Antropov, M. I. Katsnelson, M. van Schilfgaarde, and B. N. Harmon, Phys. Rev. Lett. **75**, 729 (1995).

[39] W. Koshibae, N. Furukawa, and N. Nagaosa, Phys. Rev. Lett. **103**, 266402 (2009).

[40] A. Pertsova, M. Stamenova, and S. Sanvito, Phys. Rev. B **84**, 155436 (2011).

[41] M. Sayad and M. Potthoff, New J. Phys. **17**, 113058 (2015).

[42] G.-W. Chern, K. Barros, Z. Wang, H. Suwa, and C. D. Batista, Phys. Rev. B **97**, 035120 (2018).

[43] U. Bajpai and B. K. Nikolic, Phys. Rev. B **99**, 134409 (2019).

[44] M. Onoda and N. Nagaosa, Phys. Rev. Lett. **96**, 066603 (2006).

[45] S. Bhattacharjee, L. Nordström, and J. Fransson, Phys. Rev. Lett. **108**, 057204 (2012).

[46] N. Umetsu, D. Miura, and A. Sakuma, J. Appl. Phys. **111**, 07D117 (2012).

[47] B. Skubic, J. Hellsvik, L. Nordström, and O. Eriksson, J. Phys.: Condens. Matter **20**, 315203 (2008).

[48] R. F. L. Evans, W. J. Fan, P. Chureemart, T. A. Ostler, M. O. A. Ellis, and R. W. Chantrell, J. Phys.: Condens. Matter **26**, 103202 (2014).

[49] P.-W. Ma, S. L. Dudarev, A. A. Semenov, and C. H. Woo, Phys. Rev. E **82**, 031111 (2010).

[50] C. Lupo and C. Weber, Phys. Rev. B **100**, 195431 (2019).

[51] M. Elbracht and M. Potthoff, Phys. Rev. B **102**, 115434 (2020).

[52] H. Elze, Phys. Rev. A **85**, 052109 (2012).

[53] M. Sayad, R. Rausch, and M. Potthoff, Phys. Rev. Lett. **117**, 127201 (2016).

6 – Prerelaxation in Quantum, Classical, and Quantum-Classical Two-Impurity Models

In the last paper [III] we investigated the relaxation dynamics of three different types of impurity models. A purely quantum mechanical model, a purely classical model and a mixed quantum-classical model. Although they are different in nature, they all share a similar geometry: a one-dimensional host system, to which we attach two impurities.

6.1 – Stub Impurity Model

In the stub impurity model, we attach two impurity sites of spinless fermions to the center of a one-dimensional host system of also spinless fermions. This is depicted in Fig. III-2. We calculate the real-time dynamics and investigate how the occupation numbers at each site evolve over time. As the fermions are non-interacting this can be done relatively easy using the one-particle reduced density matrix.

Initially, the host system is in its ground state, and the impurities are fully occupied but decoupled from the host system. At $t = 0$, the coupling between the host system and the impurities V is switched on instantaneously. As the total system (host and impurities) is not in an equilibrium anymore, a dynamics is initiated. We find that for the dynamics there is a huge discrepancy between impurities coupled to nearest-neighbor sites and impurities coupled to next-nearest-neighbor sites of the host system. While the system relaxes completely for neighboring impurities as one might expect, the system does not relax fully for next-nearest-neighbor impurities and rather becomes trapped in some kind of metastable state with an ongoing oscillation.

We find that this phenomenon is caused by the existence of localized single particle eigenstates in the Hamiltonian of the full system (host system and impurities). These eigenstates only exist for the full system and were not there before the impurities were attached. One can treat this act of attaching the impurities to the host system as a quantum quench, and in this sense by attaching the impurities, we performed a quantum quench from a system with no localized eigenstates to a system with some localized eigenstates.

As already explained in Sec. 3.6, the existence of localized eigenstates in the post-quench Hamiltonian after a quantum quench can lead to non-vanishing fluctuations

in the GGE. Non-vanishing fluctuations have the consequence that the system cannot relax fully as it keeps on fluctuating forever. For next-nearest-neighbor impurities there are multiple localized eigenstates caused by attaching the impurities to the host system. These very states then lead to non-vanishing fluctuations and therefore no complete relaxation of the system.

Interestingly, there are also localized eigenstates in the post-quench Hamiltonian for nearest-neighbor impurities. However, their contribution to the fluctuations of the system cancel each other out due to parity-symmetry of the system. Therefore, all fluctuations in the system vanish after some time and the system relaxes completely.

6.2 – Classical Heisenberg Impurity Model

The second model we looked at is a one-dimensional classical Heisenberg model to which we attached two impurities. The impurities couple to the center of the model. Both the host system as well as the impurities are made up solely by classical spins of length $S = \frac{1}{2}$. Initially, the host system is in its ground state while the impurities are not. We find a similar dynamics to the stub impurity model. For nearest-neighbor impurities the system relaxes completely, while for next-nearest-neighbor impurities it does not relax into its ground state and it rather gets stuck in some kind of metastable state. However, we find a different phenomenon to be the cause of this unexpected relaxation behavior than for the stub impurity model, as the whole concept of localized states and GGE ensemble is not straightforwardly applicable for a completely classical model.

We find that for neighboring impurity spins there is a (quasi-)conserved constant of motion emerging in the dynamics after the system gets sufficiently close to its (local) ground state. This can be seen by linearizing the system and computing the linearized equations of motion. In these equations, the scalar product of the impurity spins $\boldsymbol{S}_1\boldsymbol{S}_2$ is conserved over time. In the full equations of motion, this is not the case. Of course, one has to be careful when linearizing the equations of motion, as it itself is an approximation. The thorough analysis of the linearization procedure can be found in [III] in detail, however, roughly summarized, it is fine to say that an additional conserved quantity arises over time in the dynamics, which prevents the complete relaxation of the system.

It might be surprising that changing the position of just one impurity spin by just one site has such a large effect on the nature of the system dynamics. In a work by a different author [94] it was already shown that the dynamics in the one-dimensional antiferromagnetic classical Heisenberg model can change drastically, when modifying the system just slightly. For example, following [94]: Suppose we have such a one-dimensional antiferromagnetic classical Heisenberg model with L sites, nearest-neighbor only exchange interaction $J = 1$, and periodic boundary conditions. This system is bipartite with
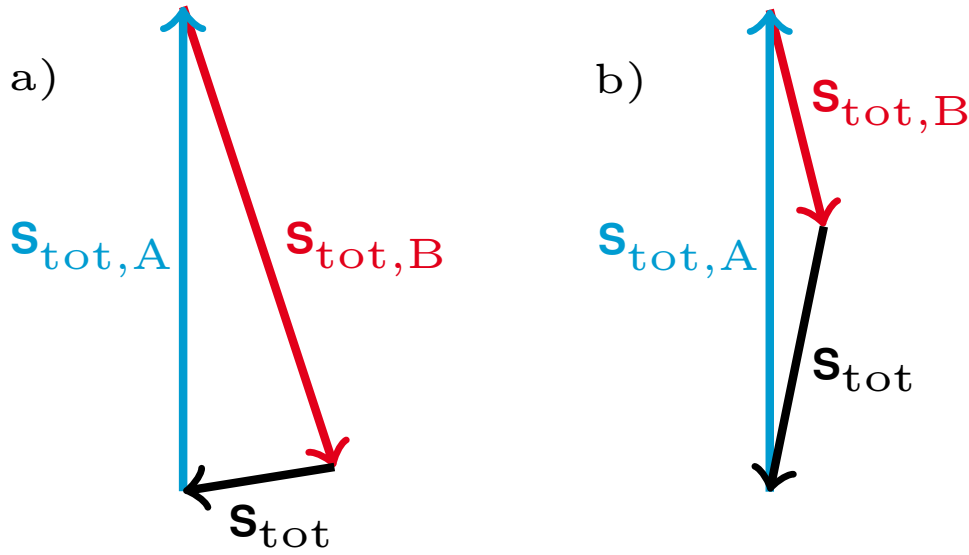
Figure 6.1: *All spins in the sublattices A and B point in the same direction respectively. Case a): The total spins of both sublattices have the same absolute value and are nearly collinear. The total spin of the system $\boldsymbol{S}_{tot} = \boldsymbol{S}_{tot,A} + \boldsymbol{S}_{tot,B}$ is nearly orthogonal to the sublattice spins. Case b): The total spins of the sublattices are nearly collinear, but have a different absolute value. The total spin of the system is nearly collinear to the sublattice spins.*

every second spin belonging to sublattice A and the remaining spins belonging to sublattice B. One solution of the system is given when the spins in sublattice A all have the same length and point in the same direction $\boldsymbol{S}_A$ and all spins in sublattice B have the same length and point also in the same direction $\boldsymbol{S}_B$. For a spin in sublattice A the equations of motion then are

$$\frac{d}{dt}\boldsymbol{S}_A(t) = 2J\boldsymbol{S}_B \times \boldsymbol{S}_A = \frac{4J}{L}\boldsymbol{S}_{\text{tot},B} \times \boldsymbol{S}_A = \frac{4J}{L}\left(\boldsymbol{S}_{\text{tot},B} + \boldsymbol{S}_{\text{tot},B}\right) \times \boldsymbol{S}_A$$
$$= \frac{4J}{L}\boldsymbol{S}_{\text{tot}} \times \boldsymbol{S}_A \, , \tag{6.1}$$

where $\boldsymbol{S}_{\text{tot}}$, $\boldsymbol{S}_{\text{tot},A}$ and $\boldsymbol{S}_{\text{tot},B}$ are the total spin of the system and the sublattices, respectively. An analogous equation can also be derived for the spins in sublattice B. From the equations of motion, we see that the spins in both sublattices precess around the same axis defined by the total spin of the system. Now suppose the system is close to its antiferromagnetic ground state. When the spins in sublattice A and sublattice B have different lengths, the total spin points approximately in the same direction as the ground state. All spins therefore precess around the ground state axis and remain in close vicinity of the ground state, see Fig. 6.1 for a graphical explanation. Contrary, when the spins in both sublattices have the same lengths, the total spin is approximately perpendicular to the ground state axis. The spins precess around an

axis not at all close to the ground state axis, see Fig. 6.1 for a graphical explanation. During the dynamics, the spins then move away from the ground state. In this case, the ground state is called unstable [94].

As the impurities destroy the translational invariance of the system and we are more interested in the local state of the system around the impurities and not in the global state, the results from [94] are not straightforwardly applicable. In general things like integrability and instability of a system are considered for the full system. Of course the total spin and energy are conserved in the full system, but that is not the case for a subset of the system around the impurities.

That is one of the reason why we decided to investigate emerging (local) conserved quantities in the linear regime, as it does not require to look at the whole system and it is sufficient to consider only a subset of the system around the impurities.

6.3 – Quantum-Classical Impurity Model

The last model we considered is a quantum-classical hybrid model consisting of a one-dimensional tight-binding model of non-interacting electrons, to which we attached two impurities in the form of classical spins. Again, we see a difference in the relaxation behavior of nearest-neighbor impurities and next-nearest-neighbor impurities. The system relaxes completely for nearest-neighbor impurities and does not for next-nearest-neighbor impurities. As it is not easy to employ one of the techniques from the prior sections, we analyze the problem in a different way by using linear-response theory. We already used linear-response theory before for the analysis of the SSH-impurity model in [II]. Of high interest is the spin susceptibility

$$\chi_{mm'}(t) = \Theta(t)e^{-\eta t}\mathrm{Im}\left[\left(e^{-i\boldsymbol{T}t}\boldsymbol{\Theta}(\boldsymbol{T}-\mu)\right)_{i_m i_{m'}} \times \left(e^{i\boldsymbol{T}t}\boldsymbol{\Theta}(\mu-\boldsymbol{T})\right)_{i_{m'} i_m}\right], \qquad (6.2)$$

which now depends on two indices $m, m' \in \{1, 2\}$ indicating one of the two impurity spins. The positive infinitesimal η ensures convergence. With the spin susceptibility, we get a set of effective equations of motion for the impurity spins:

$$\frac{d}{dt}\boldsymbol{S}_m(t) = -K^2 \boldsymbol{S}_m \times \sum_{m'=1,2} \int_0^t dt' \chi_{mm'}(t')\boldsymbol{S}_{m'}(t-t') . \qquad (6.3)$$

We can also express the spin susceptibility in frequency space via a Fourier transformation, which results in:

$$\chi_{mm'}(\omega) = \frac{1}{2L^2} \sum_k^{\text{occ.}} \sum_{k'}^{\text{unocc.}} e^{i(k'-k)(i_m - i'_m)} \left(\frac{1}{\omega - \epsilon_k + \epsilon_{k'} + i\eta} - \frac{1}{\omega + \epsilon_k - \epsilon_{k'} + i\eta} \right) ,$$

(6.4)

where the sums go over the occupied and unoccupied single-particle eigenstates with wave vectors k, k', respectively. The one-particle eigenenergies are given by $\epsilon_k = -2T\cos(k)$. One has to be cautious of the positive infinitesimal η in Eq. (6.4). It is tempting to just perform the limit $\eta \to 0$, however, this leads to unphysical results. As the system is not gapped at the Fermi edge performing the limit now can lead to problems, e.g., singularities, when performing the thermodynamic limit $L \to \infty$ afterwards. The right way is to perform the thermodynamic limit first and to always perform the $\eta \to 0$ limit last.

The analysis of the spin susceptibility is not as easy as it was for the SSH impurity model in [II], where we just looked where $\chi(\omega) \neq 0$. This is not a valid criterion for relaxation anymore, because in the effective equations of motion for the impurity spins Eq. (6.3) the right hand site depends on two different terms with different $\chi_{mm'}$. It does not really matter if an individual $\chi_{mm'}$ is zero when the other is not. Additionally, as we do not consider a gapped system, the spin susceptibilities $\chi_{mm'}$ are not expected to have a relevant extended parameter region where they are zero.

Nevertheless, to still get some insight into the relaxation and damping behavior of the impurity spins, we derive the Gilbert damping [16], which can be computed from the spin susceptibility. The Gilbert damping describes the damping and relaxation behavior of the impurity spins and is given by [17]

$$\alpha_{mm'} = iK^2 \frac{\partial}{\partial \omega} \chi_{mm'}(\omega)|_{\omega=0} .$$

(6.5)

In a similar vein, the RKKY interaction [11–13] can also be derived from the spin susceptibility and is given by

$$J_{mm'} = K^2 \chi_{mm'}(\omega = 0) .$$

(6.6)

They both can be used to formulate an even more simplified set of effective equations of motion:

$$\dot{\boldsymbol{S}}_m = \sum_{m'} J_{mm'} \boldsymbol{S}_{m'} \times \boldsymbol{S}_m + \sum_{m'} \alpha_{mm'} \boldsymbol{S}_m \times \dot{\boldsymbol{S}}_{m'} .$$

(6.7)

Inserting Eq. (6.4) into Eq. (6.5) yields an analytic form of the Gilbert damping:

$$\alpha_{mm'} = \frac{i}{2L^2} \sum_k^{\text{occ.}} \sum_{k'}^{\text{unocc.}} e^{i(k'-k)(i_m - i'_m)} \left(\frac{1}{(-\epsilon_k + \epsilon_{k'} + i\eta)^2} - \frac{1}{(\epsilon_k - \epsilon_{k'} + i\eta)^2} \right) . \quad (6.8)$$

For our model we have $J_{12} = J_{21} = 0.0342$ for the RKKY interaction. For the local Gilbert damping we find $\alpha_{11} = \alpha_{22} \approx -0.398K^2$ for both nearest-neighbor and next-nearest-neighbor impurities. For the non-local Gilbert damping, however, we find $\alpha_{12}^{(\text{nn})} \approx 0.0021K^2$ for nearest-neighbor and $\alpha_{12}^{(\text{nnn})} \approx 0.398K^2$ for next-nearest-neighbor impurities. So for next-nearest-neighbor impurities the local Gilbert damping and the non-local Gilbert damping are the same.

The exact derivation for this can be found in [III]. One can use the Gilbert dampings to calculate the dynamics via the effective equations of motion Eq. (6.7) and find that it very much resembles the full dynamics. It shows full relaxation for nearest-neighbor impurities and no relaxation for next-nearest-neighbor impurities, see Fig. III-13 and Fig. III-14.

One can also see, why the system does not relax for next-nearest-neighbor impurities. For $\alpha_{11} = \alpha_{22} = \alpha_{12} = \alpha_{21}$ it can be easily shown that the total spin $\boldsymbol{S}_1 + \boldsymbol{S}_2$ becomes a conserved quantity in Eq. (6.7). The total spin not being able to change trivially prohibits the relaxation of the impurities. In a way, one could say that the damping effects of the local and non-local Gilbert damping cancel each other out. For nearest-neighbor impurities, on the other hand, there is no additional conserved quantity in Eq. (6.7), and hence the relaxation of the spins is not prohibited.

6.4 – Further Discussion

We compared three different kinds of models, which all had the same kind of structure: two impurities connected via a host system. They all have in common that there were two different intrinsic time scales. The dynamics in the host system is fast compared to the host-impurity dynamics. This somewhat beckons the question if it is possible to construct an effective impurity only dynamics. We did this for the quantum-classical model in [III] using linear-response theory, which results in an effective LLG equation. However, due to the separation of time scales it might be worthwhile to treat the system adiabatically to obtain an impurity-only dynamics.

This means, at every point in time we assume the host system to be in the ground state corresponding to the present impurity configuration. For the quantum-classical model with just one impurity this was already done in [95]. For the purely classical model with one impurity this was done in [IV] and for an arbitrary number of impurities it can be found in [96]. In the classical case, using this adiabatic constraint, it is

possible to derive a set of effective impurity-only equations of motion that depend on
the system's parameters, like the number of spins in the host system and the exact
location of the impurities. It also features a topological spin torque. This topological
spin torque makes the effective equations of motion non-Hamiltonian, meaning they
cannot be derived from some effective Hamiltonian, and can change the precession
frequency of the impurities quite drastically. For next-nearest-neighbor impurities, the
classical adiabatic spin dynamics of [96] predicts that the impurities precess around
the total impurity spin vector $\boldsymbol{S}_1 + \boldsymbol{S}_2$ with a precession frequency of $\omega_p = \frac{K}{2}$, which
is actually exactly what we get as the final state for the full dynamics shown in Fig.
III-8. However, for nearest-neighbor impurities adiabatic spin dynamics also predicts
a precession of the impurity spins around the total impurity spin vector albeit with a
different precession frequency. This is definitely not what we see in our calculations,
see Fig. III-7, where the system relaxes straightforwardly without any precession.

So with that, it seems that adiabatic spin dynamics is not really applicable for our
problem, and the agreement in the next-nearest-neighbor impurities case was merely a
coincidence. It is probably because the adiabatic approximation, as it is done in [96], is
flawed when applied to our specific problem. We consider large systems with $L > 10^5$
spins. Even with a much smaller intrinsic time scale of the host system, it still takes a
long time for the host system to adapt to the present impurity spin configuration. The
necessary time for this is in general larger than the intrinsic time scale of the dynamics
of the impurities. Maybe for very small impurity-host interactions $K \ll \frac{J}{L}$ one would
recover adiabatic spin dynamics. However, that would require to numerically calculate
the dynamics of the system for very long times as the dynamics would be very small.
Even for a purely classical system that is not really feasible.

Of course, one could relax the adiabatic constraint a bit and restrict only a small part
of the host system in the vicinity of the impurities to the adiabatic approximation.
So we require, for example, that only the ten closest spins to the impurities in the
host system are at all times in the local ground state to the current impurity spin
configuration. However, this leads to further questions: Firstly, one has to think about
how to treat the rest of the host system and secondly, the restriction of the adiabatic
approximation to a small subset of the host system only is a bit arbitrary, and one
could always wonder why we only restrict it to, e.g., ten spins in the host system and
not eleven, twelve of twenty. This is surely an interesting avenue to explore, but it goes
beyond the scope of this section.

Similarly to the classical case, we also do not expect an adiabatic approximation to be
straightforwardly applicable to the quantum-classical and purely quantum mechanical
models, as the host systems are too large for a simple adiabatic approximation.

Prerelaxation in quantum, classical, and quantum-classical two-impurity models

Michael Elbracht[1] and Michael Potthoff[1,2]

[1]*I. Institute of Theoretical Physics, Department of Physics, University of Hamburg, Notkestraße 9, 22607 Hamburg, Germany*
[2]*The Hamburg Centre for Ultrafast Imaging, Luruper Chaussee 149, 22761 Hamburg, Germany*

We numerically study the relaxation dynamics of impurity-host systems, focusing on the presence of long-lived metastable states in the nonequilibrium dynamics after an initial excitation of the impurities. In generic systems, an excited impurity coupled to a large bath at zero temperature is expected to relax and approach its ground state over time. However, certain exceptional cases exhibit metastability, where the system remains in an excited state on timescales largely exceeding the typical relaxation time. We study this phenomenon for three prototypical impurity models: a tight-binding quantum model of independent spinless fermions on a lattice with two stub impurities, a classical-spin Heisenberg model with two weakly coupled classical impurity spins, and a tight-binding quantum model of independent electrons with two classical impurity spins. Through numerical integration of the fundamental equations of motion, we find that all three models exhibit similar qualitative behavior: complete relaxation for nearest-neighbor impurities and incomplete or strongly delayed relaxation for next-nearest-neighbor impurities. The underlying mechanisms leading to this behavior differ between models and include impurity-induced bound states, emergent approximately conserved local observables, and exact cancellation of local and nonlocal dissipation effects.

I. INTRODUCTION

A small system ("impurity") in an excited state and coupled to a large bath ("host") at zero temperature is usually expected to relax over time and to approach its ground state. After the initial excitation of the impurity, the excess energy is dissipated via the impurity-host coupling and through the coupling of the host degrees of freedom into the bulk of the host system (see Fig. 1). For a system with a macroscopically large number of degrees of freedom subject to the principles of thermodynamics, this dissipation process is irreversible. This picture of generic relaxation dynamics explains the interest in exceptional cases, where the system is trapped in a metastable state that does not decay on timescales exceeding by far the typical intrinsic timescales governing the microscopic degrees of freedom.

Incomplete or delayed relaxation and metastability in impurity-host models [1,2] is closely related to incomplete or delayed thermalization of extended lattice models. In both cases, much of the interest in metastable states is due to their promise for controlling nonequilibrium dynamics and for related functionalities [3]. Compared to notoriously difficult lattice models, models with single or few initially excited impurities embedded in a large host represent an interesting class of comparatively simple systems that may hold a key to the understanding of metastability. Here, we report on metastable

states in the real-time dynamics of three different prototypical system-bath models: an uncorrelated quantum, a classical and a quantum-classical hybrid model. In all three cases, the exact dynamics is numerically accessible on long timescales.

In recent decades, much progress has been made in understanding the thermalization of generic macroscopically large quantum systems, the main paradigm of quantum-statistical physics, and the foundation of thermodynamics [4,5]. Here, an important concept is the eigenstate thermalization hypothesis [6–10], as reviewed, e.g., in Ref. [11]. One route to *nonthermal* states of quantum-lattice models is via integrability. For (one-dimensional) systems with a large number of conserved local observables, the long-time dynamics may result in a state described by a generalized Gibbs ensemble [5,12–14]. Another route is provided via disorder, either on the single-particle level or via many-body localization [15,16].

This is similar to *classical* Hamiltonian dynamics [17]. It is known that ergodicity and the equivalence between long-time and ensemble averages of observables can be broken in the case of a large number of integrals of motion. Violations of ergodicity are found for integrable systems [17] but also for systems parametrically close to integrability [18–21] or in systems with glassy dynamics [22,23].

For quantum-lattice models, too, proximity to an integrable point in parameter space may lead to prethermalization and metastability. This has been analyzed analytically and demonstrated numerically in several studies [24–28].

For *impurity-host* systems (or open quantum systems) the situation is not very different. After an initial local excitation of the impurity, one generally expects a relaxation of the reduced density matrix of the impurity to its (canonical) thermal state if the impurity-host coupling is weak [2,29–32]. On the
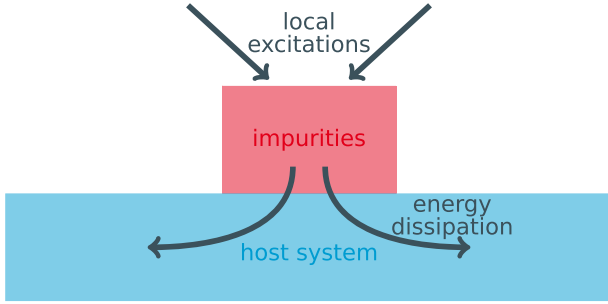
FIG. 1. Typical structure of an impurity model. The impurities are coupled to a much larger host system. After an initial local excitation, the full system, impurities plus host, is expected to relax locally in its ground state in the vicinity of the impurities after the excitation energy is dissipated into the bulk.

FIG. 2. Sketch of the stub-impurity model of spinless fermions. Two fermionic impurity sites or orbitals are coupled via a hybridization V to a one-dimensional lattice with nearest-neighbor hopping T. $T = 1$ sets the energy scale. The host system is at half-filling.

other hand, in the case of band gaps or finite bandwidths, incomplete relaxation and residual dissipationless dynamics may occur [33,34]. Relaxation to nonthermal states may be found in the gapless case for a sufficiently strong impurity-bath coupling [34–36].

Recently, a metastable state and incomplete spin relaxation have been observed in a system consisting of a classical impurity spin that is exchange coupled to a spinful Su-Schrieffer-Heeger model at an edge site [37]. Here, the topological state of the host and the associated presence or absence of a protected edge mode are found to control the relaxation of the classical spin. This is a prime example for an impurity system with prerelaxation dynamics, analogous to prethermalization in quantum-lattice models. However, the dynamical decoupling of the impurity and the stabilization of the excited state on a long timescale is due to a gapped spectrum for *two-particle* excitations, which blocks further energy dissipation. A similar effect has been observed for a classical spin locally coupled to a one-dimensional half-filled Hubbard model [38]. In this case the Hubbard-U and the narrow spectrum of (quantum) spin excitations control prerelaxation and metastability. Fast but incomplete relaxation to a metastable intermediate excited state, followed by extremely slow complete relaxation, is also known from the decay of a local doublon excitation in the Hubbard model at large U [39,40], or for a magnetic doublon [41] in the strong-J limit of the Kondo lattice.

Here, we study the exact real-time dynamics by numerical integration of the fundamental equations of motion for three different prototypical impurity models, a quantum, a classical, and a quantum-classical hybrid model. All share equivalent geometries, namely, a one-dimensional lattice model serving as the bath and two additional impurities which are locally coupled to nearest-neighbor (n.n.) or to next-nearest-neighbor (n.n.n.) sites of the lattice. Specifically, we study (i) a tight-binding quantum model of independent spinless fermions on a lattice with two stub impurities, (ii) a classical-spin Heisenberg model with two weakly coupled classical impurity spins, and (iii) a tight-binding quantum model of independent electrons with two classical impurity spins. The long-time relaxation dynamics initiated by a local excitation of the impurities can by studied numerically for large lattices in all three
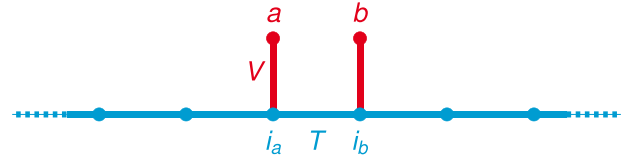
cases, and in all cases we find qualitatively very similar results: there is complete relaxation to a time-independent final state in the case of n.n. impurities, while there is incomplete relaxation or prerelaxation for n.n.n. impurities. In all three cases the effect can be understood after a thorough theoretical analysis. However, it turns out that the uncovered mechanisms are very different. The different systems are discussed separately in Secs. II, III, and IV. Our conclusions are summarized in Sec. V.

II. STUB IMPURITY MODEL

We start the discussion by considering a tight-binding model with two stub impurities. The host system is given by noninteracting spinless fermions on a one-dimensional chain of L sites with open boundaries. The nearest-neighbor hopping $T = 1$ sets the energy scale. The two impurities (a and b) are given by two additional sites or orbitals coupling via a hybridization of strength V to the host sites i_a and i_b. We will consider n.n. or n.n.n. sites i_a, i_b located at the center of the chain. A sketch of the system is shown in Fig. 2. The Hamiltonian consists of three terms:

$$H = H_{\text{host}} + H_{\text{imp}} + H_{\text{hyb}}, \tag{1}$$

the Hamiltonian of the host,

$$H_{\text{host}} = -T \sum_{i=1}^{L-1} c_i^\dagger c_{i+1} + \text{H.c.}, \tag{2}$$

the impurity sites,

$$H_{\text{imp}} = \epsilon_f (f_a^\dagger f_a + f_b^\dagger f_b), \tag{3}$$

with on-site energy $\epsilon_f = 0$, and the host-impurity hybridization,

$$H_{\text{hyb}} = V(c_{i_a}^\dagger f_a + c_{i_b}^\dagger f_b) + \text{H.c.} \tag{4}$$

Here, c_i annihilates a fermion at site i, and f_a annihilates a fermion at impurity site a.

We study the real-time dynamics of the system after a quantum quench of the hybridization from zero to a finite value V. At time $t = 0$, the state of the host is assumed to be prepared in its nondegenerate ground state with $N = L/2$ fermions, i.e., half-filling:

$$|\Psi_{\text{host}}(0)\rangle = \prod_k^{\text{occ.}} c_k^\dagger |\text{vac.}\rangle, \tag{5}$$

where k runs over the one-particle eigenstates of H_{host} with one-particle energies $\varepsilon_k < 0$. Furthermore, the impurity sites

a and b are assumed as fully occupied at time $t = 0$. Hence, the initial state of the full system is the state

$$|\Psi(t = 0)\rangle = f_a^\dagger f_b^\dagger |\Psi_{\text{host}}(0)\rangle \,. \tag{6}$$

As the system is noninteracting, it is sufficient to formulate an equation of motion in terms of the one-particle reduced density matrix $\boldsymbol{\rho}$. Its elements are defined as

$$\rho_{IJ}(t) = \langle c_J^\dagger c_I \rangle_t \,. \tag{7}$$

The indices I, J run over the $L + 2$ host and impurity sites: $I, J \in \{1, 2, \ldots, L, a, b\}$. Initially, at $t = 0$ the density matrix $\boldsymbol{\rho}(0)$ has a block-diagonal form, with an $L \times L$ block representing the host system and two 1×1 blocks representing the impurities. We are interested in the time evolution of the occupation numbers

$$n_i(t) \equiv \langle c_i^\dagger c_i \rangle_t = \rho_{ii}(t) \,,$$
$$n_a(t) \equiv \langle f_a^\dagger f_a \rangle_t = \rho_{aa}(t) \,,$$
$$n_b(t) \equiv \langle f_b^\dagger f_b \rangle_t = \rho_{bb}(t) \,. \tag{8}$$

At $t = 0$, we have

$$\boldsymbol{\rho}_{\text{host}}(t = 0) = \Theta(\mu\mathbb{I} - \boldsymbol{T}_{\text{host}}) \,, \tag{9}$$

where Θ denotes the Heaviside step function, $\mu = 0$ the chemical potential, and $\boldsymbol{T}_{\text{host}}$ the hopping matrix of the host system. Furthermore, $\rho_{aa}(0) = \rho_{bb}(0) = 1$.

The time dependence of the density matrix $\boldsymbol{\rho}(t)$ is obtained via the von Neumann equation of motion:

$$i\frac{d}{dt}\boldsymbol{\rho}(t) = [\boldsymbol{T}, \boldsymbol{\rho}(t)] \,. \tag{10}$$

Here, $\boldsymbol{T}$ is the hopping matrix of the full system, Eq. (1). The formal solution of Eq. (10) is given by

$$\boldsymbol{\rho}(t) = \boldsymbol{U} e^{-i\boldsymbol{\varepsilon}t} \boldsymbol{U}^\dagger \boldsymbol{\rho}(0) \boldsymbol{U} e^{i\boldsymbol{\varepsilon}t} \boldsymbol{U}^\dagger \,, \tag{11}$$

where the diagonal matrix of one-particle eigenenergies $\boldsymbol{\varepsilon}$ and the unitary matrix $\boldsymbol{U}$ formed by the one-particle eigenstates of $\boldsymbol{T}$ are obtained by solving the eigenvalue problem

$$\boldsymbol{T}\boldsymbol{U} = \boldsymbol{U}\boldsymbol{\varepsilon} \,. \tag{12}$$

The $t = 0$ state, Eq. (6), is not an eigenstate of the full Hamiltonian with $V > 0$. It instead represents a state that is locally excited, in the vicinity of the impurities. One naively expects that the local excess energy and the locally enhanced fermion density at the impurity sites are dissipated to the bulk of the system over time and that the system approaches the fully relaxed state that is locally characterized by the ground-state energy density and the ground-state impurity occupations.

Numerical results for a system with $L = 500$ host sites and impurities a and b coupling to nearest-neighbor (n.n.) sites $i_a = 250$ and $i_b = 251$ located symmetrically around the chain center are shown in Fig. 3. On a timescale $t \sim 100$, the impurity occupations $n_a (= n_b)$ relax and approach a value $n_a \approx 0.505$ close to their ground-state value $n_a^{(\text{gs})} = 0.5$. Similarly, the occupations $n_{i_a} = n_{i_b}$ of the host sites closest to the impurities and also the occupations at more distant sites, e.g., n_{i_a+20}, relax. The characteristic timescale for the dissipation of particles (and of energy) can be read off from Fig. 3 by comparing the dynamics of n_{i_a} with that of n_{i_a+20}. The total
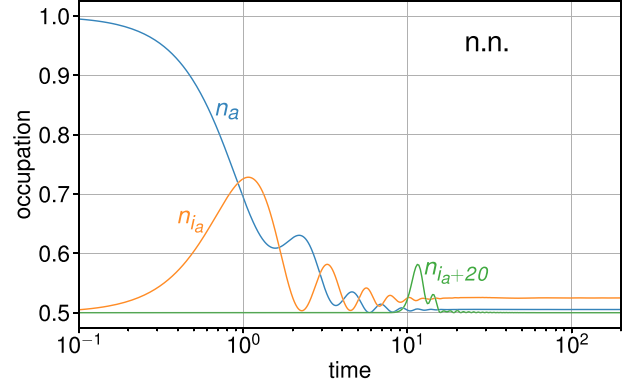

FIG. 3. Time dependence of the average occupation number n_a of the impurity sites a and of the occupation n_{i_a} of the corresponding host site i_a. In addition the occupation n_{i_a+20} of a distant site $i_a + 20$ is displayed. Calculation for a system with $L = 500$ host sites and two stub impurities at the nearest-neighbor positions $i_a = 250$ and $i_b = 251$. Hybridization strength $V = 1$. Note that inversion symmetry enforces $n_b = n_a$ and $n_{i_b} = n_{i_a}$. The time unit is set by the inverse nearest-neighbor hopping $1/T = 1$.

system size ($L = 500$) is large enough such that reflections of the propagating wave packets at the open system boundaries do not yet interfere with the dynamics in the vicinity of the impurities, on the time interval considered.

The time evolution turns out to be completely different, however, when coupling the two impurities to next-nearest-neighbor (n.n.n.) host sites. This is demonstrated with Fig. 4. While we do find a fast initial relaxation, the relaxation process stops at $t \sim 2$, and the impurity occupations start to oscillate around a value ($n_a \approx 0.625$) that is considerably larger than the ground-state value. These oscillations are undamped and persistent (until finite-size effects in form of interference with reflections from the boundaries become important).

This qualitative difference between n.n. and n.n.n. impurities, i.e., complete or incomplete relaxation, is likewise
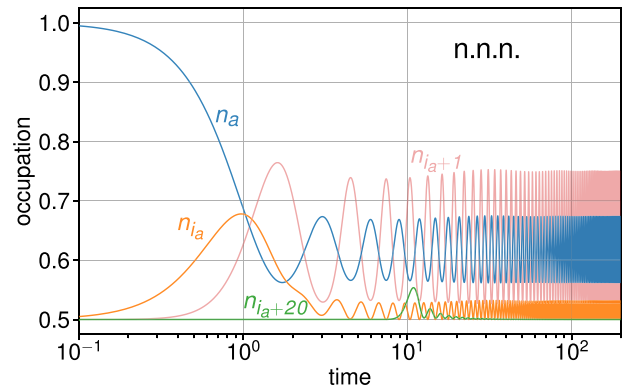

FIG. 4. The same as Fig. 3, but for stub impurities coupled to next-nearest-neighbor (n.n.n.) sites $i_a = 249$ and $i_b = 251$. We also choose $L = 499$. Therewith, inversion symmetry enforces $n_b = n_a$ and $n_{i_b} = n_{i_a}$.

observed for impurities at arbitrarily large but odd or even distances, respectively. The key to this effect is the absence or presence of bound single-particle energy eigenstates of the postquench Hamiltonian.

Two different types of localized eigenstates can be distinguished: (i) For each of the two impurities, there is a pair of bound states that split off from the lower and upper edges of the valence band. These four high-excitation-energy bound states are localized near the impurities with a weight that decays exponentially at large distances. The case of strong hybridization V is instructive. For $V \to \infty$, the hopping term, Eq. (2), can be ignored, and the Hamiltonian describes a system of two decoupled dimers with two degenerate eigenstates at $-V$, and two more degenerate states at $+V$ ($V > 0$). This degeneracy is lifted for finite $T \ll V$, and two bonding-antibonding pairs of bound states are formed, one with negative energies below the bottom of the band and one with positive energies. As V decreases, the bound states remain localized and centered around the impurities, but their weight is increasingly distributed over the lattice. At $V = 1$, only a single state from each of the two pairs remains, a spatially symmetric bound state with negative energy and an antisymmetric bound state with positive energy, while the other two states have merged with the bulk continuum. This first type of bound state is generic and thus present for both cases of impurities coupled to n.n. and to n.n.n. host sites.

(ii) A bound state of a different, second type is present in the case of n.n.n. impurities only. It is given by

$$|\psi_{\text{loc}}\rangle = \sqrt{\frac{V^2}{V^2 + 2T^2}} \left[c_{i_a+1}^\dagger + \frac{T}{V}\left(f_a^\dagger + f_b^\dagger\right) \right] |\text{vac.}\rangle, \quad (13)$$

where $i_a + 1 = i_b - 1$ denotes the host site between the sites coupled to the impurities. This state has a finite weight on this and on the two impurity sites only, it is "superlocalized." Furthermore, its eigenenergy, $\varepsilon_{\text{loc}} = 0$, resides *within* the continuum of band states. This type of states is well known from flat-band systems [42–47]. When coupling a stub impurity to every second host site, the resulting translationally invariant tight-binding lattice model has a unit cell consisting of three sites, and its band structure features a flat band, resulting from superlocalized states, besides two dispersive bands.

To discuss the impact of bound states on the postquench relaxation dynamics, we can straightforwardly adapt some concepts developed in Ref. [10]. Accordingly, we decompose the expectation value $O(t) \equiv \langle O(t) \rangle$ of a local operator O with a Heisenberg time dependence as

$$O(t) = \overline{O} + \delta O(t), \quad (14)$$

where the first term is the long-time average,

$$\overline{O} = \lim_{t \to \infty} \frac{1}{t} \int_0^t d\tau \, O(\tau), \quad (15)$$

and where the time-dependent second term $\delta O(t)$ is a fluctuation part with a vanishing long-time average. As a measure for the strength of persistent temporal fluctuations, we consider the long-time average of the absolute square of the fluctuation part:

$$\delta_O^2 = \lim_{t \to \infty} \frac{1}{t} \int_0^t d\tau \, |\delta O(\tau)|^2. \quad (16)$$
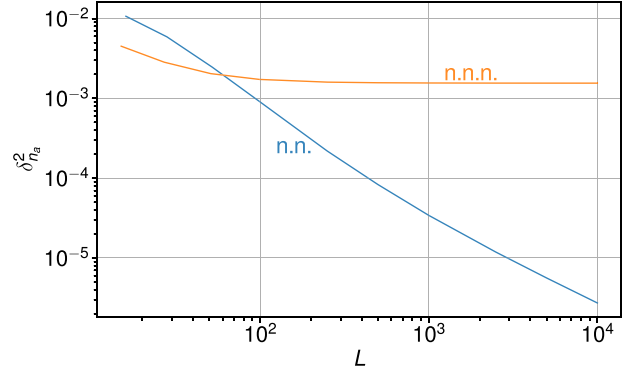

FIG. 5. Time-averaged fluctuation of the impurity occupation $\delta_{n_a}^2 = \delta_{\rho_{aa}}^2$, see Eq. (19), as a function of the system size L for n.n. and n.n.n. impurities.

For $O = O_{IJ} = c_J^\dagger c_I$, see Eq. (7), the expectation values $O_{IJ}(t) = \rho_{IJ}(t)$ are given by the elements of the one-particle reduced density matrix. A straightforward computation yields

$$\delta_{\rho_{IJ}}^2 = \sum_{\mu\nu}^{\mu \neq \nu} |U_{I\mu}|^2 |U_{J\nu}|^2 |\rho_{\mu\nu}(t=0)|^2. \quad (17)$$

Here, $U_{I\mu}$ is the Ith component of the μth eigenvector of the total hopping matrix, see Eq. (12), and

$$\rho_{\mu\nu}(t=0) = [\boldsymbol{U}^\dagger \boldsymbol{\rho}(t=0)\boldsymbol{U}]_{\mu\nu} \quad (18)$$

is an element of the one-particle reduced density matrix in the basis of the eigenstates of the total hopping matrix. Furthermore, we have assumed that there are no degeneracies and no gap degeneracies in the spectrum of the one-particle eigenenergies. In our specific case, the spectrum is indeed nondegenerate. However, particle-hole symmetry implies the presence of gap degeneracies, i.e., $\varepsilon_\mu - \varepsilon_\nu = \varepsilon_{\mu'} - \varepsilon_{\nu'}$ for $\mu \neq \mu'$ or $\nu \neq \nu'$. This modifies the derivation that led to Eq. (17), see also Ref. [10], and we find

$$\delta_{\rho_{IJ}}^2 = \sum_{\mu\nu}^{\mu \neq \nu} \sum_{\mu'\nu'}^{\mu' \neq \nu'} \delta_{\varepsilon_\mu - \varepsilon_\nu, \varepsilon_{\mu'} - \varepsilon_{\nu'}} U_{I\mu}^* U_{J\nu} U_{I\mu'} U_{J\nu'}^*$$
$$\times \rho_{\mu\nu}(t=0)\rho_{\mu'\nu'}^*(t=0). \quad (19)$$

The contribution to temporal fluctuations, measured with $\delta_{\rho_{IJ}}^2$ in Eq. (19), that stems from *extended* eigenstates must vanish for $L \to \infty$, as the components of the eigenvectors are proportional to $L^{-1/2}$ and hence $|U_{i\mu}|^2 |U_{j\nu}|^2 \sim 1/L^2 \to 0$. On the contrary, the components $U_{i\mu}$ of a localized eigenstate μ are independent of L and can be large at some sites i, as compared to the components of delocalized eigenstates, such that their contributions to $\rho_{\mu\nu}(t=0)$ in Eq. (19) become significant.

This is demonstrated with Fig. 5, where the time average of fluctuations of the occupation number is shown for one of the impurity sites. For n.n. impurities, $\delta_{n_a}^2$ decreases with increasing L and eventually vanishes in the thermodynamical limit $L \to \infty$. Note that the first type of bound states, discussed above under point (i), does not prevent relaxation due to spatial inversion symmetry, as discussed in Appendix.

Contrary, in the case of n.n.n. impurities, the strength of the fluctuations is essentially independent of the system size for $L \gtrsim 10^3$. The nonvanishing temporal fluctuations result from a bound state of the second type, see point (ii) above. This explains the observed incomplete relaxation for the n.n.n. case, see Fig. 4.

In the $L \to \infty$ limit, the effect of gap degeneracies is vanishing in the n.n. case. In the n.n.n. case and for large L, the fluctuation $\delta_{n_a}^2$, as computed via Eq. (19), is smaller by 3×10^{-4} (or by about 20%) compared to the value obtained from Eq. (17), i.e., disregarding gap degeneracies.

Note that in the n.n. case and for $L = 500$ (see Fig. 3), the plateau values for the occupation numbers at $t \approx 100$, i.e., $n_a \approx 0.505$ and $n_{i_a} \approx 0.525$, are close to but different from their $L \to \infty$ expectation values $n_a^{(\mathrm{gs})} = n_{i_a}^{(\mathrm{gs})} = 0.5$ in the ground state of the postquench Hamiltonian. The latter are fixed by particle-hole symmetry. For longer propagation times $t_{\max} \gg 100$, the plateau in the time evolution (see Fig. 3) is repeatedly interrupted by revivals (not visible on the timescale in Fig. 3). When computing the long-time averages, Eq. (15), including the revivals, we find converged $t \to \infty$ values $\bar{n}_a \approx 0.510$ and $\bar{n}_{i_a} \approx 0.526$. At $L = 500$, a propagation time $t < t_{\max} \approx 0.5 \times 10^4$ has turned out to be sufficient.

In fact, the dynamics of a system of noninteracting fermions is constrained by the constants of motion $c_\mu^\dagger c_\mu$. Hence, the system will relax to a nonthermal state with long-time averages of n_a and n_{i_a} equal to the averages in the generalized Gibbs ensemble or, equivalently, in the diagonal ensemble (see Ref. [10]). For an arbitrary operator O, the diagonal average is defined as

$$O^{(\mathrm{D})} \equiv \sum_J |C_J|^2 O_{JJ} , \qquad (20)$$

with $C_J = \langle J | \Psi(t=0) \rangle$ and with $O_{JJ} = \langle J | O | J \rangle$. At $L = 500$, for example, the numerical values $n_a^{(\mathrm{D})} \approx 0.510$ and $n_{i_a}^{(\mathrm{D})} \approx 0.526$ perfectly agree with the above-mentioned long-time averages. Repeating the computations for larger system sizes (up to $L = 5000$) and extrapolating to $L \to \infty$ yields slightly smaller values $n_a^{(\mathrm{D})} \approx 0.505$ and $n_{i_a}^{(\mathrm{D})} \approx 0.525$.

In general, for an integrable system, such as a noninteracting fermion impurity model, the expectation values of local one-particle observables generically do not relax to a thermal state, regardless of the presence or absence of bound states. However, the presence of bound one-particle eigenstates μ of the postquench Hamiltonian is crucial for the question of whether there is any relaxation at all or whether the system is trapped in a metastable state. In the case of n.n.n. impurities, there is a superlocalized bound state of the stub impurity model that prevents relaxation and forces the system into a metastable state without any further dissipation. This explains the qualitatively different relaxation dynamics for n.n. and for n.n.n. impurities.

III. CLASSICAL HEISENBERG IMPURITY MODEL

A similar effect in the relaxation dynamics is found for a purely classical-spin model, i.e., for a one-dimensional Heisenberg model of L classical spins s_i ($i = 1, ..., L$) with nearest-neighbor antiferromagnetic exchange coupling $J > 0$, where in addition two classical impurity spins S_m ($m = 1, 2$)
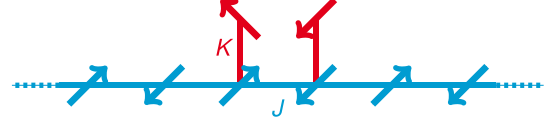

FIG. 6. Sketch of a system consisting of two classical impurity spins (red) locally exchange coupled to a one-dimensional classical Heisenberg model (blue spins) with open boundary conditions. K: weak antiferromagnetic local exchange, J: antiferromagnetic nearest-neighbor exchange interaction of the host spins.

are locally exchange coupled to the host spins at sites i_1 and i_2. The geometry is the same as for the stub impurity model, see Fig. 6 and compare with Fig. 2. The coupling strength of the local exchange is denoted by K. We assume that $K \ll J$ and $K > 0$, i.e., weak antiferromagnetic exchange interaction. The classical Hamilton function is given by

$$H = J \sum_{i=1}^{L-1} s_i s_{i+1} + K \sum_{m=1,2} S_m s_{i_m} , \qquad (21)$$

where the products of vectors are to be understood as dot products. The length of the host spins and of the impurity spins is set to $s \equiv |s_i| = \frac{1}{2}$ and $S \equiv |S_m| = \frac{1}{2}$, respectively. We consider a lattice with open boundaries. The sites i_1 and i_2, where the impurity spins are coupled to the host, are assumed to be n.n. or as n.n.n. sites in the center of the lattice. The host nearest-neighbor exchange coupling fixes the energy scale, $J = 1$, and we assume $K = 0.01$ unless otherwise stated.

The equations of motion are easily derived within the classical Hamilton formalism by making use of the spin Poisson bracket [48,49]. They attain the form of Landau-Lifshitz equations [50]. For the impurity spins we have

$$\frac{d}{dt} S_m(t) = K s_{i_m}(t) \times S_m(t) , \qquad (22)$$

where "$\times$" indicates the cross product, while for the host spins,

$$\frac{d}{dt} s_i(t) = J[s_{i-1}(t) + s_{i+1}(t)] \times s_i(t)$$
$$+ K \sum_m \delta_{i i_m} S_m(t) \times s_i(t) . \qquad (23)$$

It is immediately apparent that the length of each individual spin represents a constant of motion such that the spin dynamics is constrained to a configuration space given by the $L + 2$-fold direct product $\mathcal{S} \equiv S^2 \times \cdots S^2$ of 2-spheres with radius $1/2$. Furthermore, the total energy and, due to the SO(3) spin-rotation symmetry of H, the total spin $\sum_m S_m + \sum_i s_i$ are conserved. Moreover, the system has an SO(3)-degenerate ground-state manifold, as opposed to a nondegenerate singlet state of the quantum-spin model [51].

The spin dynamics is initiated by a parameter quench of the local exchange coupling from zero to a finite value K at time $t = 0$. We assume that the initial state of the system at $t = 0$ is given by one of the ground states for $K = 0$. For the host spins the ground state is given by an antiferromagnetic Néel state with respect to an arbitrary axis. Specifically, we choose
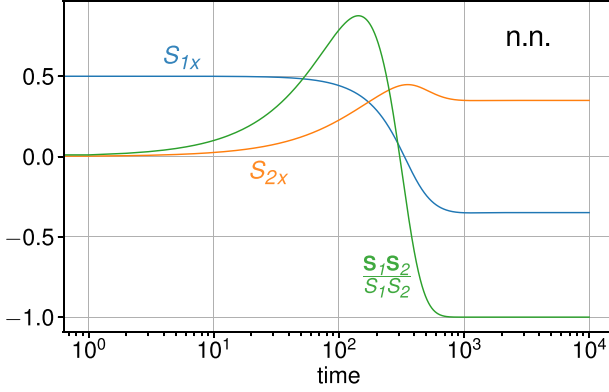
$$s_i(t=0) = (-1)^i s e_z . \qquad (24)$$

FIG. 7. Time evolution of the x components of two classical impurity spins S_1 and S_2 and of the cosine of the enclosed angle $S_1 S_2 / S_1 S_2$. Excited state at $t = 0$: host spins are in an antiferromagnetic Néel state aligned to the z axis, impurity spins point in the x and y direction, i.e., $S_1 = \frac{1}{2} e_x$ and $S_2 = \frac{1}{2} e_y$. Geometry parameters: $L = 10\,000$, $i_1 = 5000$, $i_2 = 5001$. Coupling strengths: $J = 1$ and $K = 0.01$.

The impurity-spin configuration at $t = 0$ is taken to be noncollinear, i.e., $S_1 = S e_x$ and $S_2 = S e_y$. This implies that after switching on K at $t = 0$, the spin dynamics is immediately driven by a finite spin torque.

Naively, one again expects that the excitation energy stored in the center of the chain is dissipated into the bulk of the system and that locally, in the vicinity of the impurities, the system approaches a ground-state spin configuration after a sufficiently long propagation time, assuming that the host of the system is sufficiently large to avoid unwanted interactions with excitations backscattered from the chain boundaries.

The equations of motion (22) and (23) are easily solved numerically for systems with $L \simeq 10^4$ host sites. For this system size and for $J = 1$, there are no finite-size effects in the form of reflection of spin excitations from the system boundaries up to a propagation time of $t \simeq 10^4$. Figure 7 displays the time dependence of the x components of two impurity spins and of the cosine of the enclosed angle for the case that the impurity spins are locally coupled to nearest-neighbor host spins at the chain center. We find that after $t \approx 800$ the dynamics has stopped and the system has reached one of its local ground states with an antiferromagnetic impurity-spin configuration and with an antiferromagnetic configuration of the host spins ($S_1 \uparrow\downarrow S_2$) in the vicinity of the chain center.

For two impurity spins coupled to n.n.n. sites, however, the time evolution is fundamentally different. As can be seen in Fig. 8, the system does not relax to a local ground state, at least not on the numerically accessible timescale. Rather, we find that after a propagation time $t \approx 1000$, the system state becomes trapped in a stationary state, in which the impurity spins precess around a common axis. Up to $t = 10^4$ there is hardly any relaxation to the expected ferromagnetic ($S_1 \uparrow\uparrow S_2$) impurity-spin configuration. The angle enclosed by S_1, and S_2 starts to deviate only slightly from its initial zero value (see green curve).

We also note that the qualitative difference between the relaxation dynamics for n.n. and for n.n.n. is not due to the
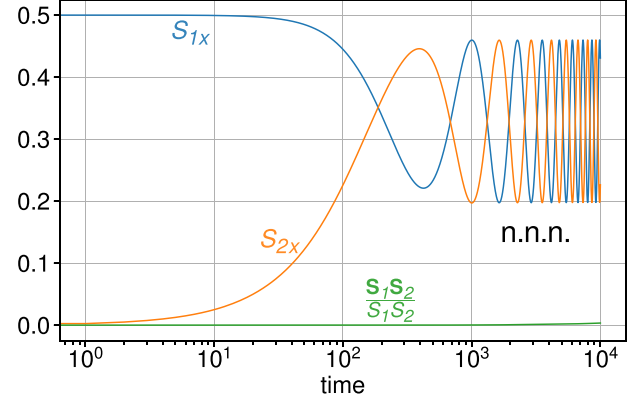

FIG. 8. The same as Fig. 7 but for impurity spins coupling to n.n.n. host spins. Geometry parameters: $L = 10001$, $i_1 = 5000$, $i_2 = 5002$.

larger distance of the impurity spins in the n.n.n. case. While the distance between the impurities does have an effect on the relaxation dynamics since it determines the time it takes for the spins to "communicate" with each other, this distance dependence turns out as negligible compared to the odd-even effect that is seen in calculations with larger interimpurity distances d. In fact, we find quick relaxation for distances $d = 1, 3, 5, \ldots$ and trapping in a stationary state for $d = 2, 4, \ldots$, very similar to the results shown in Figs. 7 and 8 and analogous to the results for the stub impurity model.

The observed odd-even effect is actually related to the different ground-state spin configurations, i.e., an antiferromagnetic and a ferromagnetic impurity-spin configuration for n.n. and for n.n.n. impurities, respectively, and to the small coupling constant $K \ll J$. This becomes obvious when looking at the time derivative of the scalar product $S_1 S_2$. From Eq. (22) we get

$$\frac{d}{dt}(S_1 S_2) = K(S_1 \times S_2)(s_{i_1} - s_{i_2}) . \qquad (25)$$

In the following we argue that, for n.n.n. impurities, the term on the right-hand side is small as compared to the inverse of the considered propagation time, in contrast to the n.n. case, and that this explains the observed odd-even effect. We consider three lines of argument with increasing level of sophistication.

In the first and crudest approach, we approximate $s_{i_2} - s_{i_1}$ in an *ad hoc* way by its ground-state value. For n.n.n. impurities, the Néel ground-state value is $s_{i_2}^{(0)} - s_{i_1}^{(0)} = 0$, and thus $S_1 S_2$ is a constant of motion that cannot relax to its ground-state value $S_1^{(0)} S_2^{(0)} = 1/4$ (see Fig. 8). On the other hand, for the n.n. case, the right-hand side is generically finite for the Néel ground state and of the order of K. In fact, there is a nontrivial dynamics of $S_1 S_2$, and $S_1 S_2$ approaches $S_1^{(0)} S_2^{(0)} = -1/4$ on a timescale $\Delta t \approx 8 \times 10^2 \sim K^{-1}$ (see Fig. 7).

In our second approach we derive an upper bound for $|s_{i_1} - s_{i_2}|$ for the case of n.n.n. impurities. For the initial state considered here, where the host spins form a Néel state, the excitation energy ΔE is solely stored in the interaction term

$\propto K$, see Eq. (21). It is given by

$$\Delta E = K\big(S_1 s_{i_1}^{(0)} + S_2 s_{i_2}^{(0)}\big) - K\big(S_1^{(0)} s_{i_1}^{(0)} + S_2^{(0)} s_{i_2}^{(0)}\big) . \quad (26)$$

Hence, for an arbitrary initial impurity-spin configuration, the maximum excitation energy is given by $\Delta E_{\max} = K$ and is realized for a ferromagnetic alignment of S_m and $s_{i_m}^{(0)}$.

Assuming that this excitation energy ΔE is distributed among the bonds between the closest host spins s_{i_1}, s_c, and s_{i_2} only ($c \equiv i_1 + 1 = i_2 - 1$), we get

$$\Delta E = J(s_{i_1}s_c + s_c s_{i_2}) - J\big(s_{i_1}^{(0)}s_c^{(0)} + s_c^{(0)}s_{i_2}^{(0)}\big)$$
$$= J(s_{i_1} + s_{i_2})s_c + J/2 . \quad (27)$$

The right-hand side is at a minimum if the central host spin is $s_c = -\frac{1}{2}\frac{s_{i_1}+s_{i_2}}{|s_{i_1}+s_{i_2}|}$. With this we find

$$\Delta E \geqslant \frac{J}{2} - \frac{J}{2}|s_{i_1} + s_{i_2}| . \quad (28)$$

Using $s_1^2 = s_2^2 = 1/4$ and the parallelogram law, $(s_1 + s_2)^2 + (s_1 - s_2)^2 = 1$, we get

$$|s_{i_1} - s_{i_2}|^2 \leqslant 4\frac{\Delta E}{J} - 4\frac{\Delta E^2}{J^2} . \quad (29)$$

With the above argument, $\Delta E \leqslant \Delta E_{\max} = K$, we find

$$|s_{i_1} - s_{i_2}| \leqslant 2\sqrt{\frac{K}{J}} . \quad (30)$$

This upper bound is a very conservative estimate as in the course of time the excitation energy will be further dissipated to the bulk of the system, and thus $|s_{i_1} - s_{i_2}|$ will be even smaller. We conclude that for $K \ll J$, the small available excitation energy of order K very much restricts the host spin dynamics. Via Eqs. (25) and (30), this implies that $S_1 S_2$ is almost conserved if S_1 and S_2 couple to n.n.n. host spins.

Our third approach is based on a linearization of the equations of motion. We start from Eqs. (22) and (23) and substitute $S_m = S_m^{(0)} + \delta S_m$ and $s_i = s_i^{(0)} + \delta s_i$, where $S_m^{(0)}$ and $s_i^{(0)}$ are ground-state spin orientations, while δS_m and δs_i denote the deviations from the ground state.

Linearization of Eqs. (22) and (23) yields

$$\dot{S}_m = J\left[\frac{K}{J}s_{i_m}^{(0)} \times S_m + \frac{K}{J}s_{i_m} \times S_m^{(0)} + \mathcal{O}\left(\frac{K^2}{J^2}\right)\right], \quad (31)$$

and

$$\dot{s}_i = J\left[\big(s_{i-1}^{(0)} + s_{i+1}^{(0)}\big) \times s_i + (s_{i-1} + s_{i+1}) \times s_i^{(0)} + \sum_{m=1}^{2}\delta_{ii_m}\left(\frac{K}{J}S_m^{(0)} \times s_i + \frac{K}{J}S_m \times s_i^{(0)}\right) + \mathcal{O}\left(\frac{K^2}{J^2}\right)\right], \quad (32)$$

where we used

$$|\delta S_m| = \mathcal{O}\left(\frac{\Delta E}{K}\right) = \mathcal{O}(1), \qquad |\delta s_i| = \mathcal{O}\left(\frac{\Delta E}{J}\right) = \mathcal{O}\left(\frac{K}{J}\right) \quad (33)$$

to estimate the magnitude of the neglected terms. We see that linearization of the equations of motion is possible although $|\delta S_m| = \mathcal{O}(1)$ is not necessarily small. The reasoning is the same that led to Eq. (30), i.e., the maximum values for $|\delta S_m|$ and $|\delta s_i|$ are limited by the available initial excitation energy $\Delta E \leqslant K$. Impurity spins contribute on the order of K to the total energy, while host spins contribute on the order of J. The estimates (33) are well supported by our numerical results underlying Fig. 8.

We proceed by computing the time derivative of $S_1 S_2$ within the linearized theory. With Eqs. (31) and (32) we find

$$\frac{d}{dt}(S_1 S_2) = J\left[\frac{K}{J}(S_1 \times S_2)\big(s_{i_1}^{(0)} - s_{i_2}^{(0)}\big) + \frac{K}{J}\big(S_2 \times s_{i_1}\big)S_1^{(0)} + \frac{K}{J}\big(S_1 \times s_{i_2}\big)S_2^{(0)}\right] + J\mathcal{O}\left(\frac{K^2}{J^2}\right) . \quad (34)$$

For n.n.n. impurity spins, the first term on the right-hand side vanishes since $s_{i_1}^{(0)} = s_{i_2}^{(0)}$. Furthermore, we can write $S^{(0)} = S_1^{(0)} = S_2^{(0)}$. Therewith we find

$$\frac{d}{dt}(S_1 S_2) = JS^{(0)}\left(\frac{K}{J}S_2 \times s_{i_1} + \frac{K}{J}S_1 \times s_{i_2}\right) + J\mathcal{O}\left(\frac{K^2}{J^2}\right). \quad (35)$$

With $S_i = S^{(0)} + \delta S_i$ and $s_m = s_m^{(0)} + \delta s_m$, exploiting that ground-state spin configurations are collinear, and finally, using Eqs. (33), one has

$$\frac{d}{dt}(S_1 S_2) = JS^{(0)}\left[\frac{K}{J}\delta S_2 \times \delta s_{i_1} + \frac{K}{J}\delta S_1 \times \delta s_{i_2} + \mathcal{O}\left(\frac{K^2}{J^2}\right)\right] = J\mathcal{O}\left(\frac{K^2}{J^2}\right) . \quad (36)$$

This means that, *within the linearized theory*, $(d/dt)(S_1 S_2)$ must be considered as zero and that $S_1 S_2$ is a constant of motion with a correction of the same order of magnitude as the linearization error only.

In the case of n.n. impurity spins, restarting from Eq. (34) with a completely analogous calculation but with an antiferromagnetic ground-state alignment $s_{i_1}^{(0)} = -s_{i_2}^{(0)}$, one finds

$$\frac{d}{dt}(S_1 S_2) = J S^{(0)} \left[2\frac{K}{J} \delta S_1 \times \delta S_2 \right] + J\mathcal{O}\left(\frac{K^2}{J^2}\right), \quad (37)$$

i.e., there is a nontrivial dynamics on an energy scale that is by an order of magnitude larger than the linearization error, such that, *even within the linearized theory*, $S_1 S_2$ cannot be considered as a constant of motion.

We have also studied the dynamics beyond the weak-coupling regime. For K and J of the same order of magnitude, one finds a relaxation of $S_1 S_2$ already after a very short propagation time of $t \simeq 100$ for both the case of n.n. and of n.n.n. impurity spins.

For the weak-coupling regime $K \ll J$, we conclude that after an initial local excitation of n.n.n. impurity spins, these show an anomalous relaxation dynamics. There is almost no relaxation of $S_1 S_2$, i.e., the enclosed angle is almost a constant of motion, on a timescale of about $t \sim 10^4$. This must be contrasted with the case of n.n. impurity spins, where complete relaxation is reached after a propagation time of $t \simeq 800$. In contrast to the stub-impurities model discussed above, there is no local symmetry of the (classical) Hamiltonian that would lead to a conserved local observable. (Quasi-)conservation of $S_1 S_2$ is rather emerging in the course of time. After a certain prerelaxation process ($t \simeq 10^3$) with a sufficient dissipation of energy and spin, the system state has evolved sufficiently close to one of the ground states *locally*, i.e., in the vicinity of the impurities, such that the further dynamics is very well captured by linearized equations of motion. Indeed, within the linearized theory, $S_1 S_2$ is strictly conserved. Its validity range, however, is not only controlled by the weak local exchange $K \ll J$ but also by the propagation time. Residual perturbative deviations from the linear dynamics accumulate over time, such that complete relaxation of the system, also for the n.n.n. case, is expected on a long timescale. In fact, indications for full long-time relaxation are seen at $t \simeq 10^4$ in Fig. 8.

IV. QUANTUM-CLASSICAL IMPURITY MODEL

In the case of the quantum-classical impurity model, we again find a qualitatively very similar effect in the relaxation dynamics. However, to explain the observed incomplete relaxation, it turns out again that a different methodological approach is necessary.

We consider a spinful single-orbital tight-binding model on a one-dimensional lattice of L sites with hopping between nearest neighbors T, where in addition, two classical impurity spins S_m ($m = 1, 2$) are locally exchange coupled to the local electron spins $s_i = \frac{1}{2}\sum_{\sigma\sigma'} c_{i\sigma}^\dagger \tau_{\sigma\sigma'} c_{i\sigma'}$ at sites $i = i_m$ of the lattice via an antiferromagnetic exchange interaction K. Here, τ denotes the vector of Pauli matrices, and $\sigma = \uparrow, \downarrow$ is the electron spin projection. A sketch of the system is shown in Fig. 9. The geometry is the same as for the previous models. As for the classical Heisenberg model, we assume that K is weak and can be treated perturbatively. The quantum-classical Hamiltonian is

$$H = -T \sum_{ij}^{\text{n.n.}} \sum_\sigma c_{i\sigma}^\dagger c_{j\sigma} + K \sum_m S_m s_{i_m}. \quad (38)$$
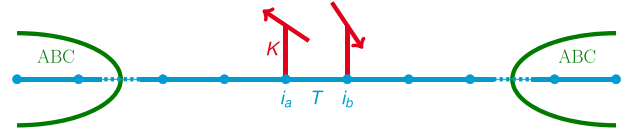

FIG. 9. Sketch of the quantum-classical hybrid model. Two classical impurity spins (red) are locally exchange coupled to a system of conduction electrons on a one-dimensional lattice (blue). K: antiferromagnetic local exchange, T: nearest-neighbor hopping. Green: absorbing boundary conditions (ABC).

We choose $T = 1$ to fix the energy (and time) scale and an antiferromagnetic exchange $K > 0$. As for the stub-impurity model, we consider half-filling, i.e., $N = L$ electrons.

The equations of motion [52,53] couple the classical and the quantum sector of the theory. For the classical impurity spins, we obtain Landau-Lifshitz–type equations,

$$\frac{d}{dt}S_m = K\langle s_{i_m}\rangle_t \times S_m(t), \quad (39)$$

similar to Eq. (22). Here, $\langle s_{i_m}\rangle_t$ is the expectation value in the N-electron state $|\Psi(t)\rangle$ at time t. For a given classical-spin configuration at time t, the quantum system is uncorrelated, and hence its real-time dynamics is completely described by the one-particle reduced density matrix $\rho(t)$ with elements

$$\rho_{i\sigma i'\sigma'}(t) = \langle \Psi(t)| c_{i'\sigma'}^\dagger c_{i\sigma}|\Psi(t)\rangle. \quad (40)$$

Its equation of motion is essentially the same as for the stub-impurity model, see Eq. (10), but the hopping matrix T is replaced by the time-dependent effective hopping matrix $T^{(\text{eff})}(t)$, which includes the classical impurity spins as time-dependent external parameters:

$$T_{i\sigma i'\sigma'}^{(\text{eff})}(t) = \delta_{\sigma\sigma'}T_{ii'} + \frac{K}{2}\delta_{ii'}\sum_{m=1,2}\delta_{ii_m}\tau_{\sigma\sigma'}S_m(t). \quad (41)$$

We study the time evolution of the full system starting at $t = 0$ from an initial state where the two impurity spins are in an excited noncollinear configuration (as in the classical Heisenberg impurities case, $S_1 = Se_x$ and $S_2 = Se_y$ with $S = \frac{1}{2}$), while the electron system is in its ground state corresponding to this spin configuration. The excitation energy stored in the vicinity of the impurities is dissipated to the bulk of the electron system on a timescale that, even for K of the order of T, typically exceeds by far the timescale that is numerically accessible when using open boundaries and when reflections of propagating excitations from the boundaries of the system shall be avoided. Since the propagation is essentially ballistic, unphysical reflections from the boundaries that disturb the dynamics near the impurities will occur at time $t \sim L/T$, i.e., one would have to work with effective hopping matrices of very high matrix dimension. For this reason and as indicated in Fig. 9, we employ so-called absorbing boundary conditions (ABC), which have been developed and extensively tested previously, see Ref. [54]. Apart from the conserving von Neumann term, the resulting equations of motion contain a dissipative term and are given by

$$i\frac{d}{dt}\rho(t) = [T_{\text{eff}}(t), \rho(t)] - i\{\gamma, \rho(t) - \rho_0\}. \quad (42)$$
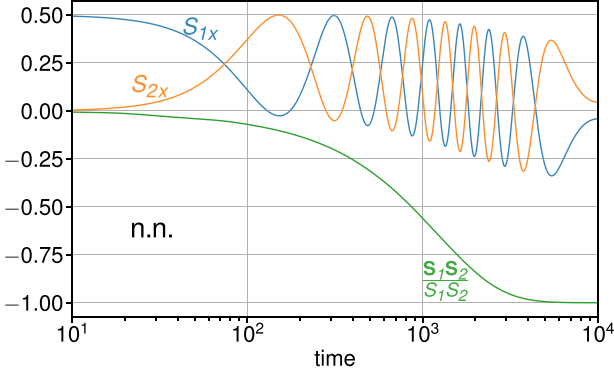
FIG. 10. Time evolution of the x components of the two classical impurity spins S_1 and S_2 (blue and orange) exchange coupled to the conduction-electron system at neighboring sites $i_1 = 34$ and $i_2 = 35$ at the center of a chain with $L = 68$ sites. Green: cosine of the angle enclosed by S_1 and S_2. Initial excited state at time $t = 0$: host electron system in its ground state corresponding to the initial (excited) impurity-spin configuration $S_1 = \frac{1}{2}e_x$ and $S_2 = \frac{1}{2}e_y$. Further parameters: $T = 1$, $K = 1$. Absorbing boundary conditions with nonzero diagonal elements $\gamma_2 = \gamma_{L-1} = 0.115$ and $\gamma_1 = \gamma_L = 0.230$ (see text).
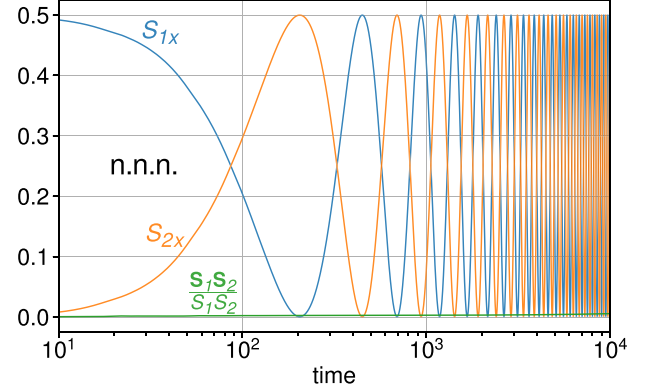

FIG. 11. The same as in Fig. 10 but for next-nearest-neighbor impurity spins at $i_1 = 34$, $i_2 = 36$ of a chain with $L = 69$ sites in total.

Here, ρ_0 is the initial ground-state one-particle reduced density matrix, $\{\cdot, \cdot\}$ denotes the anticommutator, and γ is a diagonal matrix controlling the dissipation rate. It has nonzero entries only for the outermost two "absorbing" sites on both sides of the chain. For the concrete computations, we have fixed the values for $\gamma_1 = \gamma_L$ and $\gamma_2 = \gamma_{L-1}$, as in Ref. [54], by comparing the resulting spin dynamics using ABC with the exact spin dynamics, i.e., without the dissipative term in Eq. (42). This has been done for a shorter propagation time of $t = 5 \times 10^2$ and a larger system size such that reflections from the boundaries are avoided. We find perfect agreement with $\gamma_1 = 0.230$ and $\gamma_2 = 0.115$. However, the results are quite insensitive to the precise choice. As compared to the system studied in Ref. [54], the optimal parameters are smaller because the spin dynamics is much slower.

The impurity-spin dynamics for nearest-neighbor spins as obtained by solving the coupled equations of motion (39) and (42) is displayed in Fig. 10. At short times $t \lesssim 10^3$ there is a pronounced precession dynamics with a small frequency $\omega \sim 0.01$. This is explained by the indirect RKKY exchange [55–57] mediated by the electron system, which is rather weak, even for an exchange interaction of $K = T = 1$. On a longer timescale $t \sim 10^4$, the system shows complete relaxation and the two spins reach their antiferromagnetic ground-state configuration (see green line in the figure).

For impurity spins coupled to n.n.n. sites, see Fig. 11, the same precessional motion is found, but with an even smaller precession frequency. This reflects the smaller RKKY exchange due to the increased distance between the spins. However, the real-time dynamics is qualitatively different, as there is hardly any relaxation to the ferromagnetic ground-state spin configuration visible on the numerically accessible timescale. At time $t = 10^4$, the angle enclosed by S_1 and S_2 deviates by less than 1% from its initial value only. We conclude that, as for the other models studied, the system is trapped in an intermediate stationary state and that complete relaxation, if at all, takes place on a still much longer timescale.

For smaller K (not shown here), the time evolution is essentially the same in qualitative terms. The only notable difference is that the dynamics is even slower, i.e., characterized by smaller precession frequencies and longer relaxation times.

None of the explanations for incomplete relaxation used for the previously discussed systems is easily applicable to the quantum-classical model. The linearization of the coupled equations of motion is not helpful to identify possible local conserved observables and in fact is not informative due to the large number of $\sim 4L^2$ of degrees of freedom in the quantum sector, i.e., the density-matrix elements.

With linear-response theory [37,53,58–60], we choose a different approach. Conceptually, this is limited to the weak exchange-coupling regime and directly addresses the dynamics of the classical impurity spins. For weak K, the expectation value of the local spin at site i_m can be obtained via the Kubo formula as

$$\langle s_{i_m} \rangle_t = K \sum_{m'=1,2} \int_0^t dt' \, \chi_{mm'}(t') S_{m'}(t - t') . \quad (43)$$

Here, the response function, the $K = 0$ retarded magnetic susceptibility of the electron system, is isotropic $\chi_{m\alpha,m'\alpha'}(t) = \delta_{\alpha\alpha'} \chi_{mm'}(t)$ and independent of the spatial direction $\alpha = x, y, z$. It is given by

$$\chi_{m\alpha,m'\alpha'}(t) = -i\Theta(t)e^{-\eta t}\langle [s_{i_m\alpha}(t), s_{i_{m'}\alpha'}(0)] \rangle , \quad (44)$$

where $\langle \cdots \rangle$ is the $K = 0$ ground-state expectation value and where η is a positive infinitesimal. A straightforward computation yields

$$\chi_{mm'}(t) = \Theta(t)e^{-\eta t}\text{Im}\Big[\big(e^{-iTt}\Theta(T - \mu)\big)_{i_m i_{m'}}$$
$$\times \big(e^{iTt}\Theta(\mu - T)\big)_{i_{m'} i_m} \Big]. \quad (45)$$

Note that the chemical potential $\mu = 0$ at half-filling. For the evaluation of Eq. (45), we consider large systems with up to $L = 10^5$ sites and choose periodic boundary conditions. Hence, the hopping matrix is diagonalized as $T = U \varepsilon U^\dagger$, where the unitary matrix U with elements $U_{ik} = e^{ikR_i}/\sqrt{L}$

describes Fourier transformation from lattice sites i to wave "vectors" k in the first Brillouin zone. The entries of the diagonal matrix are given by the tight-binding dispersion $\varepsilon_k = -2T\cos(k)$. We define $A_{i_m i_{m'}}(k,k') = U^\dagger_{k i_m} U_{i_m k'} U^\dagger_{k' i_{m'}} U_{i_{m'} k} = L^{-2} e^{i(k'-k)(i_m - i_{m'})}$. Furthermore, we write $\Delta\varepsilon_{kk'} = \varepsilon_k - \varepsilon_{k'} = -2T[\cos(k) - \cos(k')]$ for short. This yields

$$\chi_{mm'}(t) = -\frac{i}{2}\Theta(t)e^{-\eta t}\sum_k^{\text{occ.}}\sum_{k'}^{\text{unocc.}} A_{i_m i_{m'}}(k,k')$$
$$\times \left(e^{i\Delta\varepsilon_{kk'}t} - e^{-i\Delta\varepsilon_{kk'}t}\right), \quad (46)$$

or, after Fourier transformation from time to frequency space, the frequency-dependent susceptibility

$$\chi_{mm'}(\omega) = \frac{1}{2}\sum_k^{\text{occ.}}\sum_{k'}^{\text{unocc.}} A_{i_m i_{m'}}(k,k')$$
$$\times \left(\frac{1}{\omega - \varepsilon_k + \varepsilon_{k'} + i\eta} - \frac{1}{\omega + \varepsilon_k - \varepsilon_{k'} + i\eta}\right). \quad (47)$$

Note that we have the symmetry $\chi_{mm'}(\omega) = \chi_{m'm}(\omega)$ for the nonlocal elements $m \neq m'$, while the local elements are m independent, $\chi_{mm}(\omega) = \chi_{m'm'}(\omega)$, due to translation invariance. The representation (47) is well suited to compute the Gilbert damping:

$$\alpha_{mm'} = -iK^2 \frac{\partial}{\partial\omega}\chi_{mm'}(\omega)|_{\omega=0} \quad (48)$$

and the RKKY indirect magnetic exchange

$$J_{mm'} = K^2 \chi_{mm'}(\omega = 0), \quad (49)$$

which determine the effective equations of motion for the classical-spin dynamics (see Ref. [53]):

$$\dot{\boldsymbol{S}}_m = \sum_{m'} J_{mm'}\boldsymbol{S}_{m'} \times \boldsymbol{S}_m + \sum_{m'}\alpha_{mm'}\boldsymbol{S}_m \times \dot{\boldsymbol{S}}_{m'}. \quad (50)$$

In practice, the results of various calculations for different system sizes L as well as for different η must be extrapolated to obtain physical results in the thermodynamic limit $L \to \infty$ and in the limit $\eta \to 0$. Here, it is important to take the thermodynamic limit first. This is demonstrated with Fig. 12, where the local, α_{mm}, and the nonlocal (n.n.n.) Gilbert damping, $\alpha_{mm'}$ ($m \neq m'$), are shown as a function of η for different L. We start the discussion with the local damping (solid lines). First, we see that for any *fixed* $\eta \gtrsim 10^{-4}$, the values for the local Gilbert damping nicely converge with increasing L. System sizes of about $L = 100\,000$ are sufficient for numerical convergence unless even smaller values of η are considered. Second, the converged values $\lim_{L\to\infty}\alpha_{mm}$ become independent of η with decreasing η, once η is sufficiently small. We find a rather precise value $\lim_{\eta\to 0}\lim_{L\to\infty}\alpha_{mm} \approx -0.0398\,K^2$. Here, we note that taking the limits in the opposite order yields the unphysical result $\lim_{L\to\infty}\lim_{\eta\to 0}\alpha_{mm} = 0$. This is easily understood. For any finite L, the spectrum of one-particle energies is gapped. Close to $\omega = 0$, the finite-size gap is $\delta \approx 2\pi/L$. This implies that for $\eta \lesssim \delta \approx 2\pi/L$, the Gilbert damping must start to deviate from its physical value and approach $\alpha_{mm} = 0$, as there is no damping in a finite system. For the practical calculations, it has
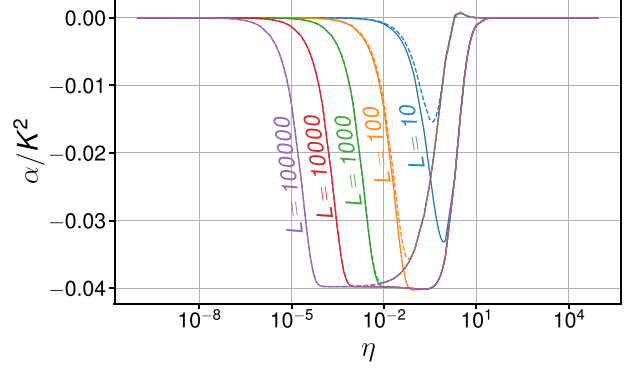

FIG. 12. Local ($m = m'$, solid lines) and nonlocal next-nearest-neighbor Gilbert damping ($m \neq m'$, dashed lines) α/K^2 as a function of η for different system sizes L as indicated. Results for large systems with periodic boundary conditions, $T = 1$.

turned out that when fixing the "infinitesimal" at $\eta \approx 2\pi/L$, it is sufficient to control the convergence with respect to L only.

Our considerations for computing the Gilbert damping likewise apply to the case of n.n.n. spins. There is, however, an important physical result that can be read off from Fig. 12. In the case of n.n.n. spins, the converged value for the nonlocal Gilbert damping (see dashed lines) is exactly the same as the local damping, i.e., $\lim_{\eta\to 0}\lim_{L\to\infty}\alpha_{mm'} \approx -0.0398\,K^2$ for both $m = m'$ and $m \neq m'$ within numerical accuracy. We note that a similar result for the nonlocal Gilbert damping has been found for metallic ferromagnets with quadratic energy-momentum dispersion [61].

The equality between the local and the nonlocal damping has in fact important consequences for the spin dynamics, as can be easily seen when rewriting Eq. (50) explicitly for two classical spins but with a single Gilbert damping constant $\alpha \equiv \alpha_{11} = \alpha_{12} = \alpha_{12} = \alpha_{21}$:

$$\dot{\boldsymbol{S}}_1 = J\boldsymbol{S}_2 \times \boldsymbol{S}_1 + \alpha\boldsymbol{S}_1 \times \dot{\boldsymbol{S}}_1 + \alpha\boldsymbol{S}_1 \times \dot{\boldsymbol{S}}_2,$$
$$\dot{\boldsymbol{S}}_2 = J\boldsymbol{S}_1 \times \boldsymbol{S}_2 + \alpha\boldsymbol{S}_2 \times \dot{\boldsymbol{S}}_2 + \alpha\boldsymbol{S}_2 \times \dot{\boldsymbol{S}}_1. \quad (51)$$

Note that only the nonlocal RKKY exchange coupling $J \equiv J_{mm'} = J_{m'm}$ ($m \neq m'$) enters the equations. We immediately see that the total impurity spin $\boldsymbol{S}_{\text{tot}} = \boldsymbol{S}_1 + \boldsymbol{S}_2$ and thus $\boldsymbol{S}_1\boldsymbol{S}_2$ are constants of motion, as in the case of the classical Heisenberg impurity model, see Sec. III. This implies that there is no relaxation to the ground-state spin configuration at all.

So far we have discussed the case of n.n.n. impurity spins, where as a consequence of $\alpha_{mm} = \alpha_{mm'}$ ($m \neq m'$), there is no relaxation to the ground-state spin configuration. While for n.n. impurity spins the local Gilbert damping $\alpha_{mm} \approx -0.398\,K^2$ stays the same, we find, on the other hand, $\alpha_{mm'} \approx 0.0021\,K^2$ ($m \neq m'$) for the nonlocal Gilbert damping. The signs are such that a solution of Eq. (50) must approach the ground state, i.e., in the n.n. case an antiferromagnetic spin configuration. This is consistent with the computed positive RKKY exchange coupling $J_{12} \approx 0.0342\,K^2$ ($H_{\text{RKKY}} = J_{12}\boldsymbol{S}_1\boldsymbol{S}_2$) for the n.n. case. On the contrary, $J_{12} \approx -0.0189\,K^2$ for the n.n.n. case with ferromagnetic ground-state spin configuration.

Returning to the n.n.n. case, the equality of the local and the nonlocal damping can be understood analytically. Using Eqs. (47) and (48) one finds

$$\alpha_{mm'} = \frac{i}{2} K^2 \sum_k^{\text{occ.}} \sum_{k'}^{\text{unocc.}} A_{i_m i_{m'}}(k, k')$$

$$\times \left(\frac{1}{(-\varepsilon_k + \varepsilon_{k'} + i\eta)^2} - \frac{1}{(\varepsilon_k - \varepsilon_{k'} + i\eta)^2} \right). \quad (52)$$

Nonzero contributions to the double sum are obtained from wave vectors close to the Fermi points, i.e., for $k, k' = \pm\pi/2 + \mathcal{O}(1/L)$ only (note that $\varepsilon(k = \pm\pi/2) = 0 = \mu$). On the contrary, for $k, k' = \pm\pi/2 + \mathcal{O}(1)$, the imaginary infinitesimal can be disregarded, since we may take $\eta = \mathcal{O}(1/L)$, as argued above, and thus $\mathcal{O}(1/L) = \eta \ll |\varepsilon_k - \varepsilon_{k'}| = \mathcal{O}(1)$, and the two fractions in Eq. (52) cancel exactly in the thermodynamical limit.

It is thus sufficient to analyze the contributions from $k = \pm\pi/2 + \delta k$ and $k' = \pm\pi/2 + \delta k'$ with $\delta k, \delta k' = \mathcal{O}(1/L)$ for $L \to \infty$ and show that these give the same result for $i_{m'} = i_m$ and for $i_{m'} = i_m + 2$. The $i_m, i_{m'}$ dependence of the Gilbert damping is due to the weight factor $A_{i_m i_{m'}}$ only. We therefore focus on $A_{i_m i_{m'}}$. Its imaginary part does not contribute to the double sum in Eq. (52). For the discussion of the real part, we first consider $k = \pi/2 + \delta k$ and $k' = \pi/2 + \delta k'$:

$$\text{Re}\, A_{i_m i_{m'}}(k, k') = \frac{1}{L^2} \cos[(-\delta k + \delta k')(i_m - i_{m'})]. \quad (53)$$

Now, if $i_{m'} = i_m$, we have $\text{Re}\, A_{i_m i_{m'}}(k, k') = L^{-2}$, and if $i_{m'} = i_m + 2$, we get

$$\text{Re}\, A_{i_m i_{m'}}(k, k') = \frac{1}{L^2} \left[1 + \mathcal{O}\left(\frac{1}{L^2}\right) \right], \quad (54)$$

and, hence, $A_{i_m i_{m'}}(k, k') = A_{i_m i_m}(k, k') + \mathcal{O}(L^{-2})$. Analogously, this also holds for $k = \pi/2 + \delta k$ and $k' = -\pi/2 + \delta k'$ and for $k = -\pi/2 + \delta k$ and $k' = \pi/2 + \delta k'$ and $k = -\pi/2 + \delta k$ and $k' = -\pi/2 + \delta k'$. This concludes our argument.

The argument extends to arbitrary $i_m, i_{m'}$ if $i_{m'} - i_m$ is even, but fails at macroscopic distances $i_{m'} - i_m = \mathcal{O}(L)$. It is also invalid for n.n. impurities and, more generally, for odd distances between the impurities, because for $k = \pi/2 + \delta k$ and $k' = -\pi/2 + \delta k'$, e.g., we have $A_{i_m i_{m'}}(k, k') = 1$ for $i_m = i_{m'}$ and $A_{i_m i_{m'}}(k, k') = -1 + \mathcal{O}(L^{-2})$ for n.n. $i_m, i_{m'}$, and for odd distances.

Since our explanation of the incomplete relaxation is based on perturbative-in-K linear-response theory, it is necessary to compare corresponding results with those of the full theory (using absorbing boundary conditions), Eqs. (39) and (42). We choose $K = T$ for this comparison. This provides us with a comparatively fast spin dynamics. Results are displayed in Figs. 13 and 14 for the cases of n.n. and n.n.n. impurity spins.

We find a slight phase offset in the precessional motion for the n.n.n. case (Fig. 14). On the logarithmic timescale, this offset is constant. Furthermore, at late times $t \sim 10^4$, a tiny deviation of the angle enclosed by the two spins from its initial $t = 0$ value is visible in the results from the full theory, hinting towards complete relaxation on a much longer timescale. This is missing in the linear-response approach.
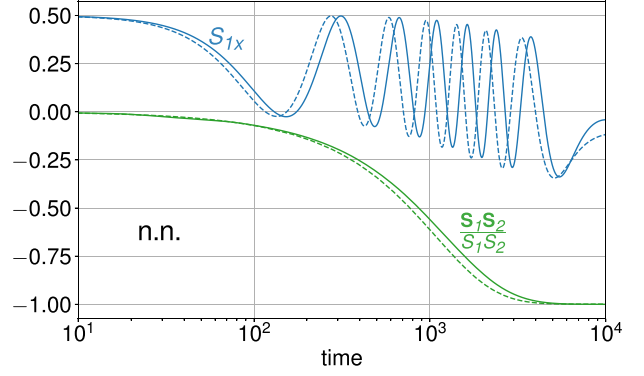

FIG. 13. Comparison between the full spin dynamics (solid lines), as obtained from the exact equations of motion (39) and (42) and absorbing boundary conditions, and linear-response spin dynamics (dashed lines), as obtained from Eq. (50) with numerically determined parameters $\alpha_{11} = \alpha_{22} = -0.0398$, $\alpha_{12} = \alpha_{21} = 0.0021$, and $J_{12} = J_{21} = 0.0342$, see Eqs. (48) and (49), respectively. Time evolution of the x component of $\mathbf{S}_1$ (blue) and cosine of the angle enclosed by $\mathbf{S}_1$ and $\mathbf{S}_2$ (green) for the case of n.n. impurity spins. All other parameters as in Fig. 10. In particular, $K = T = 1$.

For the n.n. case, where the spin dynamics is much more complicated, the perturbative method also does an almost perfect job, see Fig. 13. While we observe the same but slightly larger phase shift and a slightly longer relaxation time, all the qualitative features of the spin dynamics are fully captured.

We conclude that linear-response approach itself, i.e., perturbation theory in K, is quite reliable even for comparatively strong $K \sim T$, and errors accumulating up to a timescale $t \sim 10^4/T$ do not affect the qualitative trend of the spin dynamics. This also holds for the typical additional approximations that are necessary to arrive at Eqs. (48) and (49), i.e., weak retardation effects and time independence of the Gilbert damping, see Refs. [53,59]. All in all, the numerical results demonstrate that the proposed mechanism based on the analysis of the nonlocal Gilbert-damping term in fact captures the essence of the incomplete relaxation.
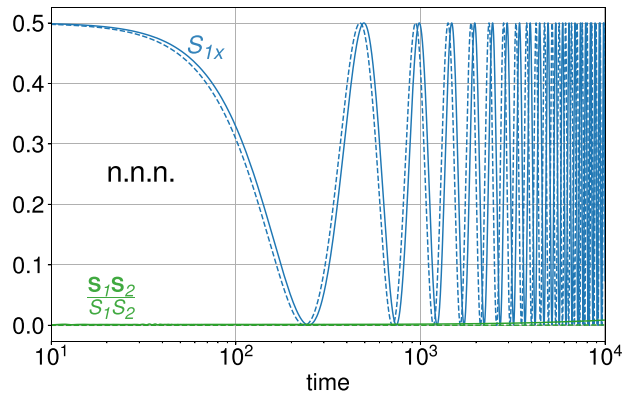

FIG. 14. Comparison between the full spin dynamics and linear-response spin dynamics (calculated damping and exchange parameters: $\alpha_{11} = \alpha_{22} = \alpha_{12} = \alpha_{21} = -0.0398$, and $J_{12} = J_{21} = -0.0189$) as in Fig. 13 but for next-nearest-neighbor impurity spins. All other parameters as in Fig. 11. In particular, $K = T = 1$.

V. CONCLUSIONS

Using numerical simulations, we have studied the exact real-time dynamics of three different prototypical one-dimensional model systems with two impurities coupled locally to nearest-neighbor or to next-nearest-neighbor sites of the host. In all cases we considered an initial state with a local excitation at or near the impurities. The unifying theme of all three models studied is the conservation (or the approximate conservation) of observables that are localized in the vicinity of the impurities. Furthermore, in all cases the presence of these (quasi) conserved observables depends on the system geometry, and in all cases this is crucial for the relaxation dynamics.

The independent-electron tight-binding quantum model with two stub impurities is conceptually the simplest. Due to the lack of interactions, it is integrable; its real-time dynamics is strongly constrained by a macroscopically large number of conserved observables. This implies that local one-particle observables do not relax to their ground-state values but to a nonthermal GGE-like state respecting the constraints. However, it depends crucially on the geometry, i.e., on the relative position of the impurities, whether or not a complete relaxation to a time-independent state for $t \to \infty$, for an infinitely extended system, actually occurs. In the case of impurities coupled to n.n.n. sites, we find persistent oscillations up to the numerically accessible timescale, i.e., before unwanted reflections from the boundaries set in.

The classical Heisenberg model with two locally exchange coupled classical impurity spins shows very similar behavior. For n.n. impurity positions, there is a fast and complete relaxation to the ground-state impurity-spin configuration. In contrast, in the n.n.n. case, an (almost) undamped oscillatory spin dynamics is found, when the local exchange coupling K is weak compared to the host exchange J. Complete relaxation to the ground-state configuration is not observed on the numerically accessible timescale. However, the numerical data indicate that complete relaxation is possible on a much longer timescale, so that the system actually exhibits prerelaxation. This is an essential difference from the noninteracting quantum system.

Qualitatively the same results are found for the quantum-classical hybrid model with two classical impurity spins locally exchange coupled to an independent-electron system on the one-dimensional lattice, i.e., fast complete relaxation to the ground-state spin configuration in the n.n. case, while in the n.n.n. case and after a fast prerelaxation, a metastable intermediate state is formed in which the impurity spins undergo an (almost) undamped oscillation. This intermediate state is stable up to $t \gtrsim 10^4$ in units of the inverse hopping. Again, we assume that the impurity-host coupling, the local exchange K, is sufficiently weak.

An explanation for the observed very different behavior for n.n. vs n.n.n. geometries, common to all three models, does not seem obvious. In fact, quite different theoretical concepts have been put forward as explanations.

The incomplete relaxation of the quantum system with n.n.n. impurities is due to the presence of a superlocalized energy eigenstate bound to the impurities and thus due to a local observable commuting with the Hamiltonian. The superlocalized state is reminiscent of the states forming flat bands in tight-binding models on lattices with characteristic geometries.

The metastability of the classical-spin model, on the other hand, could be traced back to an *approximately* conserved local observable, reminiscent of explanations for the prethermalization of interacting lattice models parametrically close to an integrable point. In fact, we had to assume that $K \ll J$, which places the model parametrically close to the trivial $K = 0$ point. Here, the weak-coupling limit has allowed us to linearize the equations of motion and thus to understand the approximate conservation law. This is remarkable because the fluctuations δS_m of the impurity spins around their ground-state configuration $S_m^{(0)}$ are not at all small, since the metastable state is far from the ground state. Rather, the argument can be based on the fact that the excitation energy is of the order of $K \ll J$, and that each impurity spin contributes of the order of K to the total energy, as opposed to the host spins which contribute of the order of J. We note that this reasoning seems possible only for impurity models.

The analysis of the real-time dynamics of the quantum-classical hybrid model is much more complicated, since a simple linearization of the equations of motions is not very feasible and not justified. However, the limit of weak local exchange coupling $K \ll T$ could be exploited in another way, namely, by time-dependent perturbation or linear-response theory. This turns out to be reliable even up to intermediate couplings $K \sim T$ and propagation times $t \lesssim 10^4$ in units of the inverse hopping parameter. *Within* the linear-response framework, the *stability* of persistent oscillations in the spin dynamics in the case of n.n.n. impurities is nicely explained by a perfect cancellation of local with nonlocal Gilbert damping constants. However, the exact dynamics obtained numerically clearly indicates that, beyond the perturbatively accessible timescale, the nonequilibrium steady state is actually metastable and that there is further relaxation on a much longer timescale.

While it seems to make no qualitative difference for the relaxation dynamics if quantum degrees of freedom are replaced by classical ones or vice versa, the geometry is a crucial factor. Common to all three models studied is the bipartite system geometry, i.e., the one-dimensionality of the host lattice with nearest-neighbor couplings between host sites, and the local host-impurity coupling. Admittedly, we expect that next-nearest-neighbor host or nonlocal host-impurity couplings (hopping or spin-exchange couplings) break the (meta)stability of the nonequilibrium state in the case of n.n.n. impurities and lead to (faster) complete relaxation. However, parametric proximity to the bipartite geometry, e.g., weak nonlocal host-impurity couplings, should still lead to a significantly different relaxation dynamics between impurities at n.n. and n.n.n. positions. Thus, we believe that our results provide valuable insights for our understanding of metastable states and the control of nonequilibrium dynamics. The study of the relaxation dynamics of impurities coupled to a host system on a two- or three-dimensional lattice is one of the promising avenues of further research.

Furthermore, it would be very interesting to study the relaxation dynamics for systems including quantum rather than classical spins or, more generally, for correlated quantum

impurity models and to check the robustness of the results against quantum fluctuations. It is quite conceivable that also in such systems the geometry plays a crucial role for the existence of (approximately) conserved local quantities. Of course, it will be technically more challenging to reach the relevant timescales. For one-dimensional systems, however, matrix-product-state approaches [62] seem to be suitable to study relaxation dynamics, e.g., see Ref. [63].

APPENDIX: COMPLETE RELAXATION IN THE CASE OF NEAREST-NEIGHBOR STUB IMPURITIES

We consider the model Eq. (1) with n.n. stub impurities for $V = 1$ (corresponding to Figs. 3 and 5), where there are two bound states at energies outside the band continuum. Let us refer to these bound eigenstates of the postquench Hamiltonian as $\mu = b_1$ and $\mu = b_2$, respectively. When calculating the fluctuations via Eq. (17), the only contributions to the double sum that are nonvanishing in the thermodynamical limit $L \to \infty$ are due to these bound eigenstates. Hence, there are essentially only two terms to be taken into account: $\mu = b_1$, $\nu = b_2$ and $\mu = b_2$, $\nu = b_1$. Consider a corresponding element of the initial one-particle reduced density matrix at time $t = 0$ in the basis of the eigenstates of the postquench Hamiltonian:

$$\rho_{b_1 b_2}(t = 0) = \sum_{IJ} U_{b_1 I}^\dagger \rho_{IJ}(t = 0) U_{J b_2} . \tag{A1}$$

To exploit the mirror symmetry of the system under reflection at the chain center, we define $\tilde{I} = L - I$, if I is a host site, while $\tilde{I}$ shall refer to the other impurity site, if I is an impurity site. With this notation we can symmetrize the summation as follows:

$$\rho_{b_1 b_2}(0) = \frac{1}{2} \sum_{IJ} \left[U_{b_1 I}^\dagger \rho_{IJ}(0) U_{J b_2} + U_{b_1 \tilde{I}}^\dagger \rho_{\tilde{I}\tilde{J}}(0) U_{\tilde{J} b_2} \right]. \tag{A2}$$

The node theorem in quantum mechanics requires that the lowest-energy state, say U_{b_1}, be symmetric under reflection, i.e., $U_{b_1 I} = U_{b_1 \tilde{I}}$, while the highest-energy state U_{b_2} is antisymmetric, $U_{\tilde{J} b_2} = -U_{J b_2}$. This immediately implies $\rho_{b_1 b_2}(0) = 0$. We conclude that there are no fluctuations surviving the thermodynamical limit $L \to \infty$ in the case of n.n. impurities. Note that this argument is invalid for the n.n.n. case. The reason is that the inversion symmetry is different due to a different inversion center, i.e., there is an invariant site $i_a + 1 = i_b - 1$, as opposed to the n.n. case.

[1] H. P. Breuer and F. Petruccione, *The Theory of Open Quantum Systems* (Oxford University Press, New York, 2002).

[2] I. de Vega and D. Alonso, Dynamics of non-Markovian open quantum systems, Rev. Mod. Phys. **89**, 015001 (2017).

[3] A. de la Torre, D. M. Kennes, M. Claassen, S. Gerber, J. W. McIver, and M. A. Sentef, Colloquium: Nonthermal pathways to ultrafast control in quantum materials, Rev. Mod. Phys. **93**, 041002 (2021).

[4] E. T. Jaynes, Information theory and statistical mechanics, Phys. Rev. **106**, 620 (1957).

[5] E. T. Jaynes, Information theory and statistical mechanics. II, Phys. Rev. **108**, 171 (1957).

[6] J. M. Deutsch, Quantum statistical mechanics in a closed system, Phys. Rev. A **43**, 2046 (1991).

[7] M. Srednicki, Chaos and quantum thermalization, Phys. Rev. E **50**, 888 (1994).

[8] M. Rigol, V. Dunjko, and M. Olshanii, Thermalization and its mechanism for generic isolated quantum systems, Nature (London) **452**, 854 (2008).

[9] L. F. Santos and M. Rigol, Onset of quantum chaos in one-dimensional bosonic and fermionic systems and its relation to thermalization, Phys. Rev. E **81**, 036206 (2010).

[10] S. Ziraldo and G. E. Santoro, Relaxation and thermalization after a quantum quench: Why localization is important, Phys. Rev. B **87**, 064201 (2013).

[11] A. Polkovnikov, K. Sengupta, A. Silva, and M. Vengalattore, Colloquium: Nonequilibrium dynamics of closed interacting quantum systems, Rev. Mod. Phys. **83**, 863 (2011).

[12] M. Rigol, A. Muramatsu, and M. Olshanii, Hard-core bosons on optical superlattices: Dynamics and relaxation in the superfluid and insulating regimes, Phys. Rev. A **74**, 053616 (2006).

[13] M. Rigol, V. Dunjko, V. Yurovsky, and M. Olshanii, Relaxation in a completely integrable many-body quantum system: An *ab initio* study of the dynamics of the highly excited states of 1D lattice hard-core bosons, Phys. Rev. Lett. **98**, 050405 (2007).

[14] M. A. Cazalilla, A. Iucci, and M.-C. Chung, Thermalization and quantum correlations in exactly solvable models, Phys. Rev. E **85**, 011133 (2012).

[15] P. W. Anderson, Absence of diffusion in certain random lattices, Phys. Rev. **109**, 1492 (1958).

[16] D. A. Abanin, E. Altman, I. Bloch, and M. Serbyn, Colloquium: Many-body localization, thermalization, and entanglement, Rev. Mod. Phys. **91**, 021001 (2019).

[17] V. I. Arnold, *Mathematical Methods of Classical Mechanics* (Springer, New York, 1978).

[18] N. Kolmogorov, On the conservation of conditionally periodic motions under small perturbation of the Hamiltonian, Dokl. Akad. Nauk SSSR **98**, 527 (1954).

[19] V. I. Arnold, Proof of a theorem of A. N. Kolmogorov on the invariance of quasi-periodic motions under small perturbations of the Hamiltonian, Russ. Math. Surv. **18**, 9 (1963).

[20] J. Moser, Nachr. Akad. Wiss. Göttingen Math.-Phys. Kl. II **1962**, 1 (1962).

[21] E. Fermi, P. Pasta, S. Ulam, and M. Tsingou, *Studies of the Nonlinear Problems* (Los Alamos Scientific Laboratory, NM, 1955).

[22] J. Jackle, Models of the glass transition, Rep. Prog. Phys. **49**, 171 (1986).

[23] P. G. Debenedetti and F. H. Stillinger, Supercooled liquids and the glass transition, Nature (London) **410**, 259 (2001).

[24] J. Berges, S. Borsányi, and C. Wetterich, Prethermalization, Phys. Rev. Lett. **93**, 142002 (2004).

[25] M. Moeckel and S. Kehrein, Interaction quench in the Hubbard model, Phys. Rev. Lett. **100**, 175702 (2008).

[26] A. Rosch, D. Rasch, B. Binz, and M. Vojta, Metastable superfluidity of repulsive fermionic atoms in optical lattices, Phys. Rev. Lett. **101**, 265301 (2008).

[27] M. Eckstein, M. Kollar, and P. Werner, Thermalization after an interaction quench in the Hubbard model, Phys. Rev. Lett. **103**, 056403 (2009).

[28] M. Kollar, F. A. Wolf, and M. Eckstein, Generalized Gibbs ensemble prediction of prethermalization plateaus and their relation to nonthermal steady states in integrable systems, Phys. Rev. B **84**, 054304 (2011).

[29] L. van Hove, Quantum-mechanical perturbations giving rise to a statistical transport equation, Physica **21**, 517 (1954).

[30] V. Romero-Rochin and I. Oppenheim, Relaxation properties of two-level systems in condensed phases, Physica A **155**, 52 (1989).

[31] B. B. Laird, J. Budimir, and J. L. Skinner, Quantum-mechanical derivation of the Bloch equations: Beyond the weak-coupling limit, J. Chem. Phys. **94**, 4391 (1991).

[32] E. Geva, E. Rosenman, and D. Tannor, On the second-order corrections to the quantum canonical equilibrium density matrix, J. Chem. Phys. **113**, 1380 (2000).

[33] W.-M. Zhang, P.-Y. Lo, H.-N. Xiong, M. W.-Y. Tu, and F. Nori, General non-Markovian dynamics of open quantum systems, Phys. Rev. Lett. **109**, 170402 (2012).

[34] H.-N. Xiong, P.-Y. Lo, W.-M. Zhang, D. H. Feng, and F. Nori, Non-Markovian complexity in the quantum-to-classical transition, Sci. Rep. **5**, 13353 (2015).

[35] C. Y. Cai, L.-P. Yang, and C. P. Sun, Threshold for nonthermal stabilization of open quantum systems, Phys. Rev. A **89**, 012128 (2014).

[36] J. Iles-Smith, N. Lambert, and A. Nazir, Environmental dynamics, correlations, and the emergence of noncanonical equilibrium states in open quantum systems, Phys. Rev. A **90**, 032114 (2014).

[37] M. Elbracht and M. Potthoff, Long-time relaxation dynamics of a spin coupled to a Chern insulator, Phys. Rev. B **103**, 024301 (2021).

[38] M. Sayad, R. Rausch, and M. Potthoff, Relaxation of a classical spin coupled to a strongly correlated electron system, Phys. Rev. Lett. **117**, 127201 (2016).

[39] N. Strohmaier, D. Greif, R. Jördens, L. Tarruell, H. Moritz, T. Esslinger, R. Sensarma, D. Pekker, E. Altman, and E. Demler, Observation of elastic doublon decay in the Fermi-Hubbard model, Phys. Rev. Lett. **104**, 080401 (2010).

[40] F. Hofmann and M. Potthoff, Doublon dynamics in the extended Fermi-Hubbard model, Phys. Rev. B **85**, 205127 (2012).

[41] R. Rausch, M. Potthoff, and N. Kawakami, Magnetic doublon bound states in the Kondo lattice model, Phys. Rev. Lett. **123**, 216401 (2019).

[42] E. H. Lieb, Two theorems on the Hubbard model, Phys. Rev. Lett. **62**, 1201 (1989).

[43] H. Tasaki, Ferromagnetism in the Hubbard models with degenerate single-electron ground states, Phys. Rev. Lett. **69**, 1608 (1992).

[44] H. Tasaki, From Nagaoka's ferromagnetism to flat-band ferromagnetism and beyond: An introduction to ferromagnetism in the Hubbard model, Prog. Theor. Phys. **99**, 489 (1998).

[45] B. Sutherland, Localization of electronic wave functions due to local topology, Phys. Rev. B **34**, 5208 (1986).

[46] J. Vidal, R. Mosseri, and B. Douçot, Aharonov-Bohm cages in two-dimensional structures, Phys. Rev. Lett. **81**, 5888 (1998).

[47] T. Misumi and H. Aoki, New class of flat-band models on tetragonal and hexagonal lattices: Gapped versus crossing flat bands, Phys. Rev. B **96**, 155137 (2017).

[48] K.-H. Yang and J. O. Hirschfelder, Generalizations of classical Poisson brackets to include spin, Phys. Rev. A **22**, 1814 (1980).

[49] M. Lakshmanan and M. Daniel, Comment on the classical models of electrons and nuclei and the generalizations of classical Poisson brackets to include spin, J. Chem. Phys. **78**, 7505 (1983).

[50] L. D. Landau and E. M. Lifshitz, On the theory of the dispersion of magnetic permeability in ferromagnetic bodies, Physik. Zeits. Sowjetunion **8**, 153 (1935).

[51] W. Marhall, Antiferromagnetism, Proc. R. Soc. London A **232**, 48 (1955).

[52] H.-T. Elze, Linear dynamics of quantum-classical hybrids, Phys. Rev. A **85**, 052109 (2012).

[53] M. Sayad and M. Potthoff, Spin dynamics and relaxation in the classical-spin Kondo-impurity model beyond the Landau-Lifschitz-Gilbert equation, New J. Phys. **17**, 113058 (2015).

[54] M. Elbracht and M. Potthoff, Accessing long timescales in the relaxation dynamics of spins coupled to a conduction-electron system using absorbing boundary conditions, Phys. Rev. B **102**, 115434 (2020).

[55] M. A. Ruderman and C. Kittel, Indirect exchange coupling of nuclear magnetic moments by conduction electrons, Phys. Rev. **96**, 99 (1954).

[56] T. Kasuya, A theory of metallic ferro- and antiferromagnetism on Zener's model, Prog. Theor. Phys. **16**, 45 (1956).

[57] K. Yosida, Magnetic properties of Cu-Mn alloys, Phys. Rev. **106**, 893 (1957).

[58] M. Onoda and N. Nagaosa, Dynamics of localized spins coupled to the conduction electrons with charge and spin currents, Phys. Rev. Lett. **96**, 066603 (2006).

[59] S. Bhattacharjee, L. Nordström, and J. Fransson, Atomistic spin dynamic method with both damping and moment of inertia effects included from first principles, Phys. Rev. Lett. **108**, 057204 (2012).

[60] N. Umetsu, D. Miura, and A. Sakuma, Microscopic theory for Gilbert damping in materials with inhomogeneous spin dynamics, J. Appl. Phys. **111**, 07D117 (2012).

[61] F. Reyes-Osorio and B. K. Nikolić, Gilbert damping in metallic ferromagnets from Schwinger-Keldysh field theory: Intrinsically nonlocal, nonuniform, and made anisotropic by spin-orbit coupling, Phys. Rev. B **109**, 024413 (2024).

[62] U. Schollwöck, The density-matrix renormalization group in the age of matrix product states, Ann. Phys. **326**, 96 (2011).

[63] M. Ljubotina, D. Roy, and T. Prosen, Absence of thermalization of free systems coupled to gapped interacting reservoirs, Phys. Rev. B **106**, 054314 (2022).

7 – Summary and Outlook

7.1 – Relation to Other Scientific Works

Before concluding this paper with a final summary, we would like to put it into bit more context with other scientific works. As the main focus of this thesis was the relaxation dynamics of quantum-classical impurity models, where one or two classical spins were coupled to a host system of non-interacting electrons, we would like to summarize a bit how such spin dynamics is treated in the rest of the scientific landscape.

Spin valves and magnetic tunnel junctions [97–100], for example, show a lot of similarity to the models we considered. They are built up by two ferromagnetic layers hosting many localized spins separated by a non-magnetic metallic spacer layer (spin valves) or an insulating barrier (magnetic tunnel junctions). At their ends, both ferromagnetic layers are coupled to metallic leads, enabling us to send a current through the setup. For a sketch, see Fig. 7.1. The first ferromagnetic layer is also called the polarizing layer (PL), as the incoming current is polarized by it, and the second ferromagnetic layer is also called the analyzing layer (AL), as we read out its magnetization when the now spin-polarized current runs through it.

In [99] the spin valve is treated in a quantum-classical way. The Hamiltonian for the quantum part is given by

$$
\hat{H} = -T \sum_{i,j}^{\text{n.n.}} \sum_{\sigma=\uparrow\downarrow} \left(\hat{c}_{i\sigma}^{\dagger} \hat{c}_{j\sigma} + \text{H.c.} \right) + \overline{\mu} \sum_{i\sigma} \hat{c}_{i\sigma}^{\dagger} \hat{c}_{i\sigma} + \frac{J_{\text{sd}}}{2} \sum_{j\in\text{PL,AL}} \sum_{\sigma\sigma'} \boldsymbol{S}_j \boldsymbol{\tau}_{\sigma\sigma'} \hat{c}_{j\sigma}^{\dagger} \hat{c}_{j\sigma'} \; , \quad (7.1)
$$

where $\overline{\mu}$ is a constant electrochemical potential governing the electron occupation, J_{sd} is a sd-like interaction (interaction between the s-shell and d-shell electrons) between the electrons and the classical spins $\boldsymbol{S}_j$ analogous to our K. The creation and annihilation operators $\hat{c}_{i\sigma}^{\dagger}$ and $\hat{c}_{j\sigma}$ are the same as in Eq. (3.1), and the vector of Pauli matrices $\boldsymbol{\tau}$ is also already known from Eq. (3.19). On the other hand, the Hamiltonian for the classical part is given by:

$$
H_{\text{cl}} = J_{\text{ex}} \sum_{ij}^{\text{n.n.}} \boldsymbol{S}_i \boldsymbol{S}_j - \sum_{j\in\text{PL,AL}} \boldsymbol{B} \boldsymbol{S}_j - \sum_{j\in\text{PL,AL}} \left(K_{\text{PL/AL}} \boldsymbol{S}_j \boldsymbol{e}_{\text{PL/AL}} \right)^2 + J_{\text{sd}} \sum_{j\in\text{PL,AL}} \langle \hat{\boldsymbol{s}}_j \rangle_t \boldsymbol{S}_j \; ,
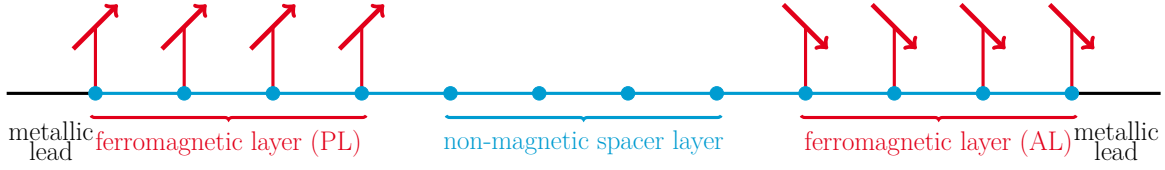$$

$$(7.2)$$

Figure 7.1: *Sketch of a one-dimensional spin valve. The two ferromagnetic layers (AL and PL), indicated by the red arrows representing localized spins, are seperated by a non-magnetic spacer layer. At both their ends, the spin valve is coupled to a metallic lead.*

with an interlayer exchange coupling J_{ex}, an external magnetic field $\boldsymbol{B}$, a layer-dependent magnetic anisotropy $K_{\text{PL/AL}}$ and unit vector $\boldsymbol{e}_{\text{PL/AL}}$ aligned with the layer-dependent anisotropy easy axis, and local magnetic moments of the electron system $\langle \boldsymbol{s}_j \rangle_t$ like in Eq. (3.22). For an electrochemical potential $\overline{\mu} = 0$ the Hamiltonian for the quantum part, Eq. (7.1) is basically the same we use for our models. The only slight difference is that there are more classical spins. On the other hand, the Hamiltonian for the classical part, Eq. (7.2), differs on two accounts. Firstly, there is an interaction J_{ex} between the classical spins, and secondly, there is a term describing the anisotropy of the system.

The metallic leads at the ends of the PL and AL are modeled via a fermionic reservoir, which leads to a non-unitary time evolution of the one-particle reduced density matrix:

$$\frac{\partial}{\partial t}\boldsymbol{\rho}(t) = - \left[\hat{H}(t), \boldsymbol{\rho}(t) \right] + \sum_{l=\text{PL,AL}} \left(\hat{\Pi}_l^{\dagger}(t) + \hat{\Pi}_l(t) \right) \;, \tag{7.3}$$

with so called current matrices $\hat{\Pi}_l$, whose definition is given in [99]. Again, this is similar to our approach. We also had a non-unitary time evolution of the one-particle reduced density matrix in our models. The cause, however, is different. In our cases the non-unitary time evolution was caused by the absorbing boundary conditions constructed via a Lindblad formalism with the aim to absorb outgoing excitations. Here, a different formalism is used to describe an electric current flowing in and out of the system.

Later on in [99], a macrospin approximation is tested, where the PL and AL are approximated by a single classical macrospin each, and it shows that for certain parameter regimes this is a satisfying approximation. This is reminiscent to our treatment of the quantum-classical model in [III], where we extracted a classical (impurity) spin only dynamics using linear-response theory. So, this shows that this kind of quantum-classical approach is also useful for different kind of problems.

Going one step further from a quantum-classical approach, in [100] a purely quantum mechanical treatment (no classical spins anymore) of a spin valve is given, where the entanglement between the PL and AL is analyzed. The PL and AL are treated as

a Kondo-Heisenberg model [101] sandwiched by electronic leads modeled by a tight-binding model. This results in a Hamiltonian:

$$\hat{H} = -T \sum_{ij}^{\text{n.n.}} \sum_{\sigma=\uparrow\downarrow} \hat{c}_{i\sigma}^{\dagger} \hat{c}_{j\sigma} - J_{\text{sd}} \sum_i \hat{\boldsymbol{s}}_i \hat{\boldsymbol{S}}_i - \sum_{ij}^{\text{n.n.}} \left[J \left(\hat{S}_i^x \hat{S}_j^x + \hat{S}_i^y \hat{S}_j^y \right) + J_z \hat{S}_i^z \hat{S}_j^z \right] \; , \quad (7.4)$$

where the quantum spins $\hat{\boldsymbol{S}}_i$ couple to the local magnetic moments $\hat{\boldsymbol{s}}_i$ of the electron system and are coupled to each other in form of a ferromagnetic nearest-neighbor Heisenberg XXZ model.

A spin valve is an open quantum system and, therefore, subject to dissipation and phase decoherence [100]. Here, the dissipation is modeled by coupling the spin operators $\hat{\boldsymbol{S}}_i$ to a bosonic heat bath using the Lindblad formalism. Because of the quantum spins a more intricate method is necessary to calculate the dynamics. Here, it is done by employing time-dependent density matrix renormalization group [48–54]. However, due to the quantum spins, it is now possible to observe entanglement between the PL and AL. All in all, in relation to our work, [100] shows a different way to employ the Lindblad formalism and also shows how it could be possible to extend our quantum-classical treatment to a purely quantum mechanical version to capture effects like entanglement between the spins.

Going on from the spin valves, in [102] a very similar setup to that in [I] is considered. The only difference is that instead of absorbing boundary conditions a fermionic reservoir is coupled to the edge of the host system. That makes it possible to apply an external voltage bias, and inspect its influence on the relaxation dynamics of the classical spin. Additionally, also an effective LLG dynamics for the classical impurity spin is calculated.

In [103], similar to our investigation for the quantum-classical model in [III], the Gilbert damping in metallic ferromagnets was investigated. This was done by using Schwinger-Keldysh non-equilibrium field theory [104]. Their findings, regarding the Gilbert damping in a metallic ferromagnet, were similar to our observation of the local and non-local Gilbert damping in [III].

We did not really cover how our research could be transferred to an experimental setup, but [100, 103, 105] go into a bit more detail how similar theoretical setups could be treated experimentally. Furthermore, in [106] experimental measurements were performed for a nanoscale magnetic spin valve structure, and [107] and [108] show how the Gilbert damping can be measured in thin films using ferromagnetic resonance measurements [109].

7.2 – Final Summary

In this thesis, we investigated the long-real-time relaxation dynamics of different kinds of one-dimensional impurity models.

We mostly considered models, in which classical impurity spins were coupled to a host system of non-interacting itinerant electrons. However, to circumvent the problems of arising finite-size effects during the time propagation, we first had to develop a framework of absorbing boundary conditions (ABC). These ABC enabled us to numerically calculate the dynamics of quantum mechanical or quantum-classical systems on time scales normally not achievable without having to deal with finite-size effects disturbing and interfering with the relaxation dynamics of the system.

We then applied the framework of ABC successfully to a toy-model, in which a classical spin, coupled to a host system of non-interacting itinerant electrons, was driven in a magnetic field $\boldsymbol{B}$. We calculated the relaxation time of the classical spin and investigated its dependence on the strength of the magnetic field $\boldsymbol{B}$. For weak field strengths we found the relaxation time to be proportional to $\frac{1}{B}$, which perfectly agrees with the spin-only LLG theory [17, 110]. From that, we concluded that, at least for our toy-model, the ABC do not cause any observable artifacts in the dynamics, even for timescales of the order of 10^5 inverse hoppings.

Following on from this, we modified our toy-model and exchanged the metallic host system with a simple band insulator with a variable energy gap, to test out the ABC for a different kind of model. The gap in the electronic structure leads to a breakdown of lowest-order perturbation theory in the exchange interaction K and standard LLG-theory as the Gilbert damping α is predicted to be zero. However, relaxation should still be possible if the spin susceptibility $\chi^{(\mathrm{ret})}(\omega)$ is non-zero at the Larmor frequency $\omega \approx B$. This is indeed possible for field strengths of the order of the gap size. Using ABC we were able to numerically calculate the long-time relaxation dynamics of this system and found this exact relaxation behavior concluding that relaxation is still possible for large enough magnetic fields.

After confirming the functionality and effectiveness of the ABCs we investigated a more intricate model. We studied the long-time relaxation dynamics of a classical spin driven in a magnetic field coupled to a topological insulator, namely a SSH model. The SSH model features a tuneable band gap and, depending on the exact parameters, topological edge states inside the gap. Building upon our earlier investigations of the simple band insulator in the previous work, we confirmed that, despite the existence of a band gap, relaxation is still possible for magnetic field strengths large enough, namely for magnetic fields larger than half the band gap: $B \geq \frac{\Delta}{2} = 2\delta T$.

However, we found an anomaly in the relaxation dynamics, once we coupled the classical impurity spin to the edge of the host system. There the impurity spin can couple

directly to the edge states if present, and these edge states can assist the relaxation process. We found that in the presence of the edge states, a smaller magnetic field strength of $B \approx 2\delta T - \epsilon_0$ suffices to enable a relaxation of the impurity spin, where ϵ_0 is the strength of the Zeeman-splitting of the edge states caused by the coupling of the host system to the classical impurity spin. The edge states inside the gap help bridging the gap by reducing the necessary energy to excite a state out of the valence band. This is further aided by a dynamical relaxation mechanism causing an exchange of population between the two Zeeman-splitted edge states.

Moving on from these single impurity models, we went on to investigate the real-time relaxation dynamics of different types of two-impurity models. A purely quantum mechanical stub impurity model, in which two fermionic impurity sites were coupled to a host system of itinerant fermions, a purely classical Heisenberg impurity model, where two classical spin impurities were coupled to a host system of classical spins and lastly, a quantum-classical hybrid model, in which two classical impurity spins were coupled to a host system of itinerant electrons. Additionally, the impurities were not driven in any kind of external (magnetic) field anymore.

We found the relaxation in all these three systems to be very similar. The system fully relaxed when the impurities were coupled to nearest-neighbor sites of the host system. On the other hand, when the impurities were coupled to next-nearest-neighbor sites, there was only an incomplete relaxation of the system. We traced back the similarity in the relaxation dynamics to partially stem from the similar geometries of the system. So two impurities coupled to a one-dimensional host system with a bipartite lattice. However, the exact reason behind the (non-)relaxation of the systems is different for the three models.

For the quantum mechanical stub impurity model, we found that the non-relaxation is caused by the existence of localized bound states in the generic post-quench dynamics of such a tight-binding lattice model. These localized bound states prohibit the relaxation dynamics in the case of next-nearest-neighbor impurities by trapping some of the initial excitation around the impurities. Although similar bound states also exist for nearest-neighbor impurities, they do not prohibit the relaxation of the system because the symmetry of the system cancels out their effect on the relaxation dynamics leading to a full relaxation of the system.

In the purely classical Heisenberg impurity model we found that the product of the impurity spins, $\boldsymbol{S}_1 \cdot \boldsymbol{S}_2$, becomes a (quasi-) conserved quantity of motion after a certain pre-relaxation process. After this process, a sufficient amount of spin and energy has been dissipated into the bulk, and the system state around the impurities evolved to be sufficiently close to one of the local ground states. There the dynamics is well described by the linearized equations of motion, and it can be easily shown that $\boldsymbol{S}_1\boldsymbol{S}_2$ becomes strictly conserved in the linearized dynamics defined by the linearized equations of

motion. However, as the validity of the linearized equations of motion is not only affected by the weak local exchange interaction $K \ll J$ but also by the total propagation time, we expect full relaxation of the system to still be possible but strongly delayed if present.

Finally, for the quantum-classical Kondo impurity model we investigated the relaxation dynamics via linear-response theory. This perturbative approach yields a local and a non-local Gilbert damping parameter describing the effective relaxation dynamics of the two impurity spins. In the case of nearest-neighbor impurities, the local Gilbert damping is much larger than the non-local one, resulting in an effective dynamics with full relaxation. For next-nearest-neighbor impurities, we found the local and non-local Gilbert damping to be the same. This leads to a new conserved quantity in the effective impurity spin relaxation dynamics in the form of the total spin of the impurities $\boldsymbol{S}_1 + \boldsymbol{S}_2$. As a result the, for the dynamics of the classical impurity spins available, configuration space becomes restricted which consequently prohibits the relaxation of the system.

Looking forward, it would be interesting to expand the research of this thesis to higher dimensional systems and/or to correlated electron systems. Higher-dimensional systems, so impurity models with two or three-dimensional host systems, suffer, even more than the one-dimensional model, from finite-size effects. As the computational power is limited, the maximum extension of the system in a dimension shrinks exponentially with the total dimension of the system. Ideally, the absorbing boundary conditions developed in [I], could enable us to compute the real-time dynamics of higher dimensional systems, as we would only need to compute the dynamics of a relatively small core system, to which we would attach the absorbing boundaries. Of course one would have to be cautious as some things are different in higher dimension. For example the ratio between the boundary and bulk of a system is much higher in two and three dimensions than in one. This could have an effect on how to choose the ABC. An example for an implementation of ABC for a two-dimensional Kane-Mele model can be found in [111].

On the other hand, the calculation of the real-time dynamics of a correlated electron system is also computationally very expensive. We cannot restrict the computation to the one-particle subspace of the Hilbert space as we do for uncorrelated electrons. As we have to consider the full Hilbert space at all times the necessary computation time becomes very large very fast for increasing system sizes. ABC could in theory alleviate the problem somewhat by keeping the system sizes small without having to worry about finite-size effects. However, one would have to keep in mind that in general the ABC and the Lindblad master equation lead to a non-unitary dynamics, which can make calculations more difficult.

8 – Bibliography

[1] G. W. E. Hairer, S. P. Norsett, *Solving Ordinary Differential Equations I: Nonstiff Problems*, (Springer Berlin, Heidelberg, 1993).

[2] J. Dormand and P. Prince, A family of embedded Runge-Kutta formulae, Journal of Computational and Applied Mathematics **6**, 19 (1980).

[3] S. A. Wolf, D. D. Awschalom, R. A. Buhrman, J. M. Daughton, S. von Molnar, M. L. Roukes, A. Y. Chtchelkanova, and D. M. Treger, Spintronics: A spin-based electronics vision for the future, Science **294**, 1488 (2001).

[4] I. Žutić, J. Fabian, and S. Das Sarma, Spintronics: Fundamentals and applications, Rev. Mod. Phys. **76**, 323 (2004).

[5] S. Bader and S. Parkin, Spintronics, Annual Review of Condensed Matter Physics **1**, 71 (2010).

[6] A. Fert, Nobel lecture: Origin, development, and future of spintronics, Rev. Mod. Phys. **80**, 1517 (2008).

[7] M. N. Baibich, J. M. Broto, A. Fert, F. N. Van Dau, F. Petroff, P. Etienne, G. Creuzet, A. Friederich, and J. Chazelas, Giant magnetoresistance of (001)Fe/(001)Cr magnetic superlattices, Phys. Rev. Lett. **61**, 2472 (1988).

[8] G. Binasch, P. Grünberg, F. Saurenbach, and W. Zinn, Enhanced magnetoresistance in layered magnetic structures with antiferromagnetic interlayer exchange, Phys. Rev. B **39**, 4828 (1989).

[9] A. A. Khajetoorians, J. Wiebe, B. Chilian, and R. Wiesendanger, Realizing all-spin–based logic operations atom by atom, Science **332**, 1062 (2011).

[10] B. Behin-Aein, J.-P. Wang, and R. Wiesendanger, Computing with spins and magnets, MRS Bulletin **39**, 696–702 (2014).

[11] M. A. Ruderman and C. Kittel, Indirect exchange coupling of nuclear magnetic moments by conduction electrons, Phys. Rev. **96**, 99 (1954).

[12] T. Kasuya, A theory of metallic ferro- and antiferromagnetism on Zener's model, Progress of Theoretical Physics **16**, 45 (1956).

[13] K. Yosida, Magnetic properties of Cu-Mn alloys, Phys. Rev. **106**, 893 (1957).

[14] A. A. Khajetoorians, S. Lounis, B. Chilian, A. T. Costa, L. Zhou, D. L. Mills, J. Wiebe, and R. Wiesendanger, Itinerant nature of atom-magnetization excitation by tunneling electrons, Phys. Rev. Lett. **106**, 037205 (2011).

[15] L. D. Landau and E. M. Lifshitz, On the theory of the dispersion of magnetic permeability in ferromagnetic bodies, Physik. Zeits. Sowjetunion **8**, 153 (1935).

[16] T. Gilbert, A phenomenological theory of damping in ferromagnetic materials, IEEE Transactions on Magnetics **40**, 3443 (2004).

[17] M. Sayad and M. Potthoff, Spin dynamics and relaxation in the classical-spin Kondo-impurity model beyond the Landau–Lifschitz–Gilbert equation, New Journal of Physics **17**, 113058 (2015).

[18] B. Skubic, J. Hellsvik, L. Nordström, and O. Eriksson, A method for atomistic spin dynamics simulations: implementation and examples, Journal of Physics: Condensed Matter **20**, 315203 (2008).

[19] B. Hillebrands and K. Ounadjela (Eds.), *Spin Dynamics in Confined Magnetic Structures I*, (Springer Berlin, Heidelberg, 2002).

[20] D. C. Mattis, *The Theory of Magnetism I: Statics and Dynamics*, (Springer Berlin, Heidelberg, 1981).

[21] M. D. Stiles and J. Miltat, *Spin Dynamics in Confined Magnetic Structures III*, chap. Spin-Transfer Torque and Dynamics, pp. 225–308, (Springer Berlin Heidelberg, 2006).

[22] M. Lakshmanan, The fascinating world of the Landau–Lifshitz–Gilbert equation: an overview, Philosophical Transactions of the Royal Society A: Mathematical, Physical and Engineering Sciences **369**, 1280 (2011).

[23] M. Sayad, R. Rausch, and M. Potthoff, Relaxation of a classical spin coupled to a strongly correlated electron system, Phys. Rev. Lett. **117**, 127201 (2016).

[24] M. Sayad, R. Rausch, and M. Potthoff, Inertia effects in the real-time dynamics of a quantum spin coupled to a Fermi sea, Europhysics Letters **116**, 17001 (2016).

[25] J. Kondo, Resistance minimum in dilute magnetic alloys, Progress of Theoretical Physics **32**, 37 (1964).

[26] A. C. Hewson, *The Kondo Problem to Heavy Fermions*, Cambridge Studies in Magnetism (Cambridge University Press, 1993).

[27] J. Wiebe, A. Wachowiak, F. Meier, D. Haude, T. Foster, M. Morgenstern, and R. Wiesendanger, A 300 mK ultra-high vacuum scanning tunneling microscope for spin-resolved spectroscopy at high energy resolution, Review of Scientific Instruments **75**, 4871 (2004).

[28] L. Schneider, P. Beck, L. Rózsa, T. Posske, J. Wiebe, and R. Wiesendanger, Probing the topologically trivial nature of end states in antiferromagnetic atomic chains on superconductors, Nature Communications **14** (2023).

[29] A. Kolmogorov, On the conservation of conditionally periodic motions under small perturbation of the Hamiltonian, Dokl. Akad. Nauk SSSR **98**, 527 (1954), engl. transl.: Stochastic Behavior in Classical and Quantum Hamiltonian Systems, Volta Memorial conference, Como, 1977, Lecture Notes in Physics, vol. 93, Springer Berlin Heidelberg, 1979, pp. 51–56.

[30] V. I. Arnol'd, Proof of a theorem of A. N. Kolmogorov on the invariance of quasi-periodic motions under small perturbations of the Hamiltonian, Russian Mathematical Surveys **18**, 9 (1963).

[31] J. Moser, On invariant curves of area-preserving mappings of an annulus, Nachr. Akad. Wiss. Göttingen, Math.-Phys. Kl. IIa **Nr. 1**, 1 (1962).

[32] J. M. Deutsch, Quantum statistical mechanics in a closed system, Phys. Rev. A **43**, 2046 (1991).

[33] M. Srednicki, Chaos and quantum thermalization, Phys. Rev. E **50**, 888 (1994).

[34] M. Rigol, V. Dunjko, and M. Olshanii, Thermalization and its mechanism for generic isolated quantum systems, Nature **452**, 854 (2008).

[35] L. F. Santos and M. Rigol, Onset of quantum chaos in one-dimensional bosonic and fermionic systems and its relation to thermalization, Phys. Rev. E **81**, 036206 (2010).

[36] E. T. Jaynes, Information theory and statistical mechanics. II, Phys. Rev. **108**, 171 (1957).

[37] M. Rigol, A. Muramatsu, and M. Olshanii, Hard-core bosons on optical superlattices: Dynamics and relaxation in the superfluid and insulating regimes, Phys. Rev. A **74**, 053616 (2006).

[38] M. Rigol, V. Dunjko, V. Yurovsky, and M. Olshanii, Relaxation in a completely integrable many-body quantum system: An ab initio study of the dynamics of the highly excited states of 1d lattice hard-core bosons, Phys. Rev. Lett. **98**, 050405 (2007).

[39] M. A. Cazalilla, A. Iucci, and M.-C. Chung, Thermalization and quantum correlations in exactly solvable models, Phys. Rev. E **85**, 011133 (2012).

[40] M. Z. Hasan and C. L. Kane, Colloquium: Topological insulators, Rev. Mod. Phys. **82**, 3045 (2010).

[41] X.-L. Qi and S.-C. Zhang, Topological insulators and superconductors, Rev. Mod. Phys. **83**, 1057 (2011).

[42] A. P. Schnyder, S. Ryu, A. Furusaki, and A. W. W. Ludwig, Classification of topological insulators and superconductors in three spatial dimensions, Phys. Rev. B **78**, 195125 (2008).

[43] A. Kitaev, Periodic table for topological insulators and superconductors, AIP Conference Proceedings **1134**, 22 (2009).

[44] S. Ryu, A. P. Schnyder, A. Furusaki, and A. W. W. Ludwig, Topological insulators and superconductors: tenfold way and dimensional hierarchy, New Journal of Physics **12**, 065010 (2010).

[45] C.-K. Chiu, J. C. Y. Teo, A. P. Schnyder, and S. Ryu, Classification of topological quantum matter with symmetries, Rev. Mod. Phys. **88**, 035005 (2016).

[46] A. Altland and M. R. Zirnbauer, Nonstandard symmetry classes in mesoscopic normal-superconducting hybrid structures, Phys. Rev. B **55**, 1142 (1997).

[47] J. Asbóth, L. Oroszlány, and A. Pályi, *The Su-Schrieffer-Heeger (SSH) Model. In: A Short Course on Topological Insulators. Lecture Notes in Physics, Vol. 919*, (Springer, Cham, 2016).

[48] U. Schollwöck, The density-matrix renormalization group in the age of matrix product states, Annals of Physics **326**, 96 (2011).

[49] J. Haegeman, J. I. Cirac, T. J. Osborne, I. Pižorn, H. Verschelde, and F. Verstraete, Time-dependent variational principle for quantum lattices, Phys. Rev. Lett. **107**, 070601 (2011).

[50] S. R. White and A. E. Feiguin, Real-time evolution using the density matrix renormalization group, Phys. Rev. Lett. **93**, 076401 (2004).

[51] P. Schmitteckert, Nonequilibrium electron transport using the density matrix renormalization group method, Phys. Rev. B **70**, 121302 (2004).

[52] A. J. Daley, C. Kollath, U. Schollwöck, and G. Vidal, Time-dependent density-matrix renormalization-group using adaptive effective Hilbert spaces, Journal of Statistical Mechanics: Theory and Experiment **2004**, P04005 (2004).

[53] A. E. Feiguin, The Density Matrix Renormalization Group and its time-dependent variants, AIP Conference Proceedings **1419**, 5 (2011).

[54] S. Paeckel, T. Köhler, A. Swoboda, S. R. Manmana, U. Schollwöck, and C. Hubig, Time-evolution methods for matrix-product states, Annals of Physics **411**, 167998 (2019).

[55] M. Sayad, D. Gütersloh, and M. Potthoff, Macrospin approximation and quantum effects in models for magnetization reversal, Eur. Phys. J. B **85**, 125 (2012).

[56] J. Gauyacq and N. Lorente, Classical limit of a quantal nano-magnet in an anisotropic environment, Surface Science **630**, 325 (2014).

[57] F. Delgado, S. Loth, M. Zielinski, and J. Fernández-Rossier, The emergence of classical behaviour in magnetic adatoms, Europhysics Letters **109**, 57001 (2015).

[58] H.-T. Elze, Linear dynamics of quantum-classical hybrids, Phys. Rev. A **85**, 052109 (2012).

[59] K.-H. Yang and J. O. Hirschfelder, Generalizations of classical poisson brackets to include spin, Phys. Rev. A **22**, 1814 (1980).

[60] M. Lakshmanan and M. Daniel, Comment on the classical models of electrons and nuclei and the generalizations of classical Poisson brackets to include spin, The Journal of Chemical Physics **78**, 7505 (1983).

[61] G. Czycholl, *Theoretische Festkörperphysik: Von den klassischen Modellen zu modernen Forschungsthemen*, (Springer Berlin, Heidelberg, 2008).

[62] G. Lindblad, On the generators of quantum dynamical semigroups, Commun. Math. Phys. **48**, 119 (1976).

[63] P. Pearle, Simple derivation of the Lindblad equation, European Journal of Physics **33**, 805 (2012).

[64] V. Gorini, A. Kossakowski, and E. C. G. Sudarshan, Completely positive dynamical semigroups of N-level systems, Journal of Mathematical Physics **17**, 821 (1976).

[65] M. Kollar, F. A. Wolf, and M. Eckstein, Generalized Gibbs ensemble prediction of prethermalization plateaus and their relation to nonthermal steady states in integrable systems, Phys. Rev. B **84**, 054304 (2011).

[66] J. Dziarmaga, Dynamics of a quantum phase transition and relaxation to a steady state, Advances in Physics **59**, 1063 (2010).

[67] A. Polkovnikov, K. Sengupta, A. Silva, and M. Vengalattore, Colloquium: Nonequilibrium dynamics of closed interacting quantum systems, Rev. Mod. Phys. **83**, 863 (2011).

[68] M. Girardeau, Decay of magnetization in the one-dimensional XY model, Physics Letters A **30**, 442 (1969).

[69] K. Sengupta, S. Powell, and S. Sachdev, Quench dynamics across quantum critical points, Phys. Rev. A **69**, 053616 (2004).

[70] M. A. Cazalilla, Effect of suddenly turning on interactions in the Luttinger model, Phys. Rev. Lett. **97**, 156403 (2006).

[71] A. Iucci and M. A. Cazalilla, Quantum quench dynamics of the Luttinger model, Phys. Rev. A **80**, 063619 (2009).

[72] C. Kollath, A. M. Läuchli, and E. Altman, Quench dynamics and nonequilibrium phase diagram of the Bose-Hubbard model, Phys. Rev. Lett. **98**, 180601 (2007).

[73] S. R. Manmana, S. Wessel, R. M. Noack, and A. Muramatsu, Strongly correlated fermions after a quantum quench, Phys. Rev. Lett. **98**, 210405 (2007).

[74] T. Kinoshita, T. Wenger, and D. S. Weiss, A quantum Newton's cradle, Nature (London) **440**, 900 (2006).

[75] D. M. Gangardt and M. Pustilnik, Correlations in an expanding gas of hard-core bosons, Phys. Rev. A **77**, 041604 (2008).

[76] T. Barthel and U. Schollwöck, Dephasing and the steady state in quantum many-particle systems, Phys. Rev. Lett. **100**, 100601 (2008).

[77] M. Eckstein and M. Kollar, Nonthermal steady states after an interaction quench in the Falicov-Kimball model, Phys. Rev. Lett. **100**, 120404 (2008).

[78] M. Kollar and M. Eckstein, Relaxation of a one-dimensional Mott insulator after an interaction quench, Phys. Rev. A **78**, 013626 (2008).

[79] M. Eckstein and M. Kollar, Measuring correlated electron dynamics with time-resolved photoemission spectroscopy, Phys. Rev. B **78**, 245113 (2008).

[80] J. Lancaster and A. Mitra, Quantum quenches in an XXZ spin chain from a spatially inhomogeneous initial state, Phys. Rev. E **81**, 061134 (2010).

[81] D. M. Kennes and V. Meden, Relaxation dynamics of an exactly solvable electron-phonon model, Phys. Rev. B **82**, 085109 (2010).

[82] J. Jackle, Models of the glass transition, Reports on Progress in Physics **49**, 171 (1986).

[83] P. G. Debenedetti and F. H. Stillinger, Supercooled liquids and the glass transition, Nature **410**, 259 (2001).

[84] S. Ziraldo and G. E. Santoro, Relaxation and thermalization after a quantum quench: Why localization is important, Phys. Rev. B **87**, 064201 (2013).

[85] P. Calabrese, F. H. L. Essler, and M. Fagotti, Quantum quench in the transverse-field ising chain, Phys. Rev. Lett. **106**, 227203 (2011).

[86] D. E. Manolopoulos, Derivation and reflection properties of a transmission-free absorbing potential, The Journal of Chemical Physics **117**, 9552 (2002).

[87] S. Selstø and S. Kvaal, Absorbing boundary conditions for dynamical many-body quantum systems, Journal of Physics B: Atomic, Molecular and Optical Physics **43**, 065004 (2010).

[88] K. C. Kulander, Multiphoton ionization of hydrogen: A time-dependent theory, Phys. Rev. A **35**, 445 (1987).

[89] M. Protopapas, C. H. Keitel, and P. L. Knight, Relativistic mass shift effects in adiabatic intense laser field stabilization of atoms, Journal of Physics B: Atomic, Molecular and Optical Physics **29**, L591 (1996).

[90] M. Monnerville and J. M. Robbe, Optical potential discrete variable representation method in the adiabatic representation, The European Physical Journal D - Atomic, Molecular, Optical and Plasma Physics **5**, 381 (1999).

[91] H. O. Karlsson, Stability of the complex symmetric Lanczos algorithm for computing photodissociation cross sections using smooth exterior scaling or absorbing potentials, Journal of Physics B: Atomic, Molecular and Optical Physics **42**, 125205 (2009).

[92] T. P. Grozdanov, L. Andric, and R. McCarroll, Calculations of partial cross sections for photofragmentation processes using complex absorbing potentials, The Journal of Chemical Physics **124**, 094303 (2006).

[93] G. S. Uhrig, Landau-Lifshitz damping from Lindbladian dissipation in quantum magnets, *arXiv preprint*, arXiv **2406.10613** (2024).

[94] L. Pantelidis, Dynamics of the Heisenberg model and a theorem on stability, Journal of Mathematical Physics **54**, 022701 (2013).

[95] C. Stahl and M. Potthoff, Anomalous spin precession under a geometrical torque, Phys. Rev. Lett. **119**, 227203 (2017).

[96] S. Michel and M. Potthoff, Non-Hamiltonian dynamics of indirectly coupled classical impurity spins, Phys. Rev. B **103**, 024449 (2021).

[97] B. Dieny, Giant magnetoresistance in spin-valve multilayers, Journal of Magnetism and Magnetic Materials **136**, 335 (1994).

[98] N. Locatelli, V. Cros, and J. Grollier, Spin-torque building blocks, Nature Materials **13**, 11 (2014).

[99] R. Smorka, P. Baláž, M. Thoss, and M. Žonda, Nonequilibrium dynamics in a spin valve with noncollinear magnetization, Phys. Rev. B **106**, 144435 (2022).

[100] A. Suresh, R. D. Soares, P. Mondal, J. P. S. Pires, J. M. V. P. Lopes, A. Ferreira, A. E. Feiguin, P. Plecháč, and B. K. Nikolić, Electron-mediated entanglement of two distant macroscopic ferromagnets within a nonequilibrium spintronic device, Phys. Rev. A **109**, 022414 (2024).

[101] A. M. Tsvelik and O. M. Yevtushenko, Chiral spin order in kondo-heisenberg systems, Phys. Rev. Lett. **119**, 247203 (2017).

[102] R. Smorka, M. Thoss, and M. Žonda, Dynamics of spin relaxation in nonequilibrium magnetic nanojunctions, New Journal of Physics **26**, 013056 (2024).

[103] F. Reyes-Osorio and B. K. Nikolić, Gilbert damping in metallic ferromagnets from Schwinger-Keldysh field theory: Intrinsically nonlocal, nonuniform, and made anisotropic by spin-orbit coupling, Phys. Rev. B **109**, 024413 (2024).

[104] A. Kamenev, *Field Theory of Non-Equilibrium Systems*, 2 edn. (Cambridge University Press, 2023).

[105] P. Mondal, A. Suresh, and B. K. Nikolić, When can localized spins interacting with conduction electrons in ferro- or antiferromagnets be described classically via the Landau-Lifshitz equation: Transition from quantum many-body entangled to quantum-classical nonequilibrium states, Phys. Rev. B **104**, 214401 (2021).

[106] A. Zholud, R. Freeman, R. Cao, A. Srivastava, and S. Urazhdin, Spin transfer due to quantum magnetization fluctuations, Phys. Rev. Lett. **119**, 257201 (2017).

[107] M. Oogane, T. Wakitani, S. Yakata, R. Yilgin, Y. Ando, A. Sakuma, and T. Miyazaki, Magnetic damping in ferromagnetic thin films, Japanese Journal of Applied Physics **45**, 3889 (2006).

[108] Z. Zhang, M. Cheng, Z. Yu, Z. Zou, Y. Liu, J. Shi, Z. Lu, and R. Xiong, Ultralow Gilbert damping in CrO_2 epitaxial films, Phys. Rev. B **102**, 014454 (2020).

[109] B. Heinrich and J. Cochran, Ultrathin metallic magnetic films: magnetic anisotropies and exchange interactions, Advances in Physics **42**, 523 (1993).

[110] R. Kikuchi, On the minimum of magnetization reversal time, Journal of Applied Physics **27**, 1352 (1956).

[111] R. Quade and M. Potthoff, Controlling the real-time dynamics of a spin coupled to the helical edge states of the Kane-Mele model, Phys. Rev. B **105**, 035406 (2022).

This thesis was typeset in LaTeX. The plots, graphics and visualizations were created using the Matplotlib Python package as well as the TikZ LaTeX package. For the enhancement of the language style in this thesis, the DeepL language tool was used.

Eidesstattliche Versicherung

Hiermit versichere ich an Eides statt, die vorliegende Dissertationsschrift selbst verfasst und keine anderen als die angegebenen Hilfsmittel und Quellen benutzt zu haben.

Sofern im Zuge der Erstellung der vorliegenden Dissertationsschrift generative Künstliche Intelligenz (gKI) basierte elektronische Hilfsmittel verwendet wurden, versichere ich, dass meine eigene Leistung im Vordergrund stand und dass eine vollständige Dokumentation aller verwendeten Hilfsmittel gemäß der Guten wissenschaftlichen Praxis vorliegt. Ich trage die Verantwortung für eventuell durch die gKI generierte fehlerhafte oder verzerrte Inhalte, fehlerhafte Referenzen, Verstöße gegen das Datenschutz- und Urheberrecht oder Plagiate.

Hamburg, den

_____

Michael Elbracht